CONJUGATE NATURAL CONVECTION BETWEEN TWO CONCENTRIC SPHERES

by

LAU MENG HOOI

A THESIS SUBMITTED IN PARTIAL FULFILMENT OF THE REQUIREMENTS FOR THE DEGREE OF MASTER OF APPLIED SCIENCE

in the Department of Mechanical Engineering

We accept this thesis as conforming to the required standard

THE UNIVERSITY OF BRITISH COLUMBIA

November, 1971

In presenting this thesis in partial fulfilment of the requirements for an advanced degree at the University of British Columbia, I agree that the Library shall make it freely available for reference and Study. I further agree that permission for extensive copying of this thesis for scholarly purposes may be granted by the Head of my Department or by his representatives. It is understood that copying or publication of this thesis for financial gain shall not be allowed without my written permission.

LAU MENG HOOI

Department of Mechanical Engineering

The University of British Columbia
Vancouver 8, Canada

Date 6th Dec. 1971

ABSTRACT

This work considers the conjugate convective heat transfer between a sphere containing heat sources and a concentric envelope maintained at a specified constant temperature. The space between the two is filled with an essentially incompressible fluid. Steady, laminar and rotationally symmetrical free convection is assumed to take place over the gap width and conduction is the sole transport mechanism considered inside the core. Two limiting cases, of an inner sphere of infinitely large relative heat conductivity, leading to an isothermal core to fluid interface; and of the converse case of small conductivity leading to a constant flux interface are considered separately.

The analysis of heat transport leads to the solution of the governing equations through regular perturbation expansions with the Grashof number as main parameter. The ratio of conductivities, radius ratio and Prandtl number appear as secondary parameters.

Streamlines, isovorticity curves and isotherms are obtained for various combinations of the parameters. The velocity distribution is determined and both local and overall values of the Nusselt number are obtained.

A flow visualization test was undertaken and the core surface temperature distribution was determined experimentally. Reasonable qualitative agreement with the analysis is found.

ACKNOWLEDGEMENTS

The author wishes to express his gratitude and sincere thanks to Professor Zeëv Rotem for his guidance and advice throughout all the stages of the program. Special thanks are due to Drs. E.G. Hauptmann and M. Iqbal for their suggestions and discussions. Also, the author wishes to thank the entire staff of the Mechanical Engineering Department, University of British Columbia, for their assistance.

Special thanks are due to Messrs. J. Hoar and P. Hurren (chief technicians) and L. Dery for their assistance during the construction and operation of the experiment.

Support of this program was provided by the National Research Council of Canada through Grant No. 67-2772 for which thanks are due. The author is grateful for the award of a University of British Columbia Graduate Fellowship from 1969 to 1971.

TABLE OF CONTENTS

Chapter Page

LIST OF TABLES

LIST OF FIGURES

Figure | Page

NOMENCLATURE

$A(R,\theta,\phi)$	dimensionless heat source function (eq. 2.2.3)
$B(R')$	heat source function per unit volume (eq. B-1)
c_p	specific heat of the fluid at constant pressure
$\mathcal{D}$	viscous dissipation number, $\dfrac{\mu\nu}{R'^2 K_f \Delta T_{ref}}$
E^2, E^4	operators
G	Grashof number, $g\gamma\Delta T_{ref} R'^3 / \nu^2$
g	acceleration of gravity
k	thermal conductivity
Nu_i	local Nusselt number for the inner sphere, $- \left(\dfrac{\beta-1}{\beta} \right) \times \dfrac{\partial\Theta}{\partial R} \Big\vert_{R=1}$
Nu_o	local Nusselt number for the outer sphere, $- \left(\dfrac{\beta-1}{\beta} \right) \times \dfrac{\partial\Theta}{\partial R} \Big\vert_{R=\beta} \times \beta^2$
$\dot{Q}$	reference rate of heat flux
Ra	Rayleigh number, $g\gamma\Delta T_{ref} R_i'^3 / (\nu\alpha)$
R	radial coordinate
T	temperature
T_{ref}	reference temperature, $\dfrac{\dot{Q} \times (\beta-1)}{4\pi\beta K_f R'_i}$
V	dimensionless velocity

α	thermal diffusivity
β	radius ratio, R_o' / R_i'
γ	expansivity at constant pressure
ε	ratio of viscous dissipation term to conduction term
ζ	dimensionless vorticity vector, $[\nabla \times \vec{V}]_\phi$
η	cos θ
∇^2	Laplace operator, spherical coordinates
θ	angular coordinate
Θ	dimensionless temperature
λ	ratio of viscous dissipation term to convection term
μ	dynamic viscosity
ν	kinematic viscosity
ρ	density of fluid
σ	Prandtl number, ν/α
ϕ	circumferential coordinate (longitude)
Φ_v	dissipation function
Ψ	dimensionless stream function, $\Psi'/\nu R_i'$
ω	thermal conductivity ratio, k_s/k_f

Superscripts, subscripts

'	refers to dimensional quantities
-	refers to average
f	refers to fluid
i , ~	refers to inner sphere
o	refers to outer sphere
ref	refers to reference values
s	refers to solid material

1. INTRODUCTION

The study of thermally induced fluid motion in enclosed spaces has been receiving increasing attention over recent years. The reason for this seems to be that such flows play a role in a wide area of technological application, ranging from convection in the annular space between a nuclear reactor core and its pressure vessel to advection in lakes and to thermal insulation of doubly-glazed windows. Furthermore, the mathematical description of such a problem leads to a set of non-linear coupled partial differential equations which is of interest in itself.

Batchelor [1], originally motivated by the problem of thermal insulation of buildings (particularly doubly-glazed windows) investigated analytically the flow régimes in a rectangular cavity. The model he considered had two vertical walls of a cavity at different temperatures, with a narrow air-space between them. The cavity is closed at the top and bottom and infinite in the third direction (the breadth). Fluid motion is generated by buoyancy and it is assumed to be essentially two-dimensional. Batchelor estimated the heat flux for various flow régimes in the cavity. He also postulated that at a sufficiently high value of the Rayleigh number the flow would consist of a core of constant vorticity and temperature surrounded by a continuous boundary layer.

Poots [2], using a doubly orthogonal expansion for the stream function and the temperature, computed Batchelor's model for several values of Rayleigh number and to some extent verified the conclusions previously arrived at.

Subsequent investigators are Wilkes and Churchill [3], Elder [4] and de Vahl Davis [5]. They all employed various finite difference schemes to obtain numerical results. In both [3] and [4] instability of the numerical scheme was a problem. Wilkes' difficulties arose apparently from the retention of the vorticity as an explicit unknown in the boundary conditions. Elder, in order to achieve numerical stability of his scheme, had to approximate by setting the normal gradient of the vorticity at the horizontal boundaries to zero. The justification for this assumption is not immediately obvious. On the other hand de Vahl Davis, in an approach similar to that of Wilkes, overcame the instability problem by calculating the vorticity from the stream function at the boundary. At sufficiently large values of the Rayleigh number, he found [5] that there was indeed a core of approximately constant vorticity, but not one of constant temperature too as previously postulated by Batchelor.

The papers reviewed above do not consider the presence of a solid core inside the enclosed space. Recently Mack et al. [6,7,8,9,10] investigated the cases of steady laminar natural convection of fluid in a gap between concentric cylinders and concentric spheres, both experimentally and

analytically. The cylinders or spheres are kept at constant temperature with the inner cylinder or sphere being the hotter. Flow visualization for both configurations and heat transfer data for the two concentric spheres were obtained. The authors reported that the flow régime in the gap between the two concentric spheres depended upon the diameter ratio of the spheres. Similar results were found for the case of concentric cylinders. Three types of flow-régimes were observed; (a) a 'kidney-shaped eddy' type (b) a 'crescent-eddy' type (c) 'falling vortices'; these correspond respectively to diameter ratios of 3.14, 1.72, and 1.19. Mack and Bishop [9], Mack and Hardee [10] obtained analytical solutions in the form of series expansions in powers of the Rayleigh number for concentric cylinders and spheres. In their expansions the coefficients of higher-order terms also depend upon the Prandtl number. A proof of convergence of their perturbation expansions was not given. Their analytical solutions for concentric spheres seem to yield convergent results up to a maximum value of the Rayleigh number of 1600 (based on gap width), while in their experimental studies the range of Rayleigh numbers used is rather higher than 1600. Thus direct comparison between experimental and analytical results is perhaps not meaningful.

It is customary in heat transfer work to specify idealized boundary conditions for both the temperature and flow velocity in order to arrive at a well-set problem. That is the boundary conditions are usually constant

temperature, constant flux or a combination of these. However, in actual practice the boundary conditions at the conducting enclosing surfaces are rarely known beforehand. They depend upon the coupled mechanisms of conduction in the solid boundary and convection of the fluid over the boundary. In technologically interesting geometries the heat transfer ('film') coefficient at the surface is virtually never uniform. This variation leads to a redistribution of heat flux in the solid, in some balance with the convective motion which takes place in the fluid. The effect of the coupled conduction/convection mechanism is most pronounced in free convective heat transfer: not only are the momentum and energy fields of the fluid coupled but in addition the energy fields of the fluid and the solid are coupled as well. Due to that complication problems of this type have only received scant attention. The following is a review of published work.

Perelman [11] considered two examples of two dimensional flow around a body with line and plane heat sources and used the term 'conjugate' for this type of problem. In his analysis the velocity profiles were assumed to be either linear or of the slip-flow type, uninfluenced by convection. In view of this assumption, the momentum field in the fluid is uncoupled from the energy field. Hence the solution to the momentum equation is known separately of the convection of heat. Some time later Rotem [12] developed an approximate method for the evaluation of interface temperature profiles

and the transfer coefficient for heat transfer to a forced laminar boundary layer with wall conduction. Again the method applies to the case of uncoupled equations only.

Kelleher and Yang [13] employed a Goertler series for the conjugate problem for the free convection of fluid over a two-dimensional conducting body with internal heat sources. Here the velocity can indeed not be specified in advance: it is coupled to the temperature distribution on the surface of the solid, which in turn depends upon both the heat source distribution and convection. The region of interest of their analysis was placed near the leading edge.

Lock and Gunn [14] considered the laminar free convection from a downward projecting fin, but solved the convection and conduction parts of the problem separately. The solution was completed by matching the interfacial temperature and heat flux.

The study of a conjugate heat transfer problem in a *confined* space is apparently not available in the literature.* Also, previous investigators of conjugate heat transfer problems, both in external and in internal flows [15], have considered the conjugate effects in one or two dimensions only. The present study considers steady conjugate laminar three-dimensional natural convection (with rotational symmetry) in

---

*An exception to this is the recent analysis of Rotem [16] of the conjugate convection for the case of horizontal concentric cylinders.

a fluid between two concentric spheres. The solutions to the quasi-linear coupled governing equations of energy and vorticity transport are obtained in the form of an asymptotic expansion of the variables stream function and temperature in terms of ascending powers of the Grashof number. The other parameters which are of importance in this problem are the Prandtl number, the radius ratio, and the thermal conductivity ratio. The range of each parameter over which the expansion scheme is valid is evaluated in detail. The cases of a constant flux or an isothermal inner sphere with an isothermal outer envelope are also considered in the present work: these are limiting cases of the conjugate problem.

An experiment was designed for the visualization of the flow pattern in the gap between two conjugate concentric spheres. The experimental results provide further insight into the nature of the convective flow and supplement the analytical results.

An application which this analysis would model is geophysical circulations. For *global* geophysical circulations the vector acceleration of gravity is everywhere normal to the boundary and convection occurs only when a certain Rayleigh number exceeds a critical value. However, insight to the local convection régime may be gained by considering the gravitational field to be oriented everywhere parallel to the vertical axis as shown in Figure 2.1.1, in this thesis. For in some geophysical models, smaller regions of closed circu-

lation are shown to exist [7], in which the conditions would not be dissimilar to those considered here.

Another application is to the design of a spherical insulating flask to minimize the heat loss: for large spherical containers it is often not feasible to have a vacuum between the concentric shells, as this would introduce buckling problems and bending stress, instead of membrane stresses, particularly near the supports. Thus a spherical gap filled with gas is retained between the spherical envelope and a configuration is obtained for which the present analysis is applicable.

2. ANALYSIS

2.1 Formulation of Conjugate Problem

The analysis considers steady conjugate laminar three-dimensional natural convection in a fluid contained between two concentric spheres. The physical configuration is that shown in Figure 2.1.1. A solid inner sphere is heated either by a constant source at its centre or by distributed sources. It is cooled by laminar natural convection of the fluid inside the gap between the concentric spheres. The outer sphere is kept at a constant temperature. Thus heat transfer at the interface between the solid inner sphere and the fluid depends upon the coupled mechanisms of conduction inside the inner sphere and convection in the fluid. By definition the transfer of heat is therefore of the *conjugate* type. Some previous investigators [10] have considered the natural convective problem for the spherical configuration *without* the additional complication of conductive effects along the boundaries and this work will be discussed later. The temperature and heat flux distributions on the surface of the inner sphere are of great importance in the numerous applications for which the problem treated here is a model.

The objectives of the present investigation are as follows: (i) determination of the temperature and heat flux

variations on the inner sphere; (ii) of the heat flux variation on the surface of the outer sphere; (iii) and lastly of the temperature, velocity and vorticity distributions of the fluid in the gap between the concentric spheres.

It will be shown that the parameters of importance in the analysis are (a) G , the Grashof number; (b) σ, the Prandtl number of the fluid; (c) ω, the ratio of the thermal conductivity of the solid inner sphere to that of the fluid; (d) β, the ratio of the radius of the outer sphere to that of the inner sphere. Spherical coordinates are used, the angular coordinate θ being measured clockwise from the apex as shown in Figure 2.1.1. All physical properties are assumed constant, except the density of the fluid in as far as its dependence on the temperature is concerned. This assumption and its implications were first introduced by Boussinesq. It is assumed that the compression work and viscous dissipation are also negligible. Hence the corresponding terms will be deleted from the energy equation. The latter assumption is checked in Appendix I of this thesis. An axisymmetrical convective flow pattern is assumed i.e. there is no azimuthal swirl. Hence all quantities are taken to be independent of the longitude, ϕ .

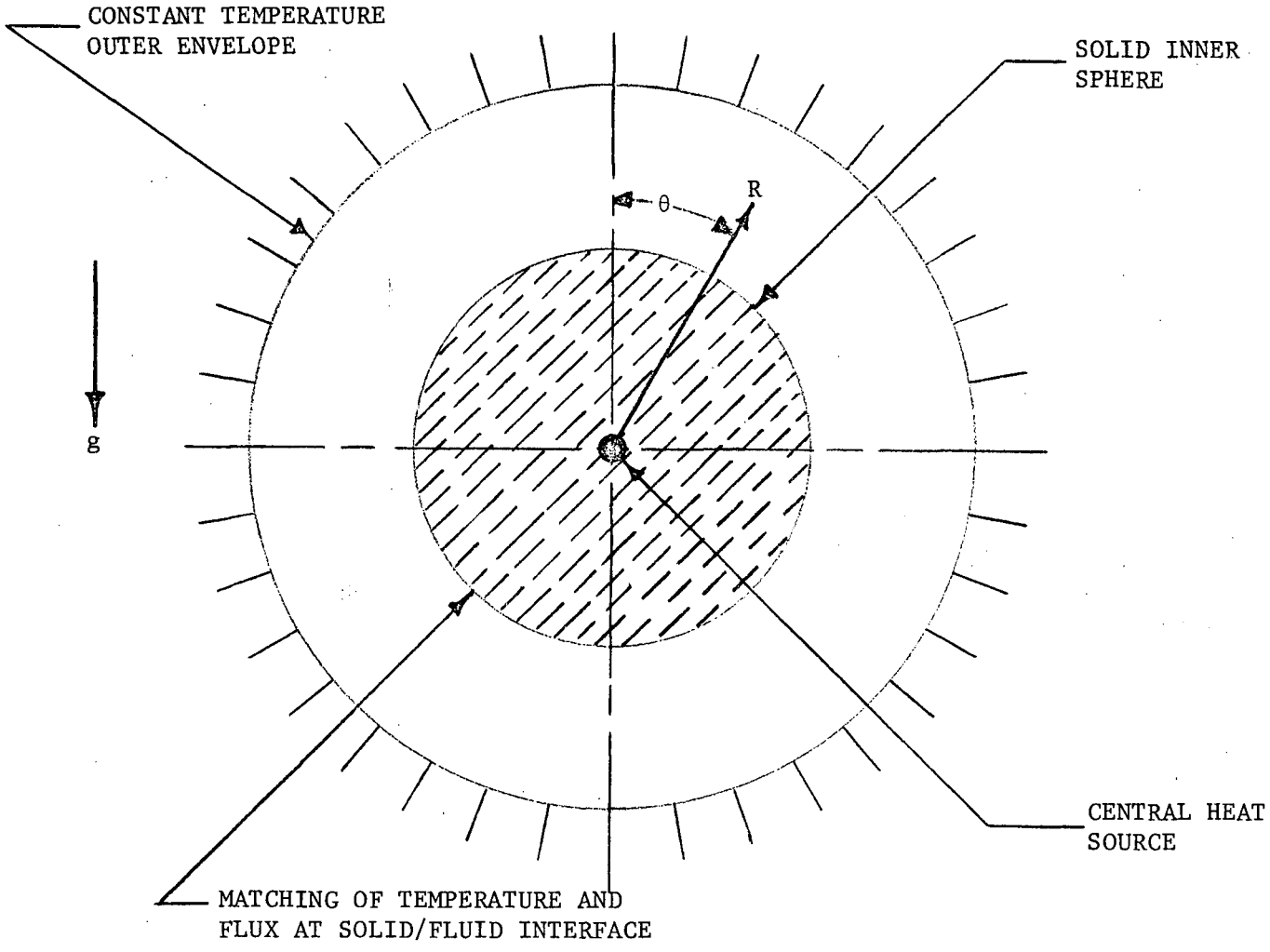

Figure 2.1.1 Physical Configuration

2.2 Governing Equations

All dimensional quantities used (except for property values) are primed in what follows and all dimensionless quantities are unprimed. Let R_i' be the radius of the inner sphere. $R = R'/R_i'$ and $\beta = R_o'/R_i'$ are the dimensionless

radial coordinate and dimensionless radius of the outer sphere respectively. $\tilde{T}$ and T are the temperatures of the inner and outer spheres respectively; g, the acceleration of gravity; γ, the volumetric coefficient of thermal expansion at constant pressure; ν, the kinematic viscosity; and α, the thermal diffusivity.

A reference temperature and temperature difference are introduced: $T_{ref} = \Delta T_{ref}$ and

$$\Delta T_{ref} = \dot{Q} \times (\beta-1)/(4\pi\beta R_i' K_f)$$

where $\dot{Q}$ is rate of heat flux, assumed constant.

Let

$$Ra = g\gamma\Delta T_{ref} R_i'^3/\nu\alpha$$

denote the Rayleigh number;

$$\sigma = \nu/\alpha$$

the Prandtl number;

$$G = g\gamma\Delta T_{ref} R_i'^3/\nu^2$$

the Grashof number;

$$\Theta = (T-T_{ref})/\Delta T_{ref}$$

the dimensionless fluid temperature;

$$\tilde{\Theta} = (\tilde{T}-T_{ref})/\Delta T_{ref}$$

the dimensionless inner sphere temperature.

The equations of continuity, motion and energy for a Newtonian, incompressible constant property fluid will not be stated here; they may be found in many textbooks. Stokes stream function Ψ will be introduced, so that the equation of continuity is fulfilled identically. Then in the dimensionless quantities introduced above the steady state governing equations reduce to the following,

$$E^4\Psi = \frac{1}{R^2}\frac{\partial(\Psi,E^2\Psi)}{\partial(R,\eta)} + \frac{2E^2\Psi}{R^2}\left(\frac{\eta}{(1-\eta^2)}\frac{\partial\Psi}{\partial R} + \frac{1}{R}\frac{\partial\Psi}{\partial\eta}\right)$$

$$+ (1-\eta^2)\, G\, \frac{\partial(R\times\eta,\Theta)}{\partial(R,\eta)} \qquad (2.2.1)$$

$$\nabla^2\Theta = \frac{\sigma}{R^2}\frac{\partial(\Psi,\Theta)}{\partial(R,\eta)} \qquad (2.2.2)$$

$$\nabla^2\tilde{\Theta} = A(R,\theta,\phi) \quad . \qquad (2.2.3)$$

The boundary conditions subject to which (2.2.1) to (2.2.3) have to be solved will be

$$\Psi = \frac{\partial \Psi}{\partial R} = 0 \qquad \text{at} \quad R = 1, \ \beta \qquad (2.2.4)$$

$$\Psi = \frac{\partial \Psi}{\partial \theta} = 0 \qquad \text{at} \quad \theta = 0, \ \pi \qquad (2.2.5)$$

or, alternatively stated

$$\Psi = -(1-\eta^2)^{\frac{1}{2}} \frac{\partial \Psi}{\partial \eta} = 0 \qquad \text{at} \quad \eta = \pm 1 \qquad (2.2.5a)$$

$$\tilde{\Theta} = \Theta \qquad \text{at} \quad R = 1 \qquad (2.2.6)$$

$$\omega \frac{\partial \tilde{\Theta}}{\partial R} = \frac{\partial \Theta}{\partial R} \qquad \text{at} \quad R = 1 \qquad (2.2.7)$$

$$\Theta = -1 \qquad \text{at} \quad R = \beta \ . \qquad (2.2.8)$$

Here $\eta = \cos \theta$ and the operators E^2, E^4 and ∇^2 are defined as follows:-

$$E^2 = \frac{\partial^2}{\partial R^2} + (1-\eta^2) \frac{\partial^2}{\partial \eta^2}$$

$$E^4 = E^2 [E^2]$$

$$= \frac{\partial^4}{\partial R^4} - \frac{4(1-\eta^2)}{R^3} \left(\frac{\eta}{R} \frac{\partial^3}{\partial \eta^3} + \frac{\partial^3}{\partial R \partial \eta^2}\right) + \frac{4(1-\eta^2)}{R^4} \frac{\partial^2}{\partial \eta^2}$$

$$+ \frac{2(1-\eta^2)}{R^2} \frac{\partial^4}{\partial R^2 \ \partial \eta^2} + \frac{(1-\eta^2)}{R^4} \frac{\partial^4}{\partial R^4}$$

$$\nabla^2 = \frac{\partial^2}{\partial R^2} + \frac{2}{R}\frac{\partial}{\partial R} + \frac{(1-\eta^2)}{R^2}\frac{\partial^2}{\partial \eta^2} - \frac{2\eta}{R^2}\frac{\partial}{\partial \eta}$$

$$= E^4 + 2\left(\frac{\partial}{\partial \eta}(\eta/R)\frac{\partial}{\partial R} + \frac{\partial}{\partial R}(\eta/R)\frac{\partial}{\partial \eta}\right) .$$

The left-hand side of the equation (2.2.1) represents the diffusion of vorticity. The first two terms on the right-hand side of the equation (2.2.1) give the convection of vorticity while the third term represents the buoyancy effect.

The left-hand side of the equation (2.2.2) represents the conduction effects, the right-hand side the convective effects. The effects of viscous dissipation and compression work were neglected in the energy equation (2.2.2). In Appendix I it will be shown that for closed spaces this is always a permissible assumption.

Lastly, equation (2.2.3) is the conduction equation for the solid inner sphere. $A(R,\theta,\phi)$ is the source function: For the case of a single heat source at the centre of the inner sphere, the source function may be set to zero everywhere except at the center pole.*

The boundary conditions (2.2.4) state that there will be no flow along and through the surfaces of the two spheres. Conditions (2.2.5) ensure that the flow is axisymmetrical

---

*The case of the inner sphere containing uniformly distributed heat sources is considered in Appendix II.

about the vertical axis $\theta = 0, \pi$ (i.e. at $\eta = \pm 1$). Boundary conditions (2.2.6) and (2.2.7) state the energy conservation principle, i.e. the equality of temperature and flux on both sides of the interface solid/fluid. The fact that both temperature and flux are specified will be seen to lead to a problem of the conjugate type. (2.2.8) is a normalization condition for the temperature.

2.3 Method of Solution

In the present analysis it is assumed that the inner sphere has a central heat source only i.e. $A(R,\theta,\phi)$ is zero in equation (2.2.3). In spherical geometry the fluid cannot be in equilibrium when there is a non-zero temperature difference between the inner sphere and the bulk of the fluid, no matter how small that difference may be as the vector acceleration of gravity is everywhere inclined to the solid to fluid interface. This is due to the tangential component of the buoyancy forces in the fluid. Initially the fluid may be at rest, but buoyancy forces will cause convective motion which after some time will become quasi-steady. The governing time-independent equations will then apply to this steady motion. It should be noted that the convective flow is the only source of vorticity available. As mentioned above, the energy equations (2.2.2) and (2.2.3) for the fluid and the solid inner sphere respectively are coupled through the boundary conditions (2.2.6) and (2.2.7). On the other hand

the vorticity transport equation and the energy equation for the fluid are also coupled through the buoyancy term in (2.2.1). As the motion of the fluid is set-up by buoyancy forces only, it will be natural to seek solutions to equations (2.2.1), (2.2.2) and (2.2.3) for the dependent variables Ψ, Θ, $\tilde{\Theta}$ in terms of perturbation expansions in the Grashof number. This is an *ad hoc* assumption in the sense that any suitable parameter characterizing the ratio of buoyancy to viscous forces might have been used with suitable scaling of the variables, e.g. Ra. That is, an expansion of the present type is not necessarily unique [18]. Moreover, the problem dealt with here is a multi-parameter one involving some other parameters, σ, β and ω.

The perturbation solutions are obtained for a range of Grashof numbers. For each value of G, combinations of various values of the other parameters σ, ω and β are considered. There is a limitation on the range of radius ratio admissible: obviously $\beta>1$; as β tends to infinity the inner sphere becomes a single sphere in an unbounded expanse of fluid. To this latter case the regular perturbation theory to be outlined will not apply [19,20].

On the other hand, if ω tends to zero or infinity the inner sphere has either a constant flux or an isothermal envelope respectively. The former of these cases leads to singularity and must be solved separately. The case of heat transfer between two concentric *isothermal* spheres has

been solved analytically by Mack and Hardee [10]. In section 2.5 the case of the constant flux inner sphere surface with an isothermal outer envelope (the solution for which had not been available) will be considered.

The influence of σ is as follows: small values present no particular difficulties. However, as $\sigma \to \infty$ the energy equation tends to become singular and not all boundary conditions for the temperature profile may be fulfilled. Therefore a different parameter perturbation starting with Ψ'/α rather than ψ'/ν as the dimensionless stream function, has to be used.

It is proposed here to solve equations (2.2.1), (2.2.2) and (2.2.3) for conjugate natural-convective heat transfer between concentric spheres with neither of the parameters G, σ, β and ω infinitely small or very large. The regular perturbation expansions for the variables Ψ,Θ and $\tilde{\Theta}$ are assumed to be

$$\Psi = \sum_{j=0}^{\infty} \sum_{k=0}^{\infty} G^j \sigma^k \Psi_j^k \quad (R, \eta) \quad , \tag{2.3.1}$$

$$\Theta = \sum_{l=0}^{\infty} \sum_{m=0}^{\infty} G^l \sigma^m \Theta_l^m \quad (R, \eta) \quad , \tag{2.3.2}$$

$$\tilde{\Theta} = \sum_{l=0}^{\infty} \sum_{m=0}^{\infty} G^l \sigma^m \tilde{\Theta}_l^m \quad (R, \eta) \quad . \tag{2.3.3}$$

It may be shown that for the case considered here, terms transcendental in the expansion parameter G do not occur: they invariably give rise to homogeneous equations with homogeneous boundary conditions which will yield only a trivial solution. Thus such terms would at most be associated with complex eigenmotions which are not considered here any further.

Substituting equations (2.3.1), (2.3.2) and (2.3.3) into the governing equations the following expansions for Ψ, Θ and $\tilde{\Theta}$ are obtained.

$$\Psi = G\,\Psi_1^{\circ}(R,\eta) + G^2\Psi_2^{\circ}(R,\eta) + G^2\sigma\Psi_2^{1}(R,\eta) + \ldots\ldots\,, \tag{2.3.4}$$

$$\Theta = \Theta_{\circ}^{\circ}(R) + G\sigma\Theta_1^{1}(R,\eta) + G^2\sigma\Theta_2^{1}(R,\eta) + G^2\sigma^2\Theta_2^{2}(R,\eta) \ldots\ldots\,, \tag{2.3.5}$$

$$\tilde{\Theta} = \tilde{\Theta}_{\circ}^{\circ}(R) + G\sigma\tilde{\Theta}_1^{1}(R,\eta) + G^2\sigma\tilde{\Theta}_2^{1}(R,\eta) + G^2\sigma^2\tilde{\Theta}_2^{2}(R,\eta) \ldots\ldots\,. \tag{2.3.6}$$

Equating coefficients of equal powers of $G^j\sigma^k$, the governing equations reduce to an infinite set of uncoupled linear differential equations,

$$\nabla^2 \tilde{\theta}_o^{\circ} = 0 \qquad (2.3.7)$$

$$\nabla^2 \theta_o^{\circ} = 0 \qquad (2.3.8)$$

$$E^4 \psi_1^{\circ} = (1-\eta^2) \frac{\partial (Rx\eta, \theta_o^{\circ})}{\partial (R,\eta)} \qquad (2.3.9)$$

$$\nabla^2 \tilde{\theta}_1^{1} = 0 \qquad (2.3.10)$$

$$\nabla^2 \theta_1^{1} = \frac{1}{R^2} \frac{\partial (\psi_1^{\circ}, \theta_o^{\circ})}{\partial (R,\eta)} \qquad (2.3.11)$$

$$E^4 \psi_2^{\circ} = \frac{1}{R^2} \left(\frac{\partial \psi_1^{\circ}}{\partial R} \frac{\partial}{\partial \eta} - \frac{\partial \psi_1^{\circ}}{\partial \eta} \frac{\partial}{\partial R}\right) E^4 \psi_1^{\circ} + \frac{2E\psi_1^{\circ}}{R^2} \left(\frac{\eta}{1-\eta^2} \frac{\partial}{\partial \eta} + \frac{1}{R} \frac{\partial}{\partial \eta}\right) \psi_1^{\circ} \qquad (2.3.12)$$

$$E^4 \psi_2^{1} = (1-\eta^2) \left(\eta \frac{\partial}{\partial \eta} - R \frac{\partial}{\partial R}\right) \theta_1^{1} \qquad (2.3.13)$$

$$\nabla^2 \tilde{\theta}_2^{1} = 0 \qquad (2.3.14)$$

$$\nabla^2 \theta_2^{1} = \frac{1}{R^2} \frac{\partial (\psi_2^{\circ}, \theta_o^{\circ})}{\partial (R,\eta)} \qquad (2.3.15)$$

$$\nabla^2 \tilde{\theta}_2^{2} = 0 \qquad (2.3.16)$$

$$\nabla^2 \theta_2^{2} = \frac{1}{R^2} \frac{\partial (\psi_1^{\circ}, \theta_1^{1})}{\partial (R,\eta)} + \frac{1}{R^2} \frac{\partial (\psi_2^{1}, \theta_o^{\circ})}{\partial (R,\eta)} \qquad (2.3.17)$$

.....

The above set of equations is solved in sequence subject to the following boundary conditions:

$$\tilde{\Theta}^{\circ}_{\circ} = \Theta^{\circ}_{\circ} = 0 \qquad \text{at } R = 1 \qquad (2.3.18)$$

$$\Theta^{\circ}_{\circ} = -1 \qquad \text{at } R = \beta \qquad (2.3.19)$$

$\tilde{\Theta}^{m}_{1}$ must not have a singularity at the centre of the inner sphere greater than the zeroeth term, namely $1/R$, for $l, m \geq 1$ (2.3.20)

$$\tilde{\Theta}^{m}_{l} = \Theta^{m}_{l} \qquad \text{at } R = 1; \quad l, m \geq 1 \qquad (2.3.21)$$

$$\Theta^{m}_{l} = 0 \qquad \text{at } R = \beta; \quad l, m \geq 1 \qquad (2.3.22)$$

$$\omega \frac{\partial \tilde{\Theta}^{m}_{l}}{\partial R} = \frac{\partial \Theta^{m}_{l}}{\partial R} \qquad \text{at } R = 1; \quad l, m \geq 1 \qquad (2.3.23)$$

$$\Psi^{k}_{j} = \frac{\partial \Psi^{k}_{j}}{\partial R} = 0 \qquad \text{at } R = 1, \beta; \quad j, k \geq 1 \qquad (2.3.24)$$

$$\Psi^{k}_{j} = -(1-\eta^{2})\frac{1}{2}\frac{\partial \Psi^{k}_{j}}{\partial \eta} = 0 \qquad \text{at } \eta = \pm 1; \quad j, k \geq 1 \qquad (2.3.25)$$

2.4 Solution

The equations (2.3.7) and (2.3.8) are solved first. They are the conduction equations for the fluid assumed immobile, and for the solid inner sphere. The solutions are the temperature distribution for pure conduction subject to boundary conditions (2.3.18) and (2.3.19).

$$\tilde{\Theta}_o^o = \frac{1}{\omega}\left(\frac{1}{R} - 1\right) \times \left(\frac{\beta}{\beta-1}\right) \qquad (2.4.1)$$

$$\Theta_o^o = \left(\frac{1}{R} - 1\right) \times \left(\frac{\beta}{\beta-1}\right) \qquad (2.4.2)$$

Upon substitution of (2.4.2) into (2.3.9),

$$E^4\Psi_1^o = (1-\eta^2)/R \times \left(\frac{\beta}{\beta-1}\right) , \qquad (2.4.3)$$

This is a 'creeping flow' equation. A solution is stream function,

$$\Psi_1^o = (1-\eta^2)\left(\frac{A_1}{R} + B_1R + C_1R^2 - \frac{R^3}{8} + D_1R^4\right)X\left(\frac{\beta}{\beta-1}\right) \qquad (2.4.4)$$

which has to satisfy the boundary conditions (2.3.25). The constants of integration A_1, B_1, C_1 and D_1 are determined by applying conditions (2.3.24) and are given here in closed form,

$$A_1 = (\beta^9 - 4\beta^8 + 6\beta^7 - 4\beta^6 + \beta^5)/8\Delta$$

$$B_1 = (-3\beta^9 + 8\beta^8 - 5\beta^7 - 5\beta^5 + 8\beta^4 - 3\beta^3)/8\Delta$$

$$C_1 = (2\beta^9 - 12\beta^7 + 10\beta^6 + 10\beta^5 - 12\beta^4 + 2\beta^2)/8\Delta$$

$$D_1 = (2\beta^7 - 6\beta^6 + 4\beta^5 + 4\beta^4 - 6\beta^3 + 2\beta^2)/8\Delta$$

where

$$\Delta = 4\beta^8 - 9\beta^7 + 10\beta^5 - 9\beta^3 + 4\beta^2 \quad ,$$

The next two equations (2.3.10), (2.3.11) are solved simultaneously after substituting (2.4.2) and (2.4.4) into (2.3.11). They are

$$\nabla^2 \tilde{\Theta}_1^1 = 0 \qquad (2.4.5)$$

$$\nabla^2 \Theta_1^1 = -2\eta \left(\frac{A_1}{R^5} + \frac{B_1}{R^3} + \frac{C_1}{R^2} - \frac{1}{8R} + D_1\right) x \left(\frac{\beta}{\beta-1}\right)^2 , \qquad (2.4.6)$$

the solutions of which are

$$\tilde{\Theta}_1^1 = \eta \left(\tilde{E}_1 R + \frac{\tilde{F}_1}{R^2}\right) x \left(\frac{\beta}{\beta-1}\right)^2 , \qquad (2.4.7)$$

and

$$\Theta_1^1 = \eta \left(-\frac{A_1}{2R^3} + \frac{F_1}{R^2} + \frac{B_1}{R} + C_1 + E_1 R - \frac{D_1 R^2}{2} + \frac{R}{12} \ln R\right) x \left(\frac{\beta}{\beta-1}\right)^2 . \qquad (2.4.8)$$

The boundary conditions (2.3.20) to (2.3.23) are used to determine the constants of integration; $\tilde{E}_1$, E_1, $\tilde{F}_1$ and F_1. They are no longer given explicitly here but were calculated directly from the boundary conditions by computer.

The next equation to be solved is obtained by substituting (2.4.4) into (2.3.12),

$$E^4\psi_2^\circ = \eta(1-\eta^2)\left(\frac{12A_1B_1}{R^5} + \frac{(12B_1^2 + A_1)}{R^3} + \frac{12B_1C_1}{R^2} - \frac{B_1}{2R} + 12B_1D_1 + C_1 - \frac{R}{8} + D_1R^2\right)x\left(\frac{\beta}{\beta-1}\right)^2 . \qquad (2.4.9)$$

The solution for Ψ_2° is

$$\Psi_2^\circ = \eta(1-\eta^2)\left(\frac{J_2^a}{R^2} - \frac{A_1B_1}{2R} + I_2^a + \frac{1}{24}(12B_1^2 + A_1)R + \frac{B_1C_1}{2}R^2 + H_2^a R^3 - \frac{1}{24}(12B_1D_1 + C_1)R^4 + G_2^a R^5 + \frac{D_1R^6}{144} + \frac{B_1}{60}R^3 \ln R - \frac{R^5}{560}\ln R\right) x \left(\frac{\beta}{\beta-1}\right)^2 , \qquad (2.4.10)$$

which satisfies boundary conditions (2.3.25). The constants of integrations G_2^a, H_2^a, I_2^a and J_2^a are determined by applying conditions (2.3.24).

The next higher-order term in the expansion of Ψ can now be determined upon substituting equation (2.4.8) into

(2.3.13):

$$E^4\Psi_2^1 = \eta(1-\eta^2)\left(-\frac{2A_1}{R^3} + \frac{3F_1}{R^3} + \frac{2B_1}{R} + C_1 + \frac{D_1R^2}{2} - \frac{R}{12}\right)x\left(\frac{\beta}{\beta-1}\right)^2 . \tag{2.4.11}$$

The solution is,

$$\Psi_2^1 = \eta(1-\eta^2)\left(\frac{J_2^b}{R^2} + I_2^b - \frac{A_1}{12}R + \frac{F_1R^2}{8} + H_2^b R^3 - \frac{C_1R^4}{24} + G_2^b R^5 + \frac{D_1R^6}{288} - \frac{B_1R^3}{15}\ln R - \frac{R^5}{840}\ln R\right) x \left(\frac{\beta}{\beta-1}\right)^2 , \tag{2.4.12}$$

which satisfies boundary conditions (2.3.25). The constants of integration G_2^b, H_2^b, I_2^b and J_2^b are determined by applying conditions (2.3.24).

It is now possible to determine the higher-order temperature terms. The next two equations (2.3.14) and (2.3.15) are solved simultaneously upon substituting (2.4.2) and (2.4.10) into (2.3.15). The equations are

$$\nabla^2\tilde{\Theta}_2^1 = 0 \tag{2.4.13}$$

$$\nabla^2\Theta_2^1 = (3\eta^2-1)\left(-\frac{D_1R^2}{144} - G_2^a R + \frac{(12B_1D_1 + C_1)}{24} - \frac{H_2^a}{R} - \frac{B_1C_1}{2R^2} - \frac{(12B_1^2 + A_1)}{24R^3} - \frac{I_2^a}{R^4} + \frac{A_1B_1}{2R^5} - \frac{J_2^a}{R^6}\right)$$

$$+ \frac{R}{560} \ln R - \frac{B_1}{60R} \ln R) x (\frac{\beta}{\beta-1})^3 \quad . \qquad (2.4.14)$$

The solutions are

$$\tilde{\Theta}_2^1 = (3\eta^2 - 1)(\tilde{K}_2^a R^2 + \frac{\tilde{L}_2^a}{R^3}) x (\frac{\beta}{\beta-1})^3 \quad , \qquad (2.4.15)$$

and

$$\begin{aligned} \Theta_2^1 = (3\eta^2 - 1) \Bigg\{ & K_2^a R^2 + \frac{L_2^a}{R^3} - \frac{D_1 R^4}{2016} - (\frac{G_2^a}{6} + \frac{1}{2880}) R^3 \\ & + (\frac{H_2^a}{4} + \frac{B_1}{320}) R + \frac{B_1 C_1}{12} + \frac{(12B_1^2 + A_1)}{144R} + \frac{I_2^a}{4R^2} \\ & - \frac{J_2^a}{6R^4} + \frac{B_1}{240} R \ln R + \frac{(12B_1 D_1 + C_1)}{120} R^2 \ln R \\ & + \frac{R^3}{3360} \ln R - \frac{A_1 B_1}{10R^3} \ln R \Bigg\} \times (\frac{\beta}{\beta-1})^3 \quad . \qquad (2.4.16) \end{aligned}$$

The constants of integration are $\tilde{K}_2^a$, K_2^a, $\tilde{L}_2^a$ and L_2^a. In view of the higher-order singularity which $\tilde{L}_2^a$ would give rise to at the centre of the inner sphere, $\tilde{L}_2^a$ will be set to zero following condition (2.3.20). The remaining unknown constants are determined using boundary conditions (2.3.21) to (2.3.23).

The last terms of the temperature expansions calculated are $\tilde{\Theta}_2^2$ and Θ_2^2. The equations are (2.3.16) and (2.3.17).

$$\nabla^2 \tilde{\Theta}_2^2 = 0 \,,$$

and (2.4.17)

$$\nabla^2 \Theta_2^2 = (3\eta^2 - 1) \left\{ -\frac{A_1^2}{2R^7} - \frac{(J_2^a - A_1 F_1)}{R^6} + \frac{3A_1 B_1}{2R^5} \right.$$

$$- \frac{(I_2^b + B_1 F_1 - 2A_1 C_1)}{R^4} - \left(\frac{5A_1}{48} - A_1 E_1 + B_1^2 + 2C_1 F_1\right)\frac{1}{R^3}$$

$$- \left(3B_1 C_1 - \frac{3A_1 D_1}{2} - \frac{F_1}{4}\right)\frac{1}{R^2} - \left(H_2^b - \frac{3B_1}{8} + B_1 E_1 + 2C_1^2 + 4D_1 F_1\right)\frac{1}{R}$$

$$- \left(\frac{7B_1 D_1}{2} - \frac{5C_1}{12}\right) - \left(G_2^b + 3C_1 D_1 - \frac{3E_1}{8}\right) R$$

$$- \left(\frac{55}{288} D_1 + 4D_1 E_1\right) R^2 - \frac{B_1}{60R} \ln R + \frac{A_1}{12R^3} \ln R$$

$$\left. + \frac{109}{3360} R \ln R - \frac{D_1}{3} R^2 \ln R \right\} \times \left(\frac{\beta}{\beta - 1}\right)^3$$

$$+ \eta^2 \left\{ \frac{4A_1^2}{R^7} - \frac{6A_1 F_1}{R^6} - \frac{2A_1 B_1}{R^5} - \frac{(2B_1 F_1 + A_1 C_1)}{R^4} \right.$$

$$+ \frac{A_1}{6R^3} + \left(4B_1 C_1 - 2A_1 D_1 - \frac{F_1}{4}\right)\frac{1}{R^2} + \left(4B_1 E_1 - \frac{B_1}{3} + 4C_1^2 + 4D_1 F_1\right)\frac{1}{R}$$

$$+ \left(3B_1 D_1 - \frac{7C_1}{12}\right) + \left(4C_1 D_1 - E_1 - \frac{1}{48}\right) R + \left(\frac{19}{24} D_1 + 10 D_1 E_1\right) R^2$$

$$+ \frac{B_1}{3R} \ln R - \frac{R}{12} \ln R + \left(\frac{5D_1}{6}\right) R^2 \ln R \Bigg\} \times \left(\frac{\beta}{\beta-1}\right)^3$$

$$+ \left\{ 2C_1E_1 - 2D_1^2 R^3 + \frac{C_1}{6} \ln R \right\} \times \left(\frac{\beta}{\beta-1}\right)^3 . \qquad (2.4.18)$$

The solutions are

$$\tilde{\theta}_2^2 = (3\eta^2 - 1) \left\{ \tilde{M}_2^b R^2 + \frac{\tilde{N}_2^b}{R^3} \right\} \times \left(\frac{\beta}{\beta-1}\right)^3 + \left(\tilde{P}_2^b + \frac{\tilde{Q}_2^b}{R}\right) \times \left(\frac{\beta}{\beta-1}\right)^3 ,$$

and

$$\theta_2^2 = (3\eta^2 - 1) \Bigg\{ M_2^b R^2 + \frac{N_2^b}{R^3} + \frac{5A_1^2}{84R^5} - \left(\frac{J_2^b + A_1F_1}{6}\right) \frac{1}{R^4}$$

$$+ \frac{(3I_2^b + 5B_1F_1 - 5A_1C_1)}{12R^2} + \left(\frac{A_1}{16} - A_1E_1 + B_1^2 + 2C_1F_1\right)\frac{1}{6R}$$

$$+ \frac{(10B_1C_1 - 5A_1D_1 - F_1)}{36} + \frac{R}{12} \left(3H_2^b - \frac{241B_1}{240} - B_1E_1\right.$$

$$\left. + 2C_1^2 + 8D_1F_1\right) - \frac{R^3}{18} \left(3G_2^b + 5C_1D_1 - \frac{E_1}{8} + \frac{107}{2880}\right)$$

$$+ \frac{R^4}{21}\left(\frac{73D_1}{448} - D_1E_1\right) - \frac{A_1B_1}{6R^3}\ln R - \frac{A_1}{72R}\ln R$$

$$- \left(\frac{17B_1}{720}\right) R \ln R - \left(\frac{B_1D_1}{2} - \frac{2C_1}{45}\right) R^2 \ln R + \left(\frac{47}{60480}\right) R^3 \ln R$$

$$- \left(\frac{D_1}{252}\right) R^4 \ln R \Bigg\} \times \left(\frac{\beta}{\beta-1}\right)^3 + \Bigg\{ \frac{A_1^2}{15R^5} - \frac{A_1F_1}{6R^4} - \frac{A_1B_1}{9R^3}$$

$$- \frac{(2B_1F_1 + A_1C_1)}{6R^2} + (4B_1E_1 - \frac{5B_1}{6} + 4C_1^2 + 4D_1F_1)\frac{R}{6}$$

$$+ \frac{R^2}{6}(B_1D_1 - \frac{C_1}{3} + 2C_1E_1) + \frac{R^3}{36}(4C_1D_1 - E_1 + \frac{1}{36})$$

$$+ \frac{R^4}{6}\left(\frac{D_1}{24} + D_1E_1\right) - \frac{D_1^2R^5}{15} + (4B_1C_1 - 2A_1D_1 - \frac{F_1}{4})\frac{\ln R}{3}$$

$$+ \left(\frac{B_1}{18}\right) R \ln R + \left(\frac{C_1}{36}\right) R^2 \ln R - \frac{R^3}{432} \ln R + \left(\frac{D_1}{72}\right) R^4 \ln R$$

$$- \frac{A_1}{18R} \ln R + \left(P_2^b + \frac{Q_2^b}{R}\right) \Bigg\} \times \left(\frac{\beta}{\beta-1}\right)^3 \quad . \qquad (2.4.20)$$

$\tilde{N}_2^b$ is set to zero since a singularity of third order is not permissible at the centre of the inner sphere (2.3.20). With-

out loss of generality $\tilde{P}_2^b$ is also set to zero since from the temperature matching conditions at the interface only one of the constants, $\tilde{P}_2^b$ or P_2^b need be retained. The other remaining constants, $\tilde{M}_2^b$, M_2^b, N_2^b, P_2^b, Q_2^b and $\tilde{Q}_2^b$ are determined by the application of boundary conditions (2.3.21) to (2.3.23).

It is seen that the functions of η appearing in the expressions for $\tilde{\Theta}_1^m$ or Θ_1^m are the set of spherical harmonics, while in Ψ_j^k Gegenbauer polynomials appear.

2.5 Solution of Constant Flux Problem

In this section, the case of free convective heat transfer between two concentric spheres with a prescribed constant flux on the surface of the solid inner sphere and an isothermal outer sphere is considered. The heat flux,

$$\dot{Q} = - k_f \frac{\partial T}{\partial R'} \Big|_{R_i'} \times 4\pi R_i'^2$$

on the surface of the inner sphere is specified in advance to be constant. Thus the conjugate effect at the interface between the solid inner sphere and the fluid is lost.

The governing equations, (2.2.1) and (2.2.2) as given in section 2.2 are applicable for this constant flux case. The energy fields of the fluid and the solid inner sphere are no longer coupled. Thus the temperature equation (2.2.3) for the inner sphere is not considered here. This case is still a multi-parameter one involving parameters of G, σ and β. It has one parameter, namely ω, less than the conjugate case. However, the limitations on the ranges of σ and β outlined in section 2.3 still hold.

The non-linear coupled governing equations (2.2.1) and (2.2.2) for this constant flux case are solved by a perturbation scheme in the similar manner as for the conjugate case. The expansions for Ψ and Θ are those of (2.3.4) and (2.3.5) respectively. The simplified boundary conditions subject to which the governing equations have to be solved will be

$$-\frac{\partial \Theta_o^o}{\partial R} = 1 \qquad \text{at } R = 1 \qquad (2.5.1)$$

$$-\frac{\partial \Theta_1^m}{\partial R} = 0 \qquad \text{at } R = 1;\ \ l, m \geq 1 \qquad (2.5.2)$$

$$\Theta_o^o = -1 \qquad \text{at } R = \beta \qquad (2.5.3)$$

$$\Theta_1^m = 0 \qquad \text{at } R = \beta;\ \ l, m \geq 1 \qquad (2.5.4)$$

$$\Psi_j^k = \frac{\partial \Psi_j^k}{\partial R} = 0 \qquad \text{at } R = 1, \beta;\ \ j, k \geq 1 \qquad (2.5.5)$$

$$\Psi_j^k = -(1-\eta^2)^{\frac{1}{2}} \frac{\partial \Psi_j^k}{\partial \eta} = 0 \qquad \text{at } \eta = \pm 1;\ j, k \geq 1\ . \qquad (2.5.6)$$

The boundary condition (2.5.1) stipulates that the flux on the surface of the inner sphere remains constant i.e. unity after normalization. The constant flux condition is fulfilled by the zeroeth order term of the temperature, Θ, expansion. Therefore no higher order terms in Θ should give a contribution to the flux on the surface of the inner sphere i.e. boundary condition (2.5.2). The boundary condition (2.5.3) is a normalization condition of the temperature at the outer sphere. (2.5.4) states that the higher order terms in the Θ expansion are zero at the outer envelope. The boundary conditions (2.5.5) and (2.5.6) have the same meaning as previously.

The set of uncoupled linear differential equations given in section 2.3 (with the exception that the equations for $\tilde{\Theta}$ are not considered here) are solved subject to the boundary conditions given above. The solution for Θ_o^o is

$$\Theta_o^o = \frac{1}{R} - \frac{(\beta+1)}{\beta}$$

which fulfilled the boundary conditions (2.5.1) and (2.5.3).

The solutions for all the higher order terms in the Θ and Ψ expansions are those given in section 2.4 except the constant factors $(\frac{\beta}{\beta-1})$, $(\frac{\beta}{\beta-1})^2$ and $(\frac{\beta}{\beta-1})^3$ will not appear in the solutions. The constants of integrations in the solutions are determined directly using the boundary conditions (2.5.1) to (2.5.6) in the computer.

3. EVALUATION OF ANALYTICAL RESULTS

In the previous chapter, the analytical solutions for the conjugate heat transfer between concentric spheres has been considered. Subject to the limitations outlined before, these solutions may be assumed to be valid for various combinations of the four characteristic parameters G, σ, ω, and β . It is anticipated that there will be limiting values for each of the parameters beyond which the perturbation expansions will no longer converge. Other factors which may limit the range of applicability of the solutions are as follows: the steady laminar axisymmetrical flow assumed in section 2.1 may become unstable leading to a flow of more complicated nature and to turbulence.

The criterion used here in determining approximately the radius of convergence of the perturbation expansions is outlined in section 3.1. The limitations on the applicability of the solutions as mentioned above will also be discussed. Contours of streamlines, vorticity lines and isotherms plotted with the aid of the computer were obtained. The radial and tangential velocity components of the fluid in the gap between the two concentric spheres were calculated by differentiating the stream function analytically and computing the results. Finally, the temperature distributions and the heat transfer rates (Nusselt Numbers) are given.

3.1 Range of Validity of Solutions

The perturbation expansions for the variables of Ψ, Θ and $\tilde{\Theta}$ are obtained up to the second order terms. The series expansions for Ψ, Θ and $\tilde{\Theta}$ are equations (2.3.4) through (2.3.6). The error made by truncating such asymptotic expansions is of the order of the first term neglected. This term will tend to zero rapidly as the parameter G is reduced to zero. In the numerical evaluations for finite, non zero G, *all* the terms for Ψ, Θ and $\tilde{\Theta}$ derived were retained for actual computation. Due to the complexity of higher order terms no extra term was derived to check convergence for each of the expansions. Thus the numerical convergence of the expansions cannot be guaranteed.

An alternative criterion is proposed here to determine the practical upper bound of the convergence of the series expansions as follows: For given values of G, σ, ω and β and at a 'typical' location the value of any higher-order terms for Ψ, Θ and $\tilde{\Theta}$ considered must not be greater than the previous term. In addition the sum of any two or more higher-order terms must not have a value greater than the previous term or the fundamental terms, i.e. Ψ_1°, $\Theta_\circ^\circ$ and $\tilde{\Theta}_\circ^\circ$.

The criterion of convergence defined here is different from that used by Mack *et al.* [9, 10]. These workers considered that as long as the maximum magnitude of any

higher order term in either series for Ψ and Θ did not exceed the maximum value of the appropriate lowest order term at a 'typical' location, convergence could be assumed. On this basis, they found from their analytical solutions at low σ that it was possible to have double cells in the flow field. Their series for Ψ and Θ were obtained by expanding in ascending powers of Rayleigh number rather than in the Grashof number. Thus the coefficient expressions for the various terms in the series are dependent on σ : they include constants with σ^{-1}.

Double cells cannot occur on the basis on which the radius of convergence is defined in this thesis. Now, the existence of a secondary cell in addition to the primary cell had been observed experimentally by Bishop et al. [7] for a Rayleigh number (as defined in this thesis) of approximately 45×10^3 at a value of β of 1.19. However, the range of Rayleigh numbers (for which the series will 'converge') considered both by Mack et al. and in the present thesis is below that quoted by Bishop for the occurrence of a secondary cell. If the radius of convergence proposed by Mack had been adopted here a secondary cell would indeed exist for a value of Ra large enough (but not necessarily at low σ or β). An example of this is illustrated in section 3.2. Therefore it can be concluded that a numerical 'demonstration' of double cells is related to the fact that the series is no longer convergent in the work cited.

For both the conjugate and constant flux cases considered, numerical investigations show that the upper bound on G or Ra decreases monotonically with σ increasing from 0.01 to 100 and/or β increasing from 1.15 to 2.5. This is shown in Figure 3.1.1. The upper bound on G is lower in the constant flux case than in the conjugate case for fixed values of σ and β. The lowest value of ω (applicable only for the conjugate case) for which the upper bound of G is sufficiently high to be of interest is 3. If the ratio of thermal conductivity ω should vanish then the boundary conditions in the temperature field (i.e. 2.3.21 and 2.3.23) can no longer be fulfilled simultaneously. This in effect corresponds to the constant flux case and the 'conjugateness' of the problem is lost.

The other possible limitations to the range of applicability of the solutions are the non-consideration of compressive work and viscous dissipative effects; more over, the flow may not be steady laminar and axisymmetrical. In Appendix I, Tables V and VI show the ratios of the magnitude of the viscous dissipation term to either the conduction term (ε) or the convection term (λ) in the energy equation (2.2.2) of the fluid in the gap between the two concentric spheres at both radial and angular positions. It is seen from the tables that the ratio of the viscous dissipation term to either term in the energy equation is at least of the order of 10^{-8}. Hence neglecting viscous heating as assumed in

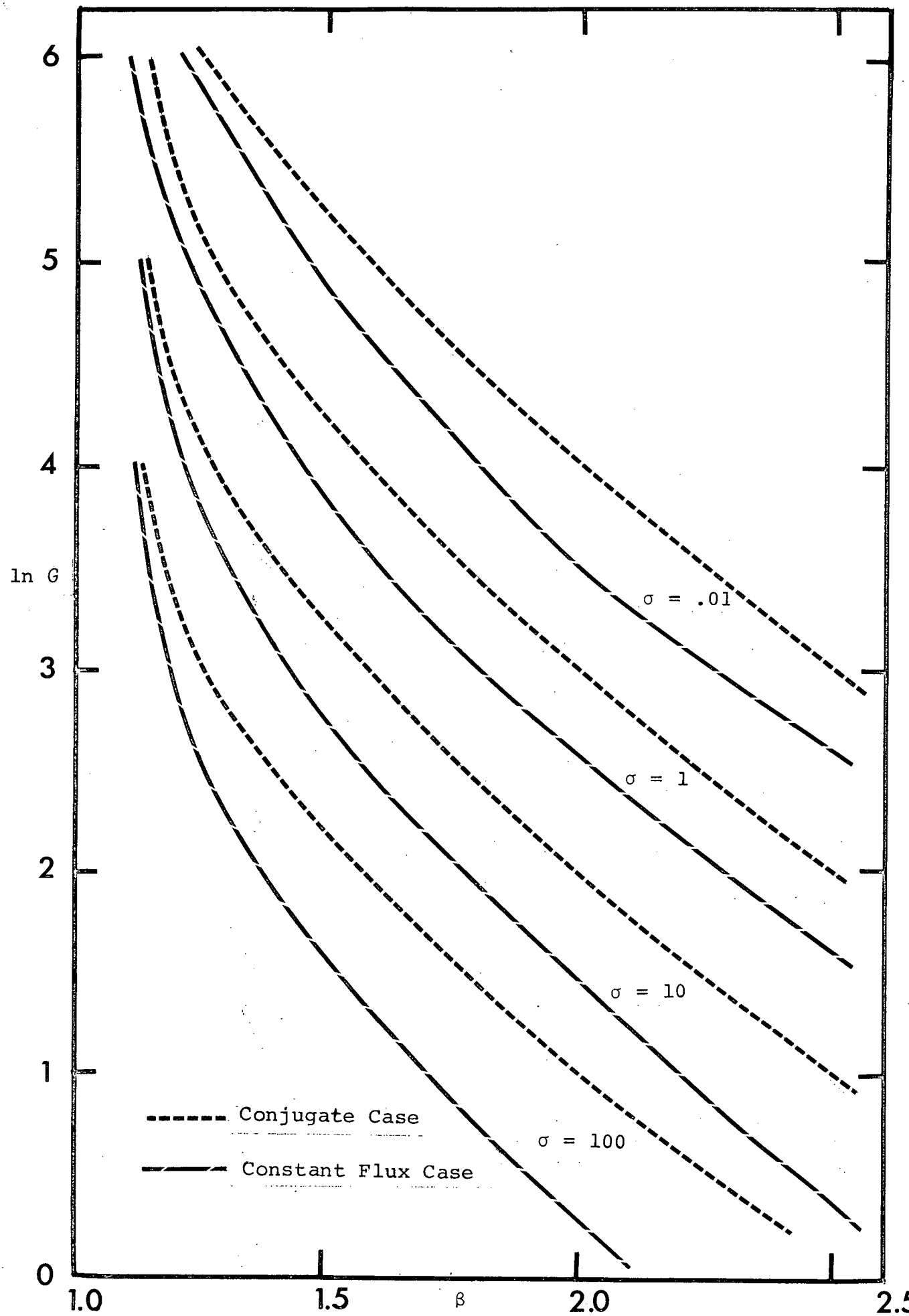

Figure 3.1.1 Approximate Upper Bound of G for Various σ/β

section 2.2 is justified. It will be shown later through the experimental investigation that the flow in the gap between the two concentric spheres is steady laminar and axisymmetrical about the vertical axis.

3.2 Streamlines

In view of the qualitative similarity for all combinations of G, σ, ω and β for which the expansions are convergent, contour plots of streamlines, isovorticity lines and isotherms are given for a fixed value of $Ra=720$ for both conjugate and the constant flux cases. The streamlines as given by Ψ equation (2.3.4) for $\sigma=.72$, $G=1000$, $\beta=2.0$ and $\omega=10$ are presented in Figure 3.2.1. A single cell of the 'crescent-eddy' type (observed previously [10] for the case of an isothermal inner sphere) is obtained. The fluid flows upward in the immediate vicinity of the inner sphere and downward along the outer sphere. The flow in the fluid space is 'toroidal' with rotational symmetry. There is a jet like flow polarization above the top of the inner sphere. The lower region of the fluid space acts like a reservoir with fluid withdrawn from it in the vicinity of the inner sphere and fluid flowing into it from the boundary of the outer sphere. The center of the circulatory motion, where Ψ has a maximum value, is in the upper half of the flow region at $\theta \simeq 82°$ and slightly past the mid point of the annular space.

Similar streamline configurations are obtained with values of Ra=720, β=2.0 for $\omega=10^{15}$ (approximately isothermal inner sphere) and the constant flux case as shown in Figures 3.2.2, 3.2.3 respectively. Figure 3.2.4 shows the streamlines for σ=.72, G=1000, ω=10 and β=1.15 with the annular space between the two concentric spheres plotted here stretched into a rectangular form for clarity. It is seen that the center of the streamlines is at θ=90°. As β tends to unity, the flow is essentially 'creeping flow' in a narrow gap. The creeping flow solution (i.e. Ψ_1°) places the center of the streamlines at θ=90°. Increasing the value of σ to 10 with the values of Ra=720, β=2.0 fixed, for the conjugate case (with ω=10, 10^{15}) and for the constant flux case, the streamline configurations remain essentially unchanged. The values of the streamline contours are lower than the previous values as the buoyancy effects are relatively reduced (G decreases when Ra is maintained constant while σ is increased), Figure 3.2.5. The center of the eddy cross section remains approximately in the same position as before for all cases. The upward and outward displacements of the center depends on the value of Ra when β is larger than 1.15 (i.e. higher order terms in Ψ then become important). Also the angular position of the center of the streamlines depends on the value of ω i.e. ω=10, $\theta \simeq 82°$; and for the constant flux case $\theta \simeq 75°$.

As stated previously in section 3.1, for convergence of the asymptotic expansion in Ψ (with all the terms actually derived used in the computations) the fundamental term Ψ_1° must always be the predominant term. If multiple cells should occur in the annular space, the adjacent cells would have values of the stream function of opposite algebraic sign However, the fundamental term is always positive throughout the flow field. Thus in order to have multiple cells the higher order terms would have to become *larger* than the fundamental term. Figure 3.2.6 shows the presence of a secondary cell at the lower region of the gap for the conjugate case with ω=10, σ=.72, G=2100 and β=2.0. The secondary cell does not extend across the gap and is much weaker than the primary cell. It may be concluded, as explained above, that here the expansion for Ψ is no longer convergent. Moreover, Bishop et al. [7] observed experimentally that the first secondary cell was formed near the top of the inner sphere. Hence, in the present analysis the occurrence of a secondary cell cannot be a genuine feature.

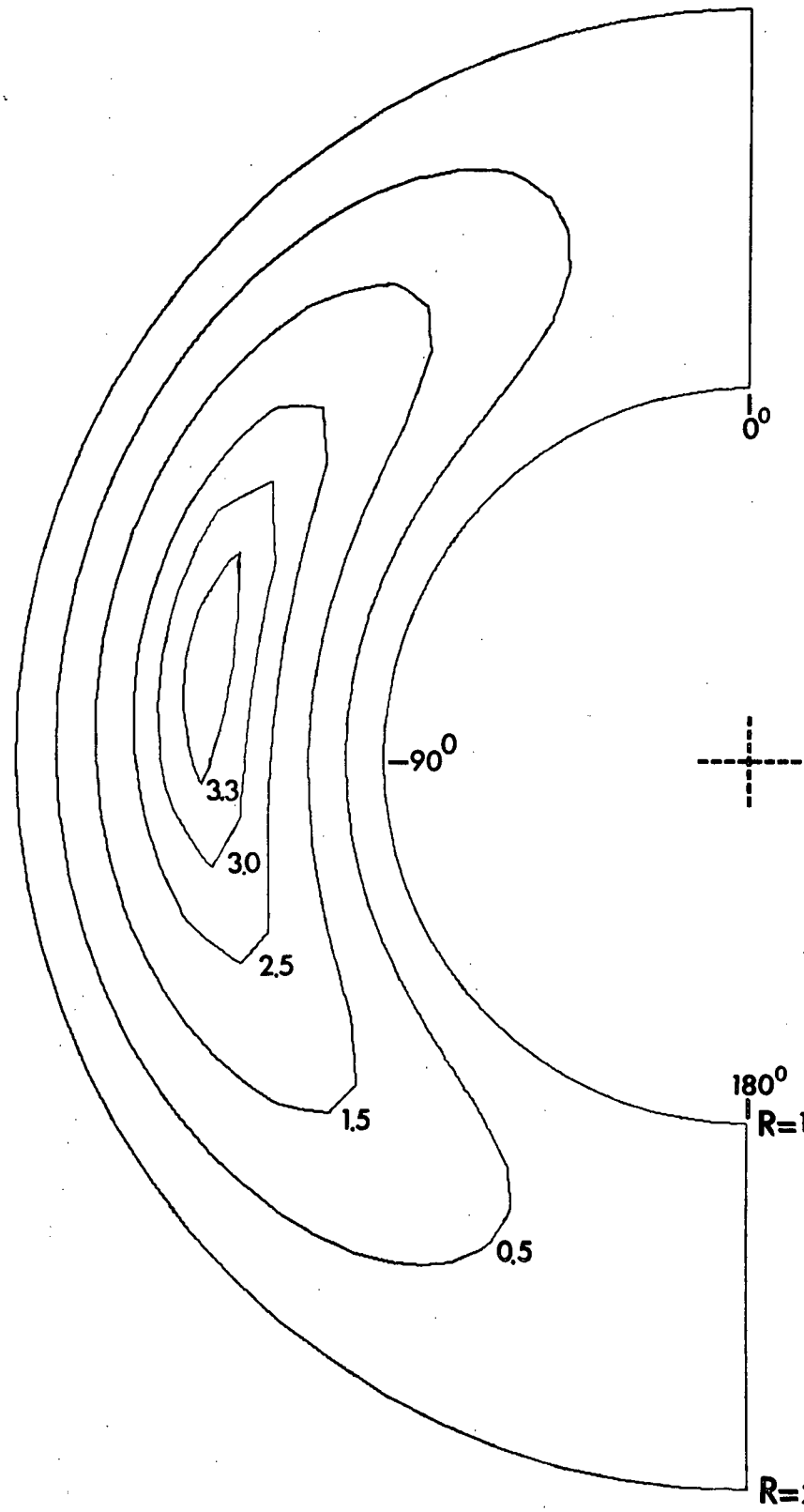

Figure 3.2.1

Streamlines for Conjugate Case, ω=10, β=2.0, σ=.72, $G=10^3$

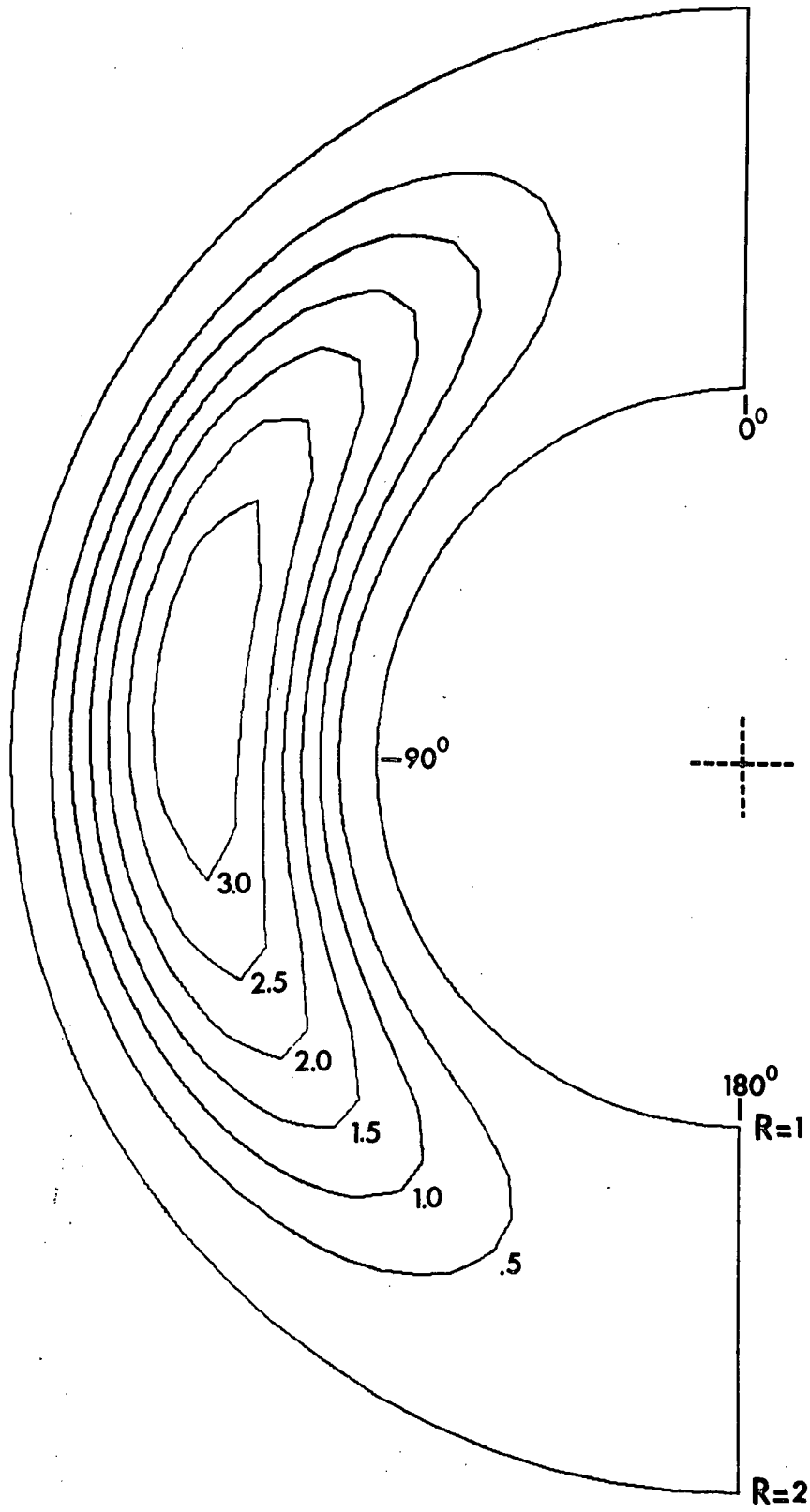

Figure 3.2.2

Streamlines for Conjugate Case, $\omega=10^{15}$, $\beta=2.0$, $\sigma=.72$, $G=10^{3}$

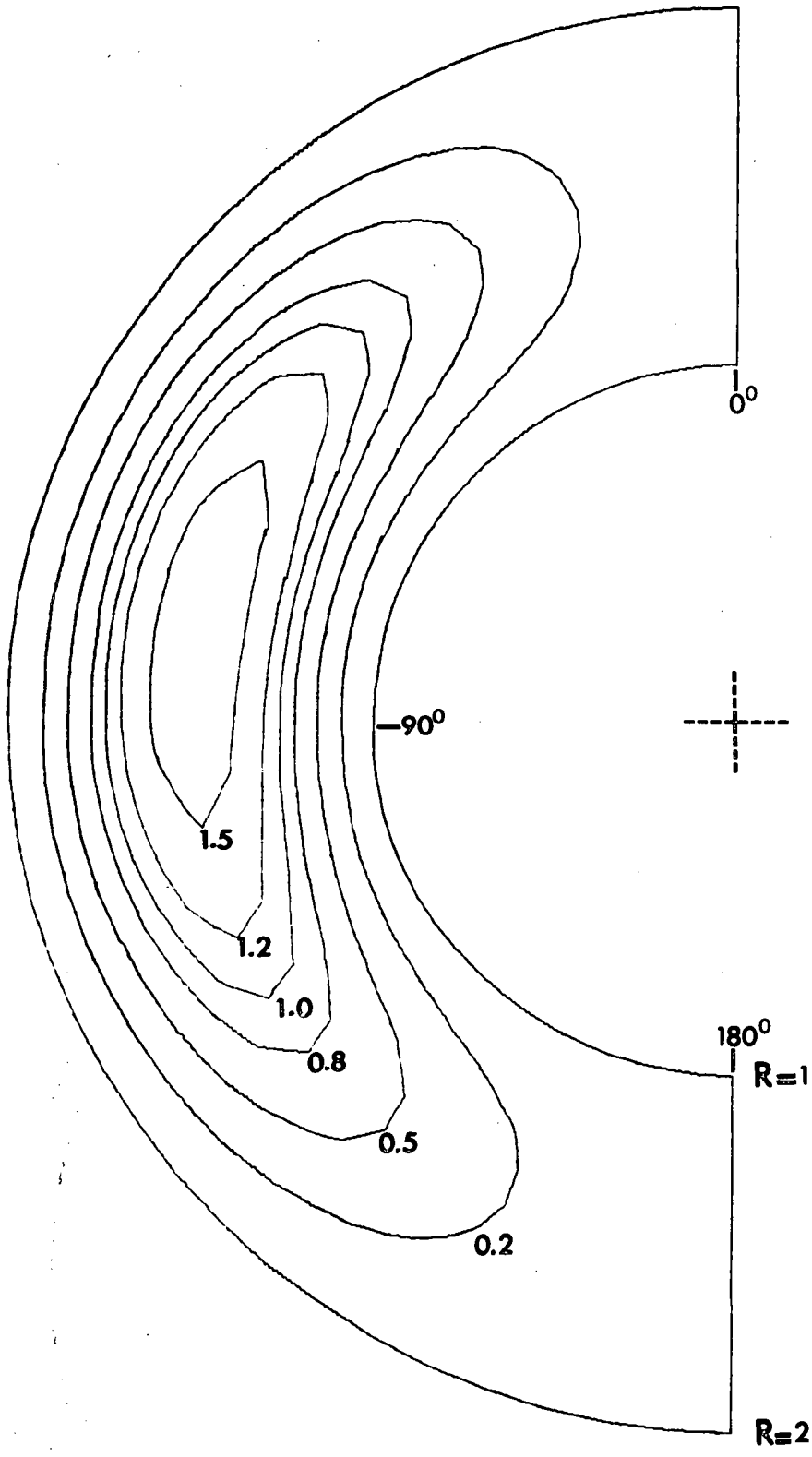

Figure 3.2.3

Streamlines for Constant Flux Case, $\beta=2.0$, $\sigma=.72$, $G=10^3$

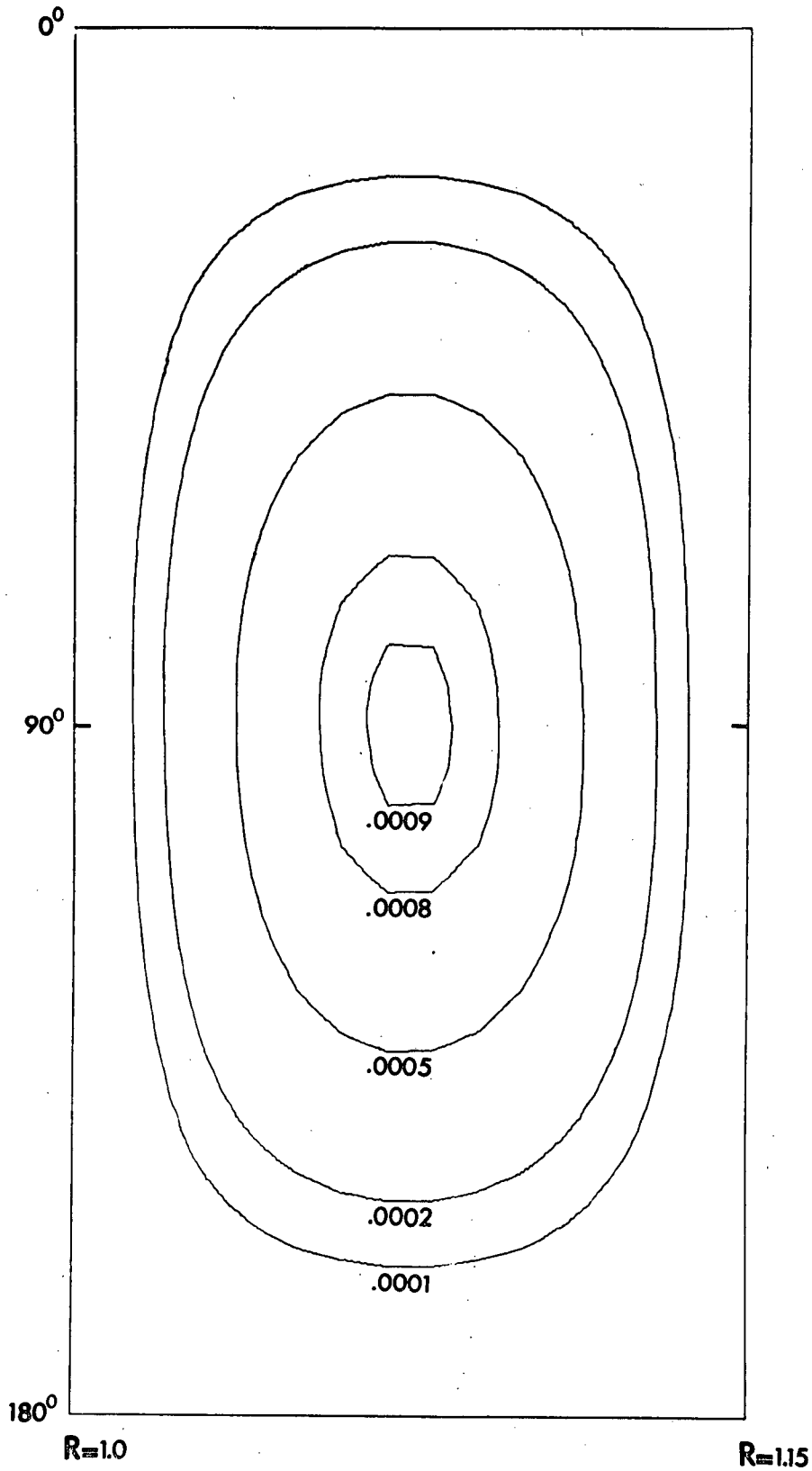

Figure 3.2.4

Streamlines for Conjugate Case, ω=10, β=1.15, σ=.72, $G=10^3$

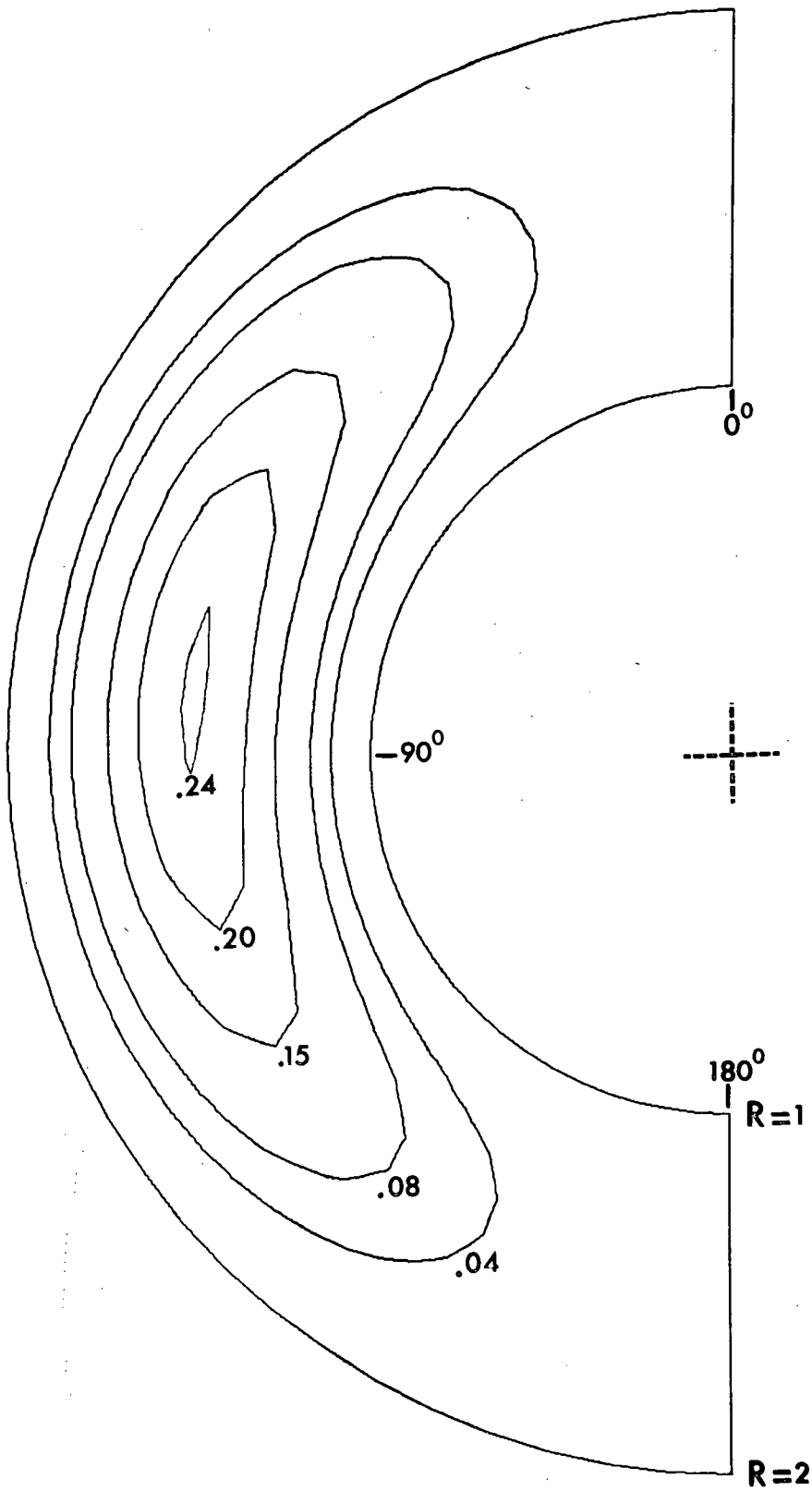

Figure 3.2.5

Streamlines for Conjugate Case, ω=10, β=2.0, σ=10, G=72

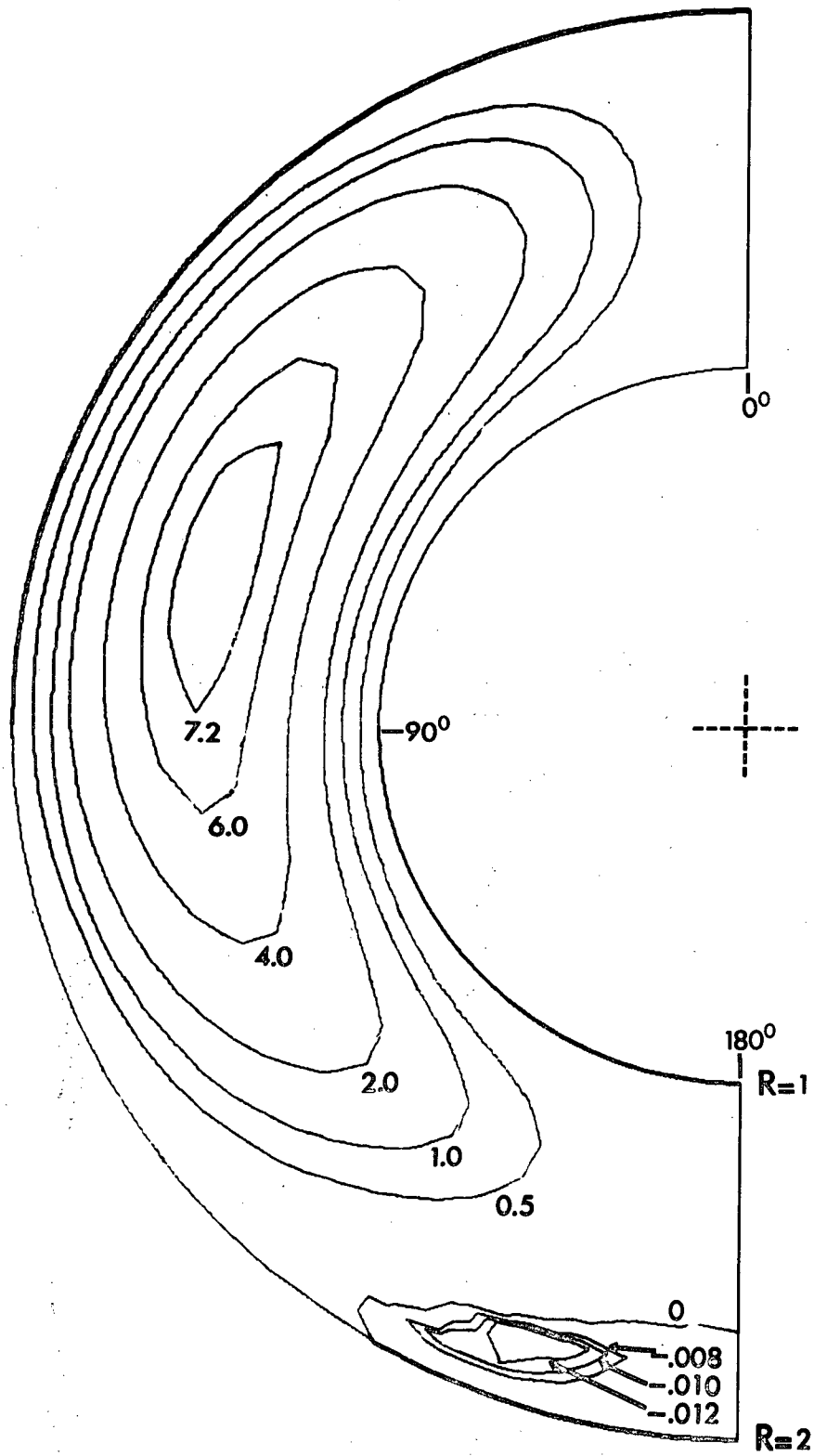

Figure 3.2.6

Streamlines for Conjugate Case, ω=10, β=2.0, σ=.72, G=2100

3.3 Velocity Distributions

It was assumed previously that the convective flow pattern is axisymmetrical. Thus there is no latitudinal velocity, V_ϕ. The radial and tangential velocity components of the fluid in the R- and θ- directions respectively are obtained analytically by differentiating the stream function, Ψ, equation (2.3.4):

$$V_R = \frac{1}{R^2 \sin\theta} \frac{\partial \Psi}{\partial \theta} = -\frac{1}{R^2} \frac{\partial \Psi}{\partial \eta} \tag{3.3.1}$$

$$= G \times 2\eta \left\{ \frac{A_1}{R^3} + \frac{B_1}{R} + C_1 - \frac{R}{8} + D_1 R^2 \right\} \times \left(\frac{\beta}{\beta-1}\right)$$

$$+ G^2 \times (3\eta^2 - 1) \left\{ G_2^a R^3 + H_2^a R + \frac{I_2^a}{R^2} + \frac{J_2^a}{R^4} \right.$$

$$- \frac{A_1 B_1}{2R^3} + \frac{1}{24R} (12B_1^2 + A_1) + \frac{B_1 C_1}{2} - \frac{R^2}{24} (12B_1 D_1 + C_1)$$

$$\left. + \frac{D_1 R^4}{144} - \frac{1}{560} R^3 \ln R + \frac{B_1}{60} R \ln R \right\} \times \left(\frac{\beta}{\beta-1}\right)^2$$

$$+ G^2 \sigma \times (3\eta^2 - 1) \left\{ G_2^b R^3 + H_2^b R + \frac{I_2^b}{R^2} + \frac{J_2^b}{R^4} \right.$$

$$- \frac{A_1}{12R} + \frac{F_1}{8} - \frac{C_1 R^2}{24} + \frac{D_1 R^4}{288} - \frac{B_1}{15} R \ln R$$

$$- \frac{R^3}{840} \ln R \Bigg\} \times \left(\frac{\beta}{\beta-1}\right)^2 \qquad (3.3.1a)$$

$$V_\theta = \frac{1}{R\sin\theta} \frac{\partial \Psi}{\partial R} = - \frac{(1-\eta^2)^{-\frac{1}{2}}}{R} \frac{\partial \Psi}{\partial R} , \qquad (3.3.2)$$

$$= (1-\eta^2)^{\frac{1}{2}} \Bigg[G \left\{ \frac{A_1}{R^3} - \frac{B_1}{R} - 2C_1 + \frac{3R}{8} - 4D_1 R^2 \right\} \times \left(\frac{\beta}{\beta-1}\right)$$

$$+ G^2 \times \eta \left\{ - 5G_2^a R^3 - 3H_2^a R + \frac{2J_2^a}{R^4} - \frac{A_1 B_1}{2R^3} \right.$$

$$- \frac{(12B_1^2 + A_1)}{24R} - B_1 C_1 + \frac{R^2}{6} (12B_1 D_1 + C_1) - \frac{D_1 R^4}{24}$$

$$\left. + \frac{R^3}{560} (1 + 5 \ln R) - \frac{B_1 R}{60} (1 + 3 \ln R) \right\} \times \left(\frac{\beta}{\beta-1}\right)^2$$

$$+ G^2 \sigma \times \eta \left\{ - 5G_2^b R^3 - 3H_2^b R + \frac{2J_2^b}{R^4} + \frac{A_1}{12R} \right.$$

$$\left. - \frac{F_1}{4} + \frac{C_1 R^2}{6} - \frac{D_1 R^4}{48} + \frac{B_1 R}{15} (1 + 3 \ln R) \right.$$

$$+ \frac{R^3}{840}(1 + 5 \ln R)\Big\} \times \left(\frac{\beta}{\beta-1}\right)^2 \Bigg] . \qquad (3.3.2a)$$

The radial and tangential velocities were evaluated numerically using the expressions (3.3.1a) and (3.3.2a).

For ω=10, β=2.0, G=1000, σ=.72; the radial velocity V_R is plotted against radius R for various angular positions θ as shown in Figure 3.3.1. At a given radial position the magnitude of the radial velocity increases with decreasing θ. Each profile has either a maximum or a minimum value occuring at an approximate radial position between $1.4 \leq R \leq 1.55$. For $0° \leq \theta \leq 60°$, the fluid has a radial outflow and a radial inflow when $90° \leq \theta \leq 180°$. It is seen that the radial outflow at θ=0° is about twice that of the radial inflow at θ=180°. Finally, the radial velocity gradient near the inner sphere's surface (i.e. R=1.0) is higher than that near the outer sphere's surface (i.e. R=2.0).

For the same values of ω, β, G and σ as before, the profiles of the tangential velocity, V_θ, against the radial position, R, for various θ are shown in Figure 3.3.2. Each profile shows a maximum value for upward flow and a minimum value of downward flow. The upward flow speed near the inner sphere is higher than the downward flow speed near the outer sphere. For θ=90°, the tangential velocity, V_θ, is zero at R=1.5 indicating that the upward and the downward flow

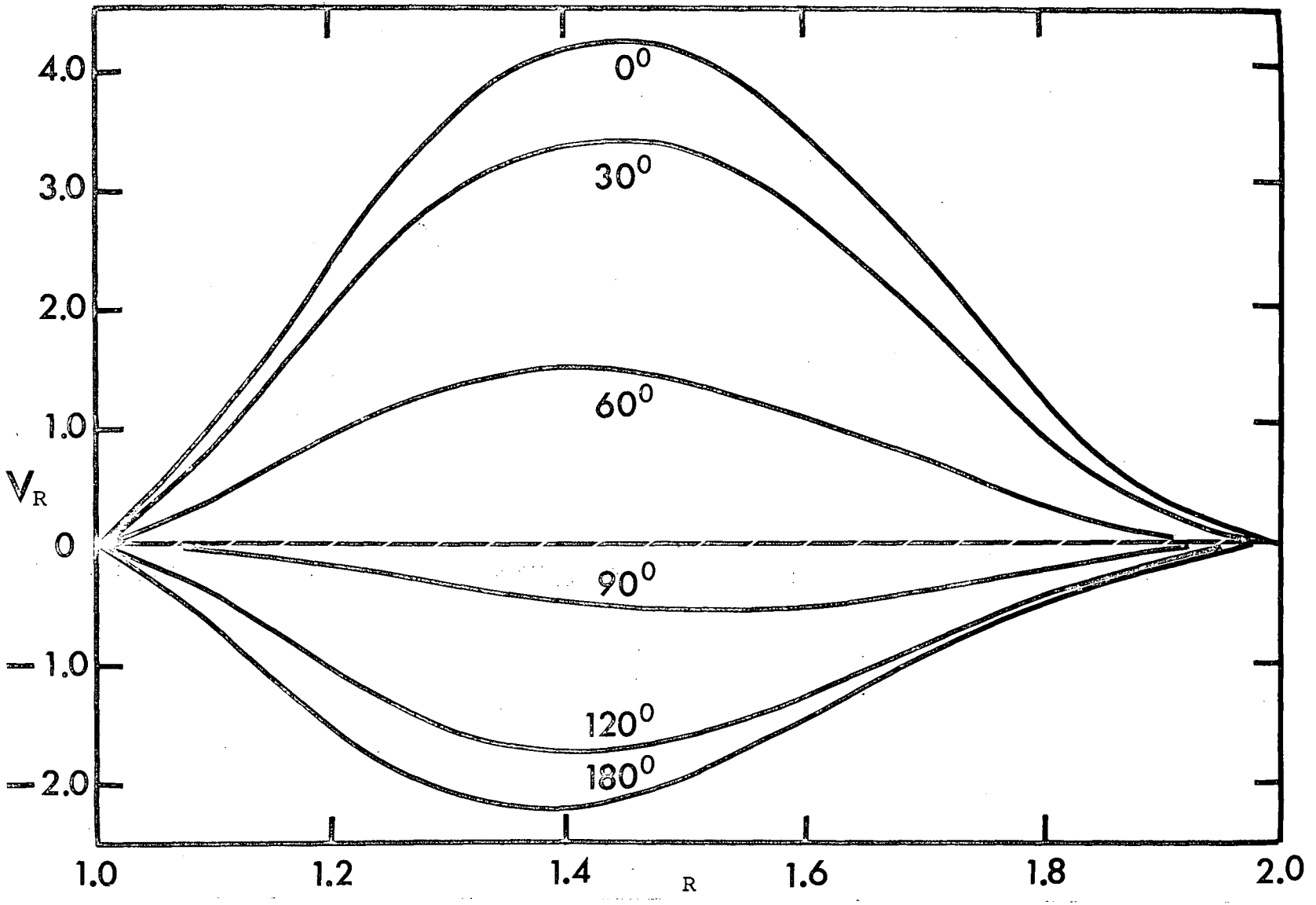

Figure 3.3.1 Radial Velocity V_R vs. Radius (Various Angular Positions)
ω=10, β=2.0, σ=.72, $G=10^3$

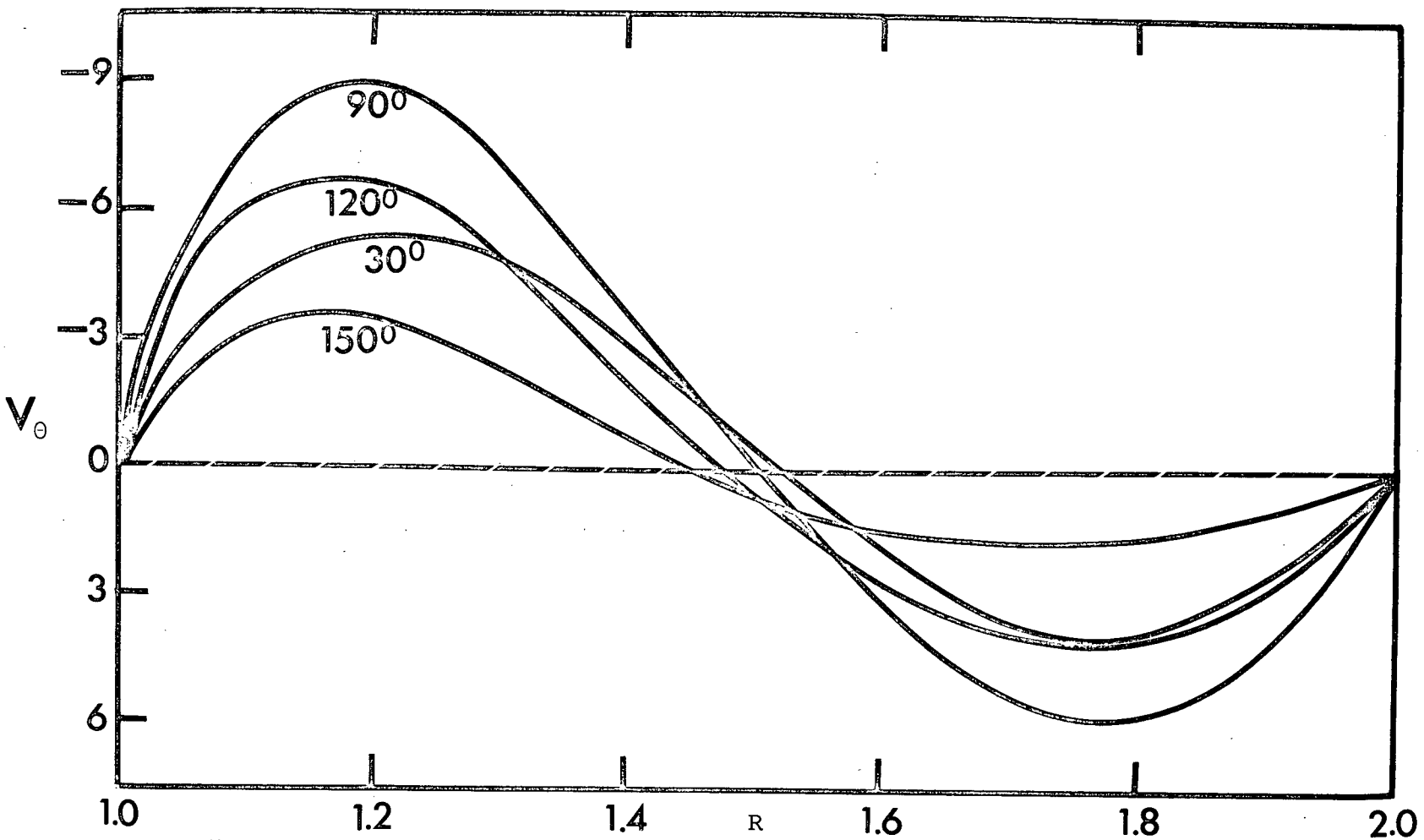

Figure 3.3.2 Tangential Velocity, V_θ vs. Radius (Various Angular Positions), ω=10, β=2.0, σ=.72, G=10^3

are approximately equal. However, the upward velocity is still greater then the downward velocity. The crossover point from upward flow to downward flow occurs in the region $1.4 \leq R \leq 1.55$. This crossover point moves towards the inner sphere as θ increases.

The general features of the radial and tangential velocity profiles are similar for other combinations of ω, β, G and σ.

3.4 Vorticity Contours

As mentioned in section 2.3, the convective motion of the fluid due to buoyancy forces is the only source of vorticity available in the gap between the concentric spheres. With rotational symmetry, the vorticity vector in the positive ϕ -direction is given by:

$$\zeta = [\nabla \times \vec{V}]_{\phi}$$

$$= \frac{\partial V_{\theta}}{\partial R} + \frac{V_{\theta}}{R} + \frac{(1-\eta^2)^{\frac{1}{2}}}{R} \frac{\partial V_R}{\partial \eta}$$

$$= (1-\eta^2)^{\frac{1}{2}} G \left\{ \left[\frac{2B_1}{R^2} - 10D_1 R + \frac{1}{2} \right] \times \left(\frac{\beta}{\beta-1}\right) \right.$$

$$+ G \times \eta \left[- 14\, G_2^a\, R^2 + \frac{6I_2^a}{R^3} - \frac{2A_1B_1}{R^4} \right.$$

$$+ \frac{1}{4R^2}(12B_1^2 + A_1) + \frac{2B_1C_1}{R} + \frac{R}{4}(12B_1D_1 + C_1)$$

$$- \frac{D_1R^3}{6} + \frac{R^2}{560}(9 + 14 \ln R) - \frac{B_1}{12} + \sigma x$$

$$\left(- 14 G_2^b R^2 + \frac{6I_2^b}{R^3} - \frac{A_1}{2R^2} + \frac{F_1}{2R} + \frac{C_1R}{4} - \frac{D_1R^3}{12}\right.$$

$$\left. + \frac{B_1}{3} + \frac{R^2}{840}(9 + 14 \ln R))\right] \times \left(\frac{\beta}{\beta-1}\right)^2 \Bigg\} \qquad (3.4.1)$$

The overall features of the vorticity contours shown in Figures 3.4.1 through 3.4.4 are similar. The vorticity field may be conveniently divided into three regions which may vary in radial extent. The meridional length of the isovorticity lines and their radial position depend upon the four parameters G, σ, ω and β. These three regions are defined as: the immediate vicinity of the inner sphere where the vorticity is generated; the central vortex region where the vorticity from the inner sphere is transferred by diffusion and convection; the boundary at the outer sphere where vorticity of the fluid is dissipated. Note that this arrangement into three regions resembles qualitatively that described

by Batchelor for free convection between parallel plane boundaries.

In the immediate vicinity of the inner sphere the vorticity of the fluid is generated by the convective motion set up by the heated inner sphere. Thus the isovorticity lines have the highest magnitude and in angular extent here in comparison to those in the other two regions. The fluid particles are rotating in the clockwise direction. The vorticity vector defined by equation (3.4.1) is at right angles and into the plane of the paper in each of the figures for this region.

The central vortex region is separated from the other two regions by the two isovorticity lines of value zero. The most notable feature in this region is the 'toroidal-shaped' surfaces of the vorticity sheets. With rotational symmetry, each of these tori extends around the whole annular space between the concentric spheres. They can be considered as 'vortex tubes' and the whole of the central region as a 'vortex ring'. The centre line of the vortex is in the upper region of the flow field and quite near to the mid-point of the gap. This position is different from that of the centre of the streamlines (section 3.2), for each of the corresponding cases. Near the centre of the vortex is a region of *nearly constant vorticity* e.g. Figure 3.4.3. The magnitude of the vorticity is the highest in this region. The sense of rotation of the fluid is opposite (i.e. counter-

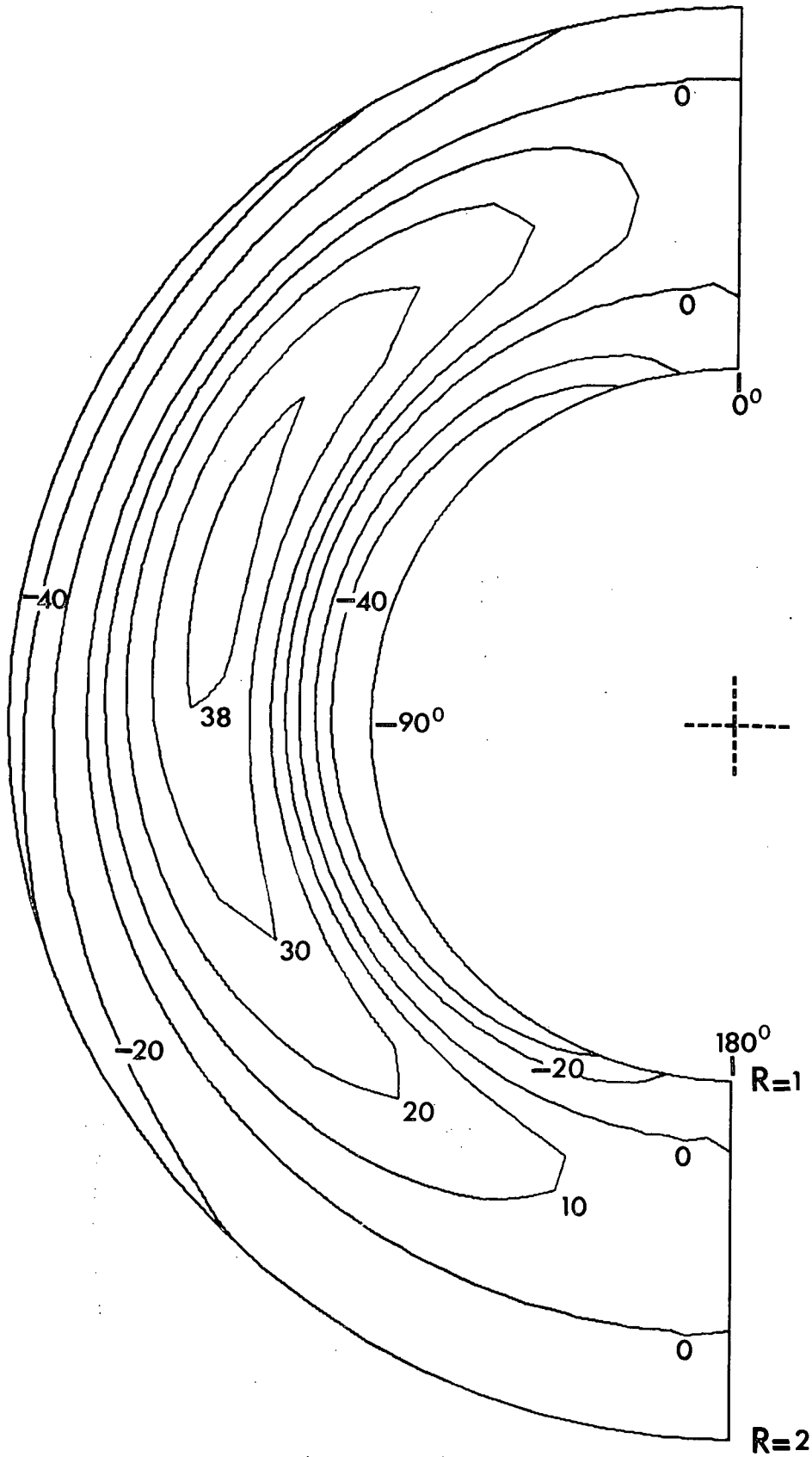

Figure 3.4.1

Vorticity Contours, Conjugate Case, ω=10, β=2.0, σ=.72, $G=10^3$

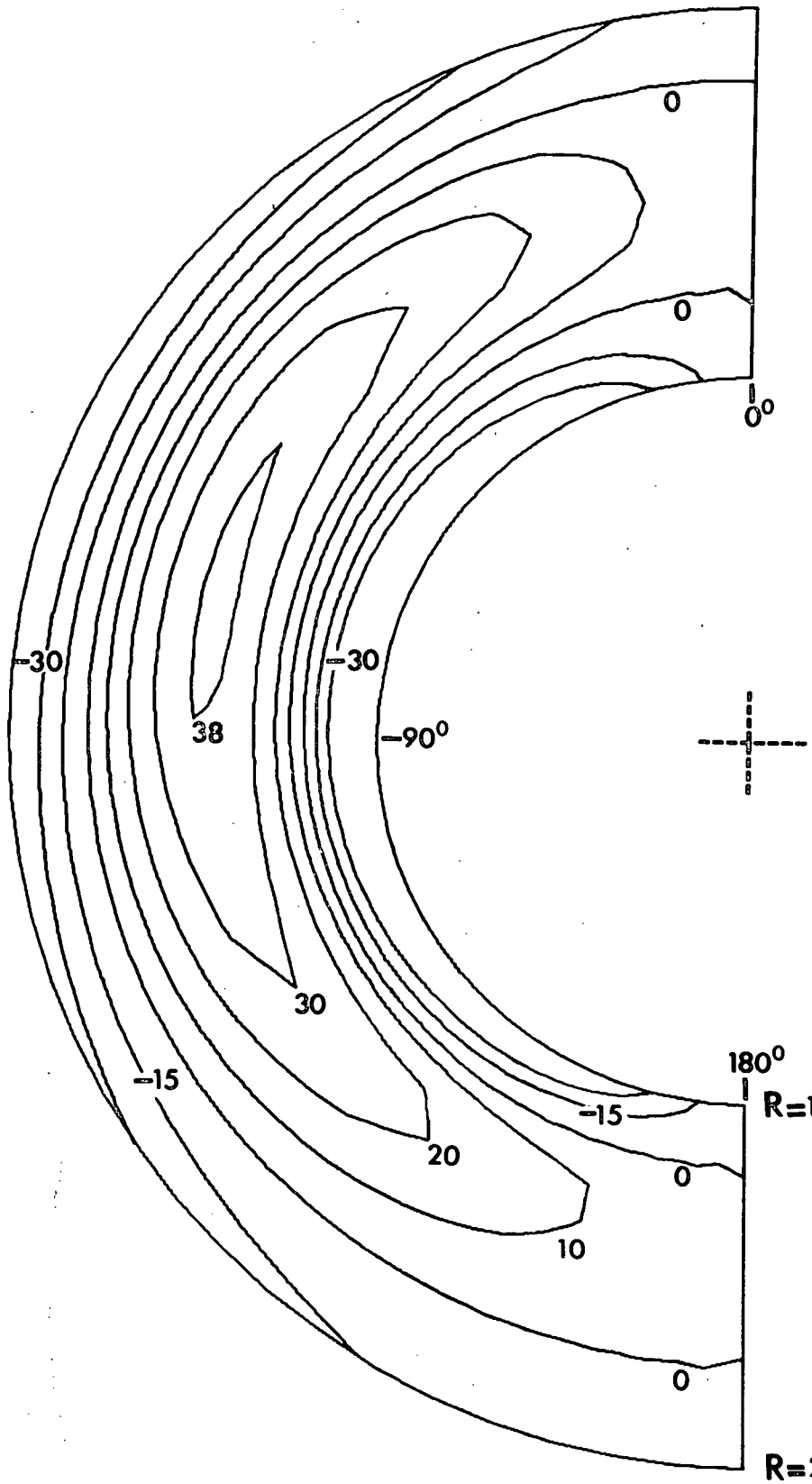

Figure 3.4.2

Vorticity Contours, Conjugate Case, $\omega=10^{15}$, $\beta=2.0$, $\sigma=.72$, $G=10^{3}$

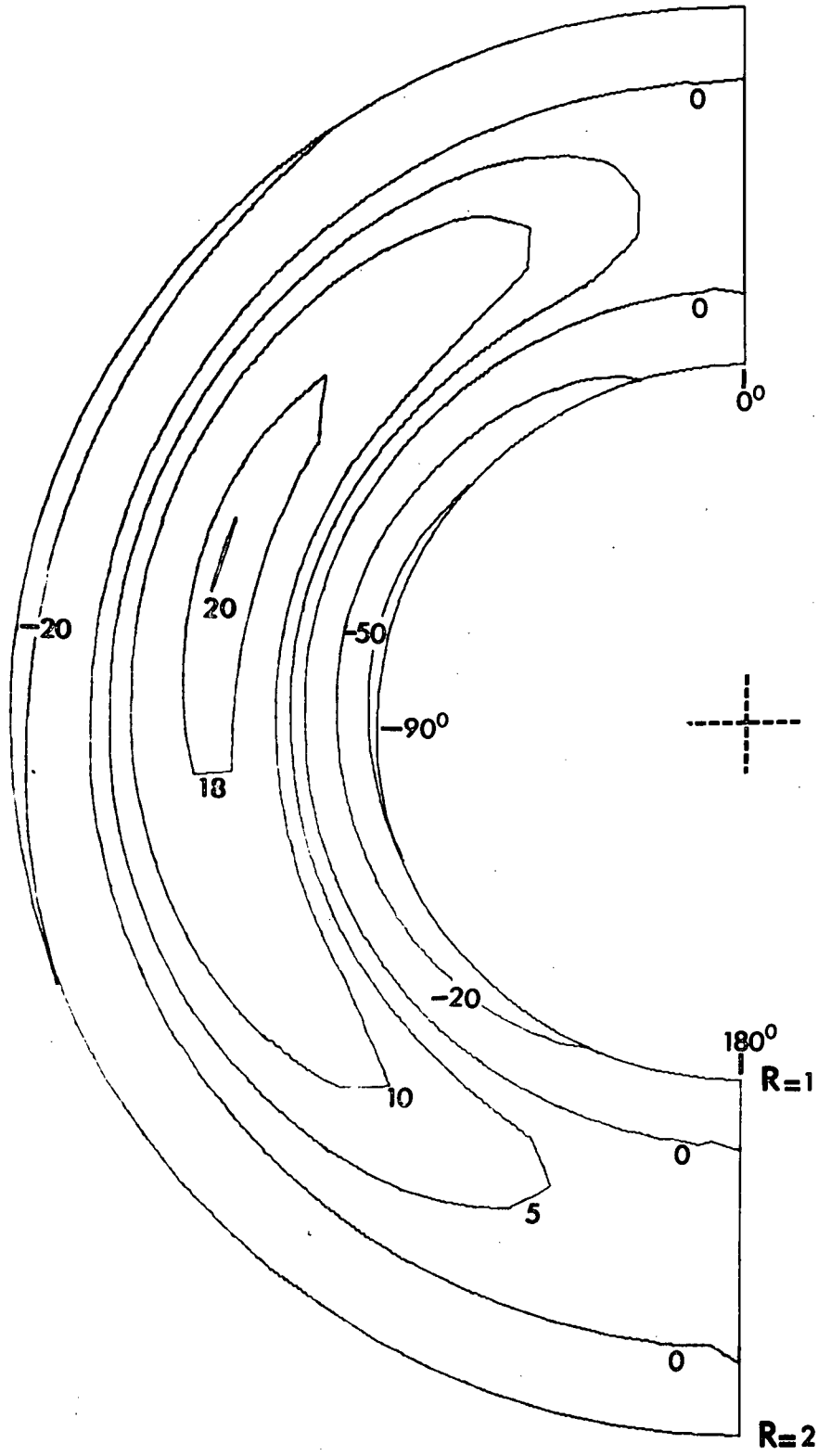

Figure 3.4.3

Vorticity Contours, Constant Flux Case, $\beta=2.0$, $\sigma=.72$, $G=10^3$

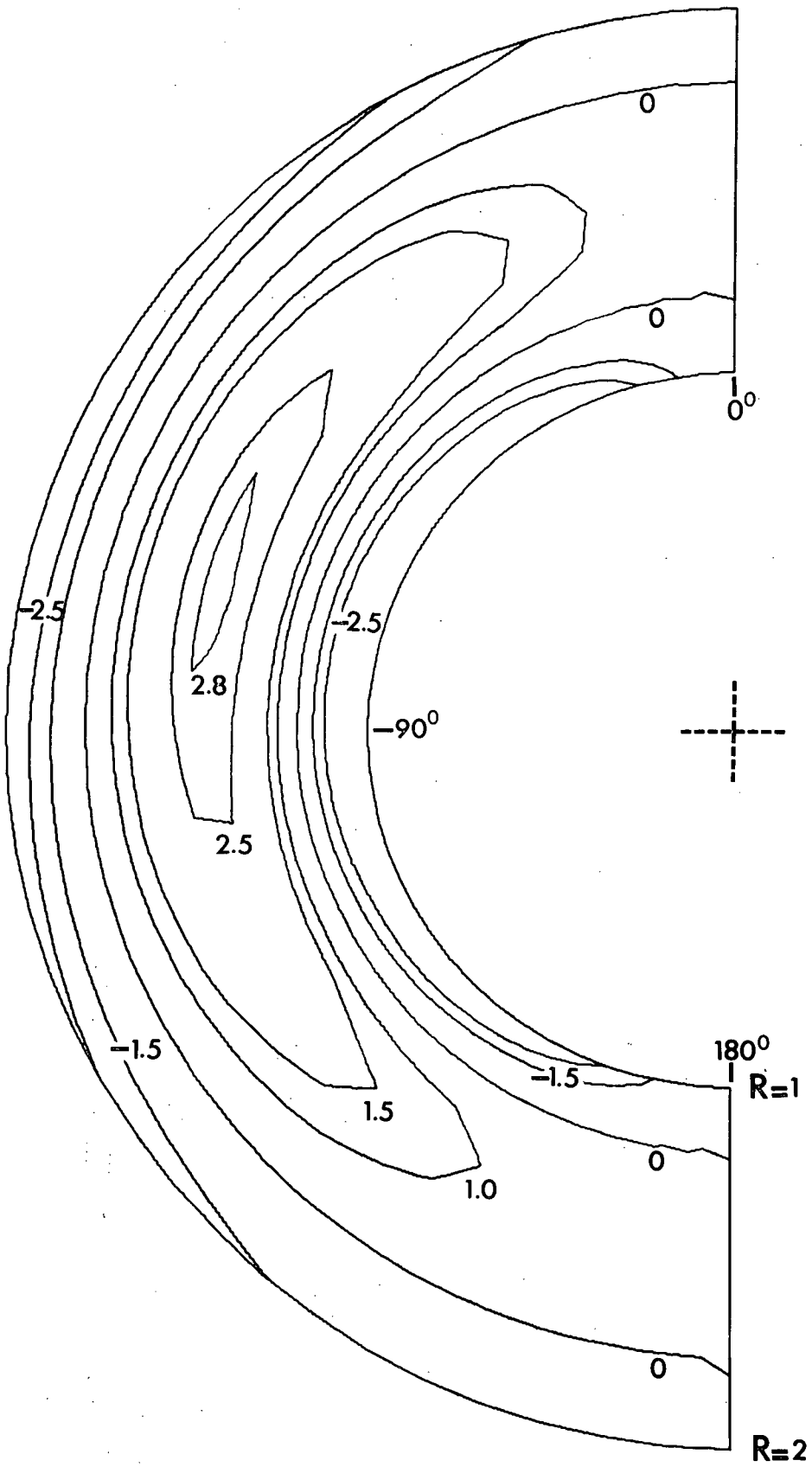

Figure 3.4.4

Vorticity Contours, Conjugate Case, ω=10, β=2.0, σ=10, G=72

clockwise) to that in the region at the inner sphere surface as the vorticity is transferred from there.

The vorticity is transferred to and dissipated at the boundary region of the outer sphere. Hence the vorticity vector is in the same direction as that in the immediate vicinity of the inner sphere. The features of the vorticity contours are there qualitatively similar to those in the region near the inner sphere. But for each corresponding magnitude of the vorticity the individual contour does not have the same angular extent in this region, at the outer sphere.

As in the streamline configuration, the features of the vorticity contours change little with a change of σ, provided Ra, β and ω be kept constant. While the position of the centre of the vortex does not change with σ, it is affected by Ra, β and ω.

3.5 Temperature Distribution and Contours

The temperature distribution of the fluid in the annular space between the concentric spheres is given by equation (2.3.5). For the conjugate case; equation (2.3.6) yields the temperature distribution in the solid inner sphere with a single heat source at the centre. Calculation of the temperature inside the inner sphere is irrelevant for both the constant flux case and when ω is very large

e.g. $\omega=10^{15}$ (i.e. an isothermal inner sphere) even in the conjugate case. It is seen from the Figures 3.5.1 and 3.5.3 that for $.72 \leq \sigma \leq 10$ and with Ra, β and ω fixed, a change in σ does not alter the temperature profiles or the contours, Figures 3.5.6 and 3.5.7. This indicates that the temperature distribution and the heat transfer rates are quite independent of σ, at least in that range. Alternatively expressed, *the influence of σ is a higher order effect* on both the temperature distribution and heat transfer rates. A proof of this is given later in section 3.6.

The general features of the temperature profiles are similar for the conjugate and constant flux cases, Figures 3.5.1 to 3.5.5. The temperature distribution due to pure conduction (i.e. θ_o°) is given by the dashed line for comparison. For the conjugate case, at any particular radial position $1 \leq R \leq \beta$, the temperature (as seen from the figures) increases with decreasing θ. The profiles for $\theta=0°$ and 60° lie below the curve for pure conduction while the profiles for 90° and 150° lie above this curve. The profiles for 120° and 150° are relatively close together compared to any two profiles. This indicates that the local heat transfer rates for both the inner sphere and the outer sphere is quite independent of θ for $120° \leq \theta \leq 180°$.

In their experimental work, Scanlan et al. [21] postulated that for the occurrence of multicellular flow, a reversal of the ordering of the temperature profiles would occur (see their Figures 8 to 10). Direct comparison of

their results with those given here is perhaps not meaningful since their range of Ra used in their experiments was considerably higher and with a smaller β than that considered here. However, it is seen that the temperature profiles illustrated here, there is no reversal of their order. Hence the existence of multicellular flow does not occur here in accord with the discussion in section 3.2 above.

The temperature on the surface of the inner sphere varies with angular position except in the conjugate case where $\omega=10^{15}$ (i.e. an isothermal inner sphere). The temperature variation on the inner sphere's surface is most pronounced for the constant flux case. For it is in this case that it is assumed the heat flux on the surface of the inner sphere is uniform even though convection is taking place in the fluid. On the other hand for the conjugate case, there is a redistribution of heat flux inside the inner sphere when there is convection in the fluid. Also the temperature of the fluid at the interface must be matched with inner sphere temperature i.e. at R=1, Figures 3.5.1, 3.5.2 and 3.5.6.

The temperature contours will be essentially those of concentric circles for pure conduction of heat from the single source at the centre of the concentric spheres. The resulting convective motion of the fluid displaces the isotherms upwards, Figures 3.5.6 to 3.5.9. This is due to the relatively cold fluid from the bottom being heated up by both conduction and convection as it rises to the top of the

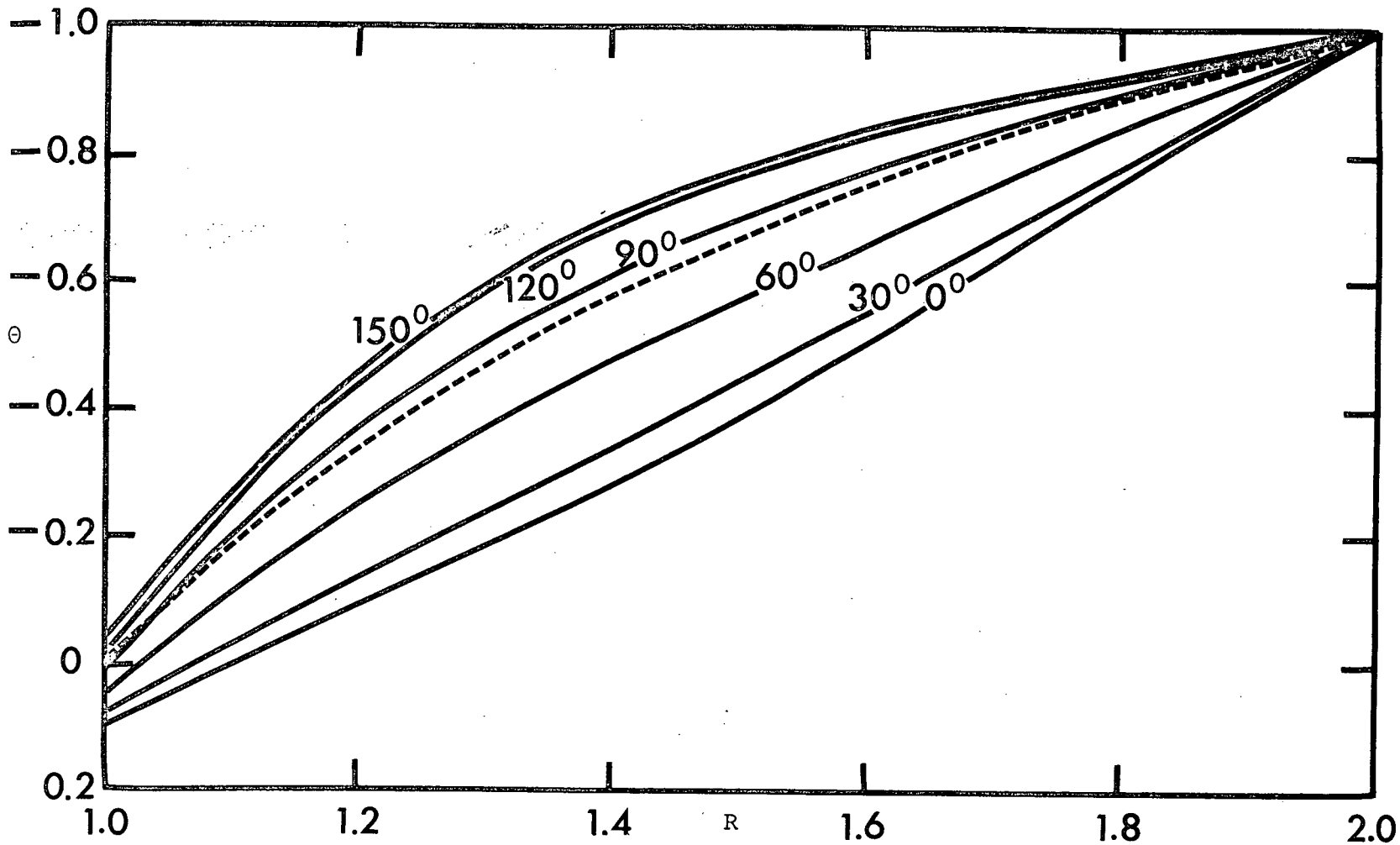

Figure 3.5.1 Temperature Distribution, Conjugate Case, ω=10, β=2.0, σ=.72, $G=10^3$

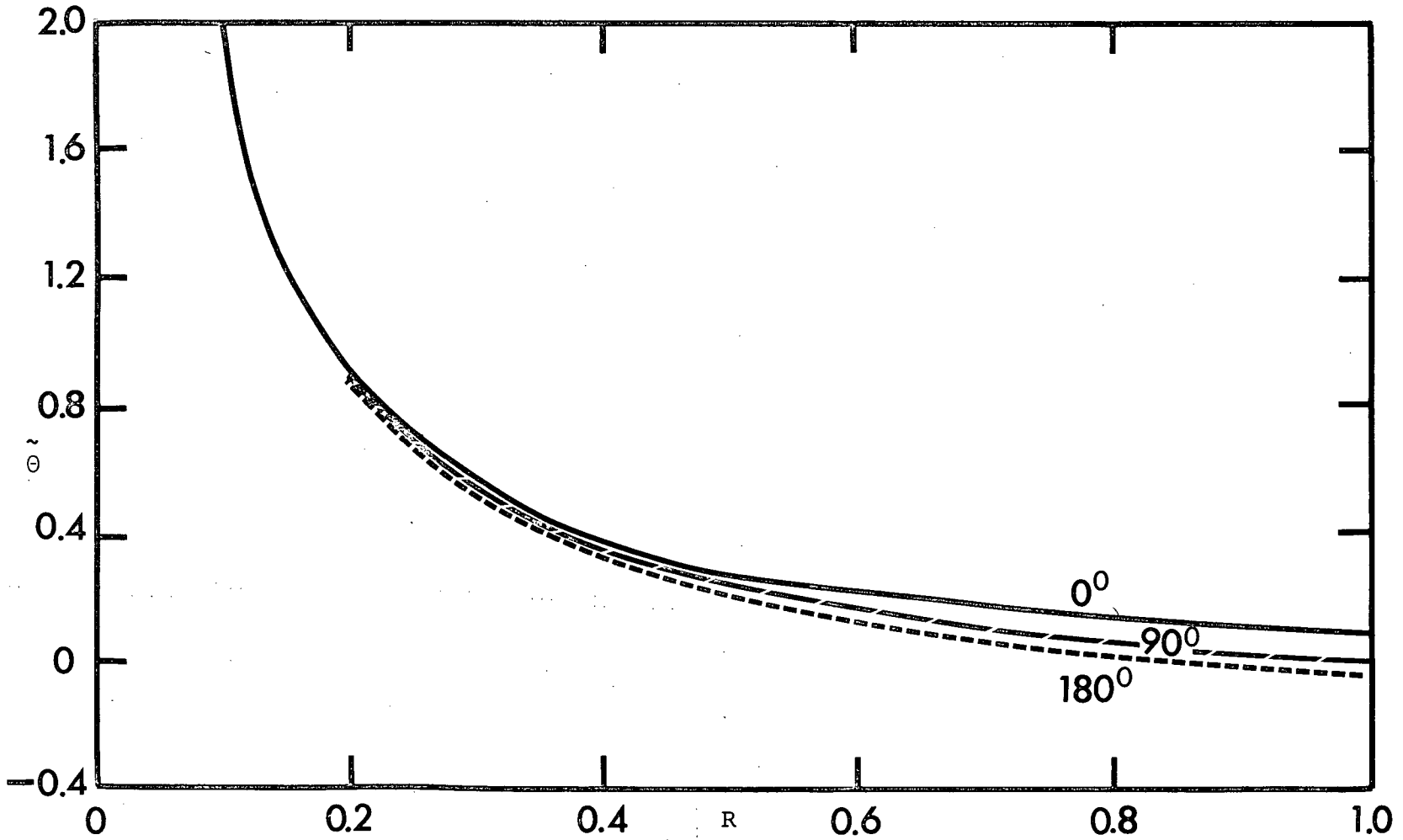

Figure 3.5.2 Temperature Distribution of Inner Sphere, Conjugate Case; $\acute{\omega}$=10, β=2.0, σ=.72, $G=10^3$

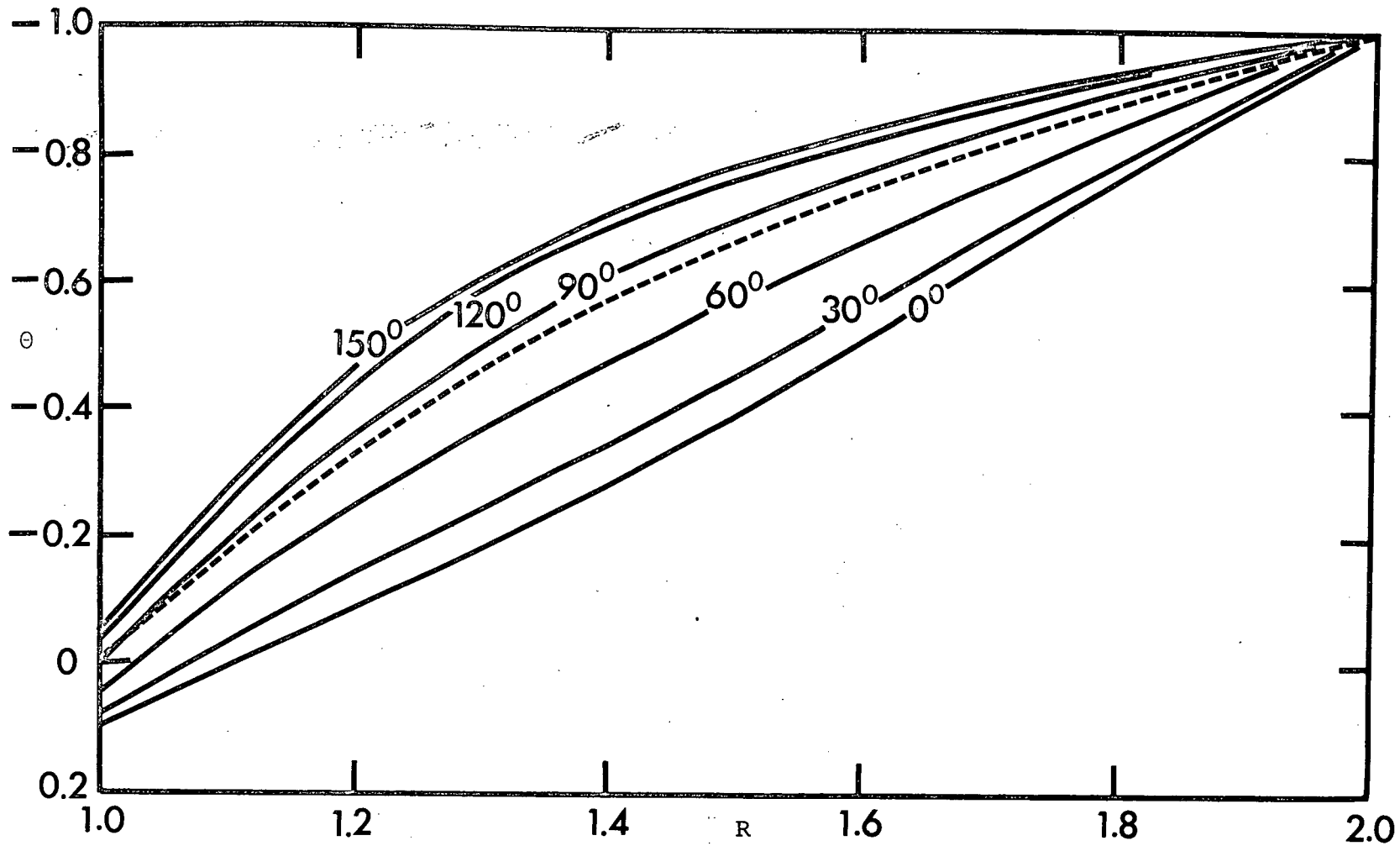

Figure 3.5.3 Temperature Distribution, Conjugate Case, ω=10, β=2.0, σ=10, G=72

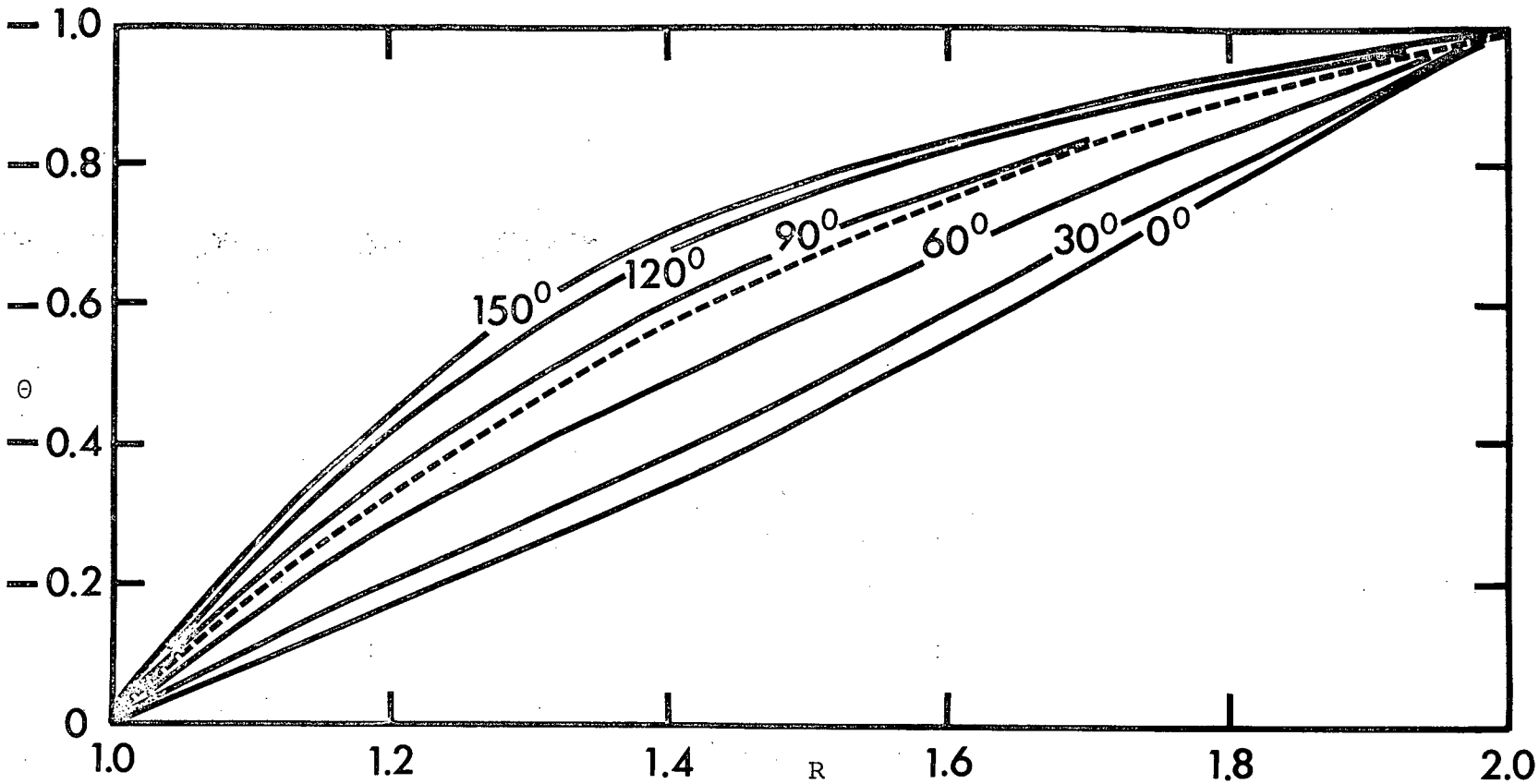

Figure 3.5.4 Temperature Distribution, Conjugate Case, $\omega=10^{15}$, $\beta=2.0$, $\sigma=.72$, $G=10^{3}$

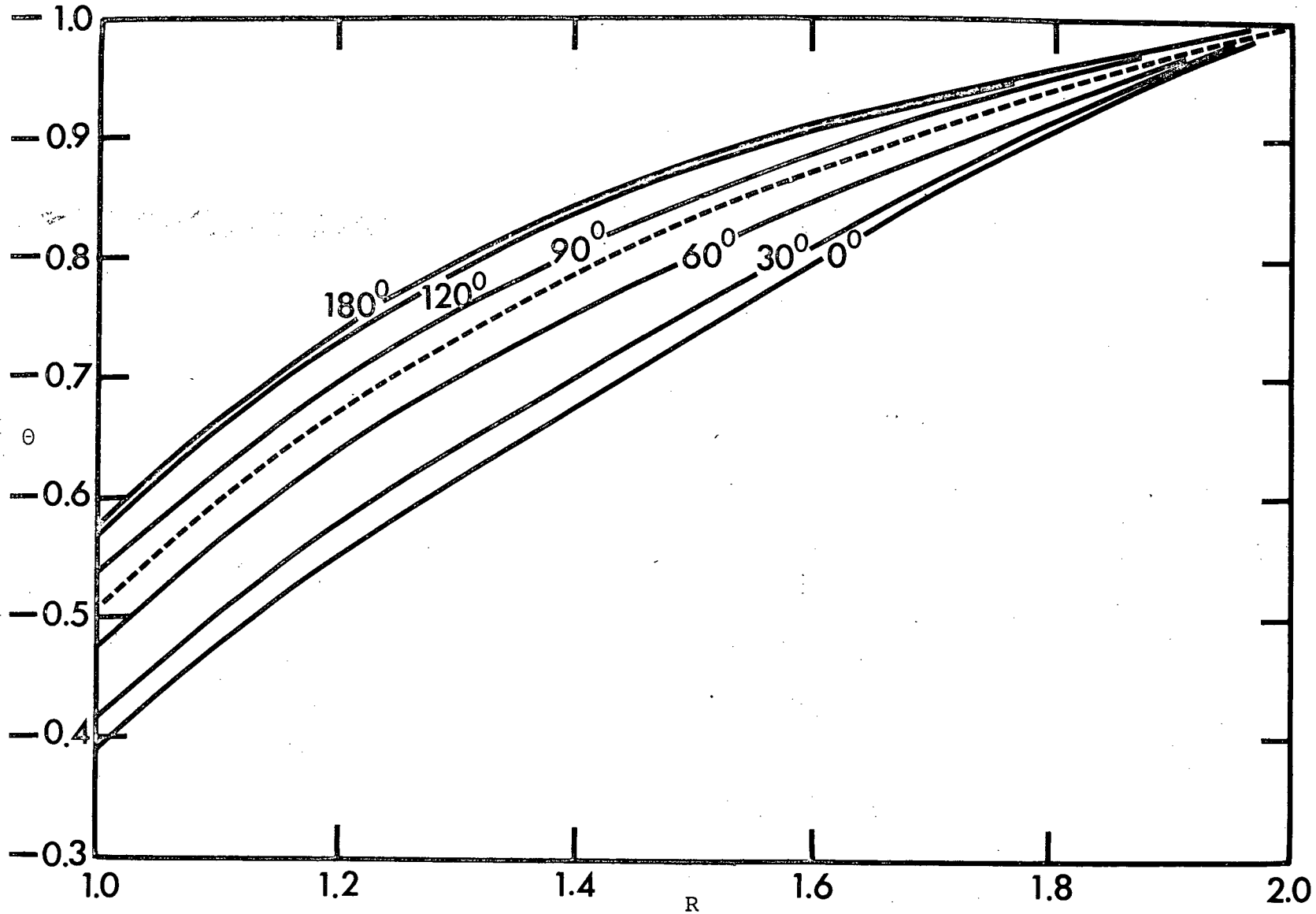

Figure 3.5.5 Temperature Distribution, Constant Flux Case, $\beta=2.0$, $\sigma=.72$, $G=10^3$

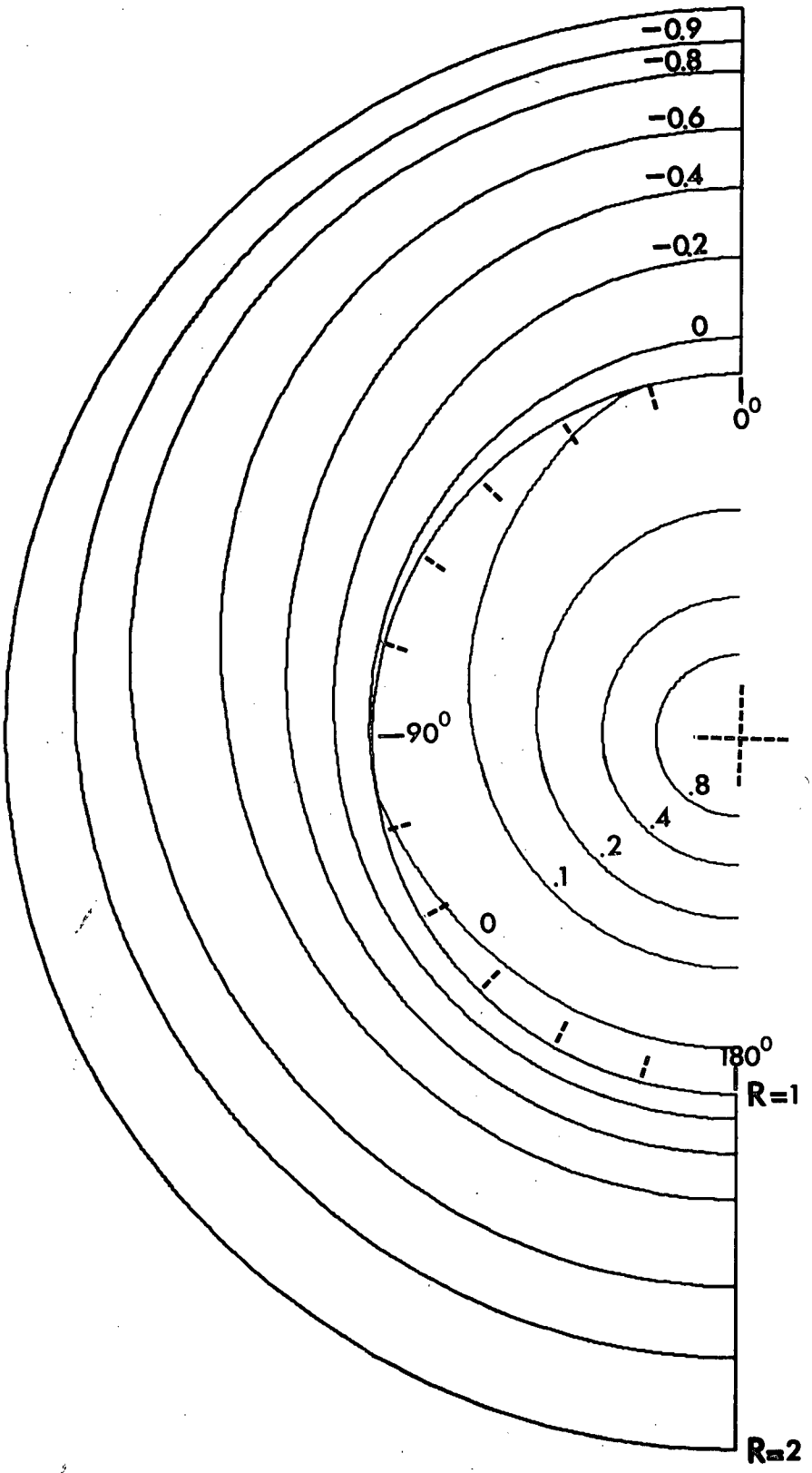

Figure 3.5.6

Isotherms, Conjugate Case, $\omega=10$, $\beta=2.0$, $\sigma=.72$, $G=10^3$

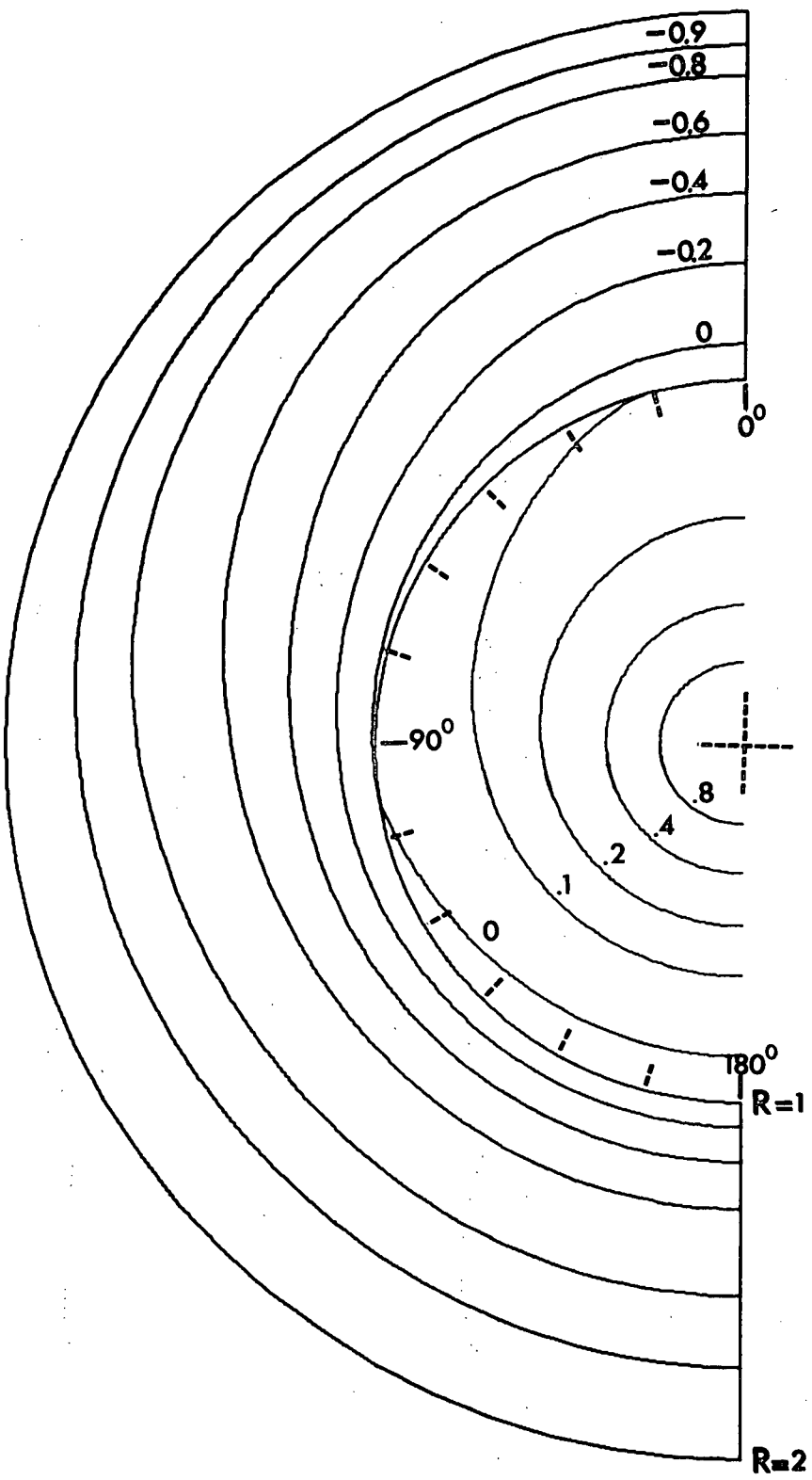

Figure 3.5.7

Isotherms, Conjugate Case, ω=10, β=2.0, σ=10, G=72

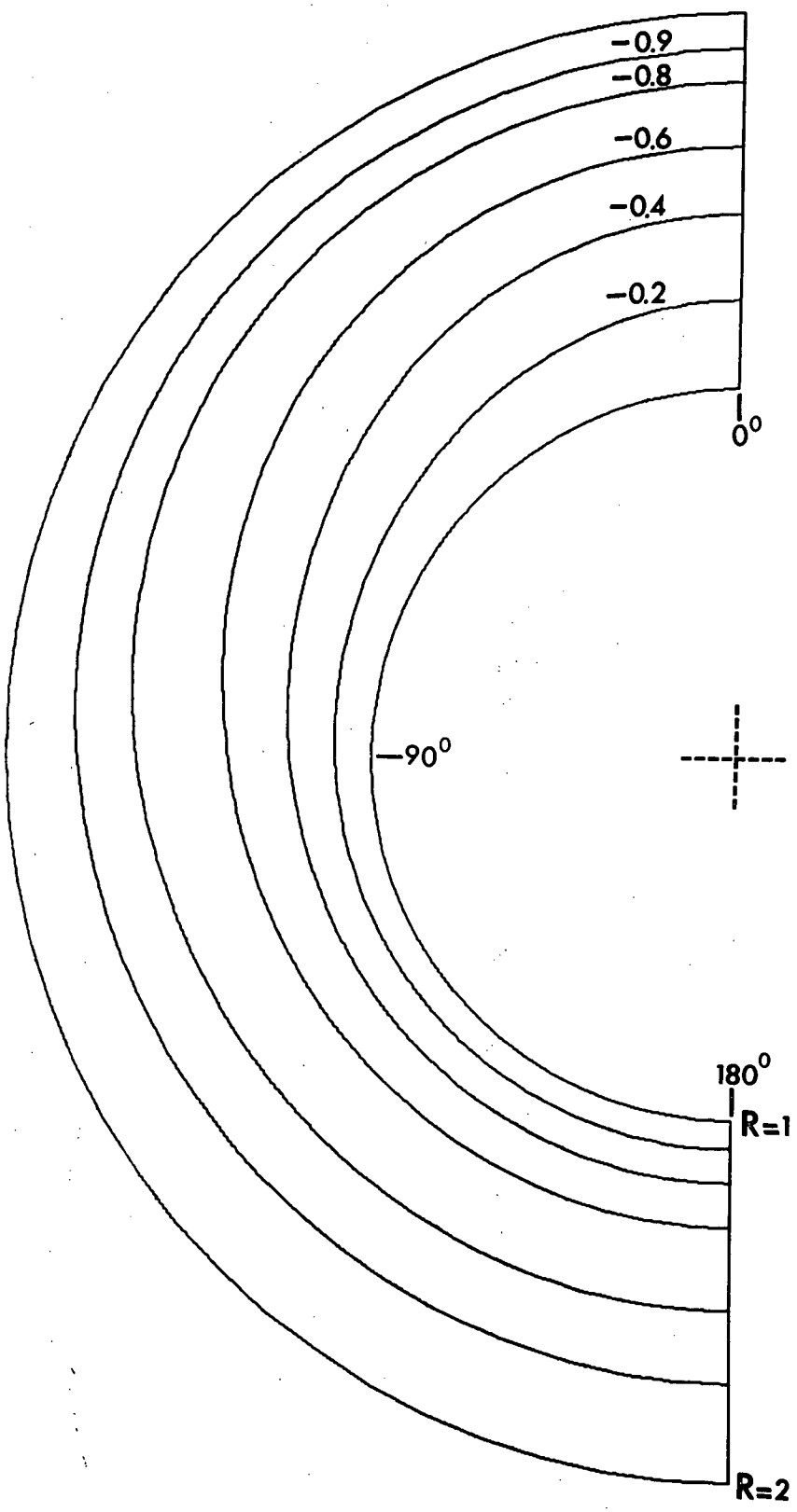

Figure 3.5.8

Isotherms, Conjugate Case, $\omega=10^{15}$, $\beta=2.0$, $\sigma=.72$, $G=10^{3}$

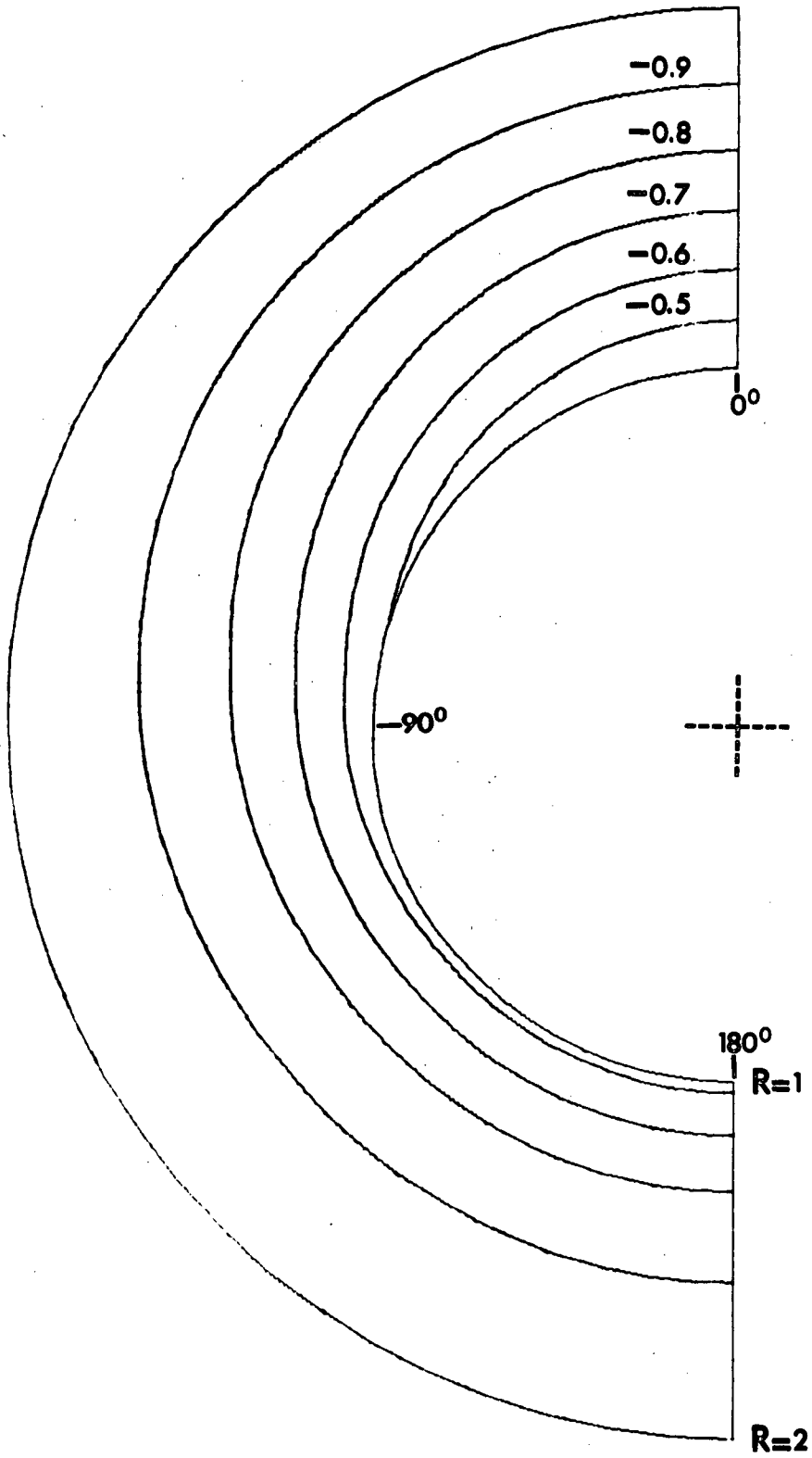

Figure 3.5.9

Isotherms, Constant Flux Case, $\beta=2.0$, $\sigma=.72$, $G=10^3$

gap. The shape of the isotherms is still similar to circles since pure conduction is predominant. In section 2.2, it is shown that at the beginning of the solution of the energy equation the inner sphere's surface is isothermal and/or of constant flux thus for pure conduction alone, the zero isotherm coincides with the surface of the inner sphere. When convective motion takes place, the portion of the zero isotherm approximately in the upper half region is displaced upwards into the annular space. The lower portion is displaced into the solid sphere where there is a redistribution of flux, Figure 3.5.6. When ω is very large the surface of the inner sphere can be considered to be isothermal even though there is a redistribution of heat flux.

The temperature contours are 'distorted' from that of concentric circles around the region for $\theta=120°$ approximately e.g. Figure 3.5.9. This shows that in this region vigorous convection is taking place in the immediate vicinity of the inner sphere.

3.6 Heat Transfer Rates

The local Nusselt numbers

$$Nu_i(\theta) = -\frac{(\beta-1)}{\beta} \times \frac{\partial \Theta}{\partial R}\Big|_{R=1}$$

and

$$Nu_o(\theta) = -\frac{(\beta-1)}{\beta} \times \beta^2 \times \frac{\partial\Theta}{\partial R}\Big|_{R=\beta}$$

are defined for the inner sphere and outer sphere respectively. The Nusselt numbers defined here have the radius of the inner sphere as the common length scale. The overall heat transfer rate is then obtained by integrating the local Nusselt numbers over the entire surface of the inner sphere or the outer sphere. The overall Nusselt numbers for the inner sphere and outer sphere are given respectively by:

$$\overline{Nu_i} = -\frac{(\beta-1)}{2\beta}\int_0^{\pi} \frac{\partial\Theta}{\partial R}\Big|_{R=1} \sin\theta \, d\theta \qquad (3.6.1)$$

$$\overline{Nu_o} = -\frac{(\beta-1)}{2\beta}\int_0^{\pi} \beta^2 \frac{\partial\Theta}{\partial R}\Big|_{R=\beta} \sin\theta \, d\theta \qquad (3.6.2)$$

It is seen that $\overline{Nu_i}$ must be equal to $\overline{Nu_o}$. Evaluating separately both $\overline{Nu_{i,o}}$, will serve as a check on the value of the overall Nusselt number.

The Nusselt numbers, $Nu_{i,o}$, are dependent upon θ, Ra, ω and β and as shown in Figures 3.6.1 to 3.6.4. The curves of $Nu_{i,o}$ show that in comparison to the pure conduction value

(shown as a dashed line in the figures) the heat transfer rate has been increased for about the lower two-thirds of the inner sphere and nearly half of the upper outer sphere and reduced elsewhere. The greatest deviation of the heat transfer rate from the pure conduction value is at $\theta=0°$ in each case. There is an angular position in the upper half of the spheres where the heat transfer rate from both the inner and outer spheres is the same. This angular position moves towards the top of the spheres i.e. $\theta=0°$ as ω decreases and as Ra increases, Figures 3.6.1, 3.6.3 and 3.6.4. For $120° \leq \theta \leq 180°$ and $Ra=720$, $Nu_{i,o}$ do not vary much with θ as inferred in section 3.5 from the temperature profiles for 120° and 150°. However, in this region there exists a maximum value for Nu_i and a minimum value for Nu_o. The locations of these turning points depend on the values of Ra, σ and the conjugateness of the inner sphere i.e. ω. Figure 3.6.5 shows the turning points at $\theta \simeq 130°$ and 125° for Nu_i and Nu_o respectively with $Ra \simeq 1000$, $\omega=10$. As inferred in section 3.5 from the temperature contours in this region near the inner sphere, there is vigorous convective motion taking place in the fluid. Thus this is the location where the heat transfer rate (or flux) from the inner sphere is a maximum. As mentioned before in section 3.3, the bottom of the annular space between the concentric spheres acts as if it were a reservoir. The hot fluid is cooled as it flows downwards along the outer sphere. Hence, the heat transfer rate decreases as the fluid flows into the reservoir.

In the region around $\theta \simeq 130°$ there is vigorous convection of the fluid near the inner sphere. So some of the 'cold' fluid near the outer sphere will be entrained by the relatively hotter rising fluid near the inner sphere. The remaining cold fluid will flow into the 'reservoir'. This will reduce the heat transfer rate to a value *lower* than that of pure conduction. Nu_o will be a minimum near $\theta \simeq 125°$ since most of the heat flux is convected away by the fluid near the inner sphere. This results in the distortion of the isotherms, see section 3.5.

The influence of σ on $Nu_{i,o}$ is not very significant for the range of Ra considered in this thesis. For a fixed ω, low Ra corresponds to low convection thus conduction plays the predominant role. Hence for a fixed value of ω and $Ra=720$, a change of σ does not alter $Nu_{i,o}$ significantly, Figures 3.6.1 and 3.6.2. For a value of $\sigma=.72$, Nu_o is greater than that for $\sigma=10$. It is usual to consider a fluid to be more conductive as σ decreases. Thus for a fixed low Ra, as σ decreases, G (buoyancy effects) increases. This will displace the isotherms further upwards in this case. Therefore Nu_o will increase near the top of the outer sphere as σ decreases.

It will now be shown that the influence of σ is a higher order effect for the overall Nusselt numbers.

Let

$$\frac{\partial\Theta}{\partial R} = -\frac{\beta}{(\beta-1)} + TN1 \times \cos\theta + (TN2 + TN3)\times(3\cos^2\theta - 1)$$

$$+ TN4$$

where $$TN1 \times \cos\theta = (G\sigma) \times \frac{\partial\theta_1^\circ}{\partial R}$$

$$TN2 \times (3\cos^2\theta - 1) = (G^2\sigma) \times \frac{\partial\theta_2}{\partial R}$$

$$TN3 \times (3\cos^2\theta - 1) + TN4 = (G^2\sigma^2) \times \frac{\partial\Theta_2^2}{\partial R}$$

i.e. $$\frac{\partial\Theta}{\partial R} = \frac{\partial\Theta_o^\circ}{\partial R} + G\sigma\,\frac{\partial\Theta_1^\circ}{\partial R} + G^2\sigma\,\frac{\partial\theta_2^1}{\partial R} + G^2\sigma^2\,\frac{\partial\Theta_2^2}{\partial R}$$

Hence $$\overline{Nu_i} = -\frac{(\beta-1)}{2\beta}\int_0^\pi \frac{\partial\Theta}{\partial R}\Big|_{R=1} \sin\theta\, d\theta$$

$$= 1 - TN4\Big|_{R=1} \qquad (3.6.3)$$

Similarly

$$\overline{Nu_o} = 1 - \beta^2 \times TN4 \Big|_{R=\beta}$$

Equations (3.6.3) and (3.6.4) show that the values of the overall Nusselt numbers are altered from that of pure conduction alone by TN4. The term TN4 comes from Θ_2^2 and is independent of θ i.e. the zeroeth spherical harmonic. Therefore $\overline{Nu}_{i,o}$ are functions of Ra only since the coefficient of Θ_2^2 is Ra^2.

$\overline{Nu}_{i,o}$ increases with increase of β and Ra, and as ω decreases, Figure 3.6.5 and Table I. For fixed values of β and Ra, and as ω tends to unity, this implies that the fluid in the gap of the concentric spheres becomes as conductive as the solid inner sphere. Therefore the heat transfer rate increases. If β is small i.e. $1 \leq \beta \leq 1.25$, the overall heat transfer rate is essentially that of pure conduction as there is relatively no convective motion in the fluid.

The same value of 1.12 for the overall Nusselt number as that given by Mack and Hardee for $\beta=2.0$, $Ra=1000$ is obtained here for computing the conjugate case when $\omega=10^{15}$.

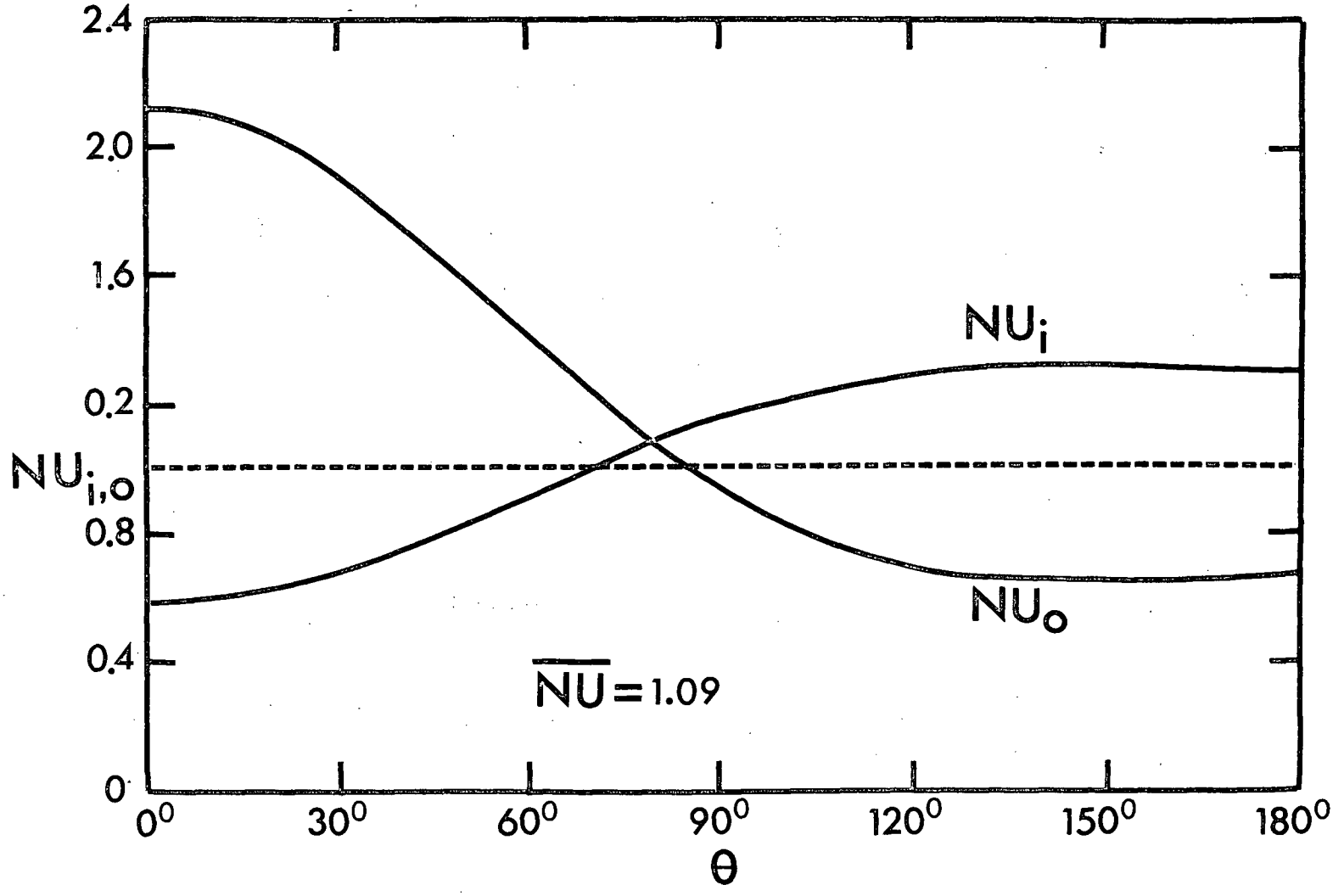

Figure 3.6.1 Nusselt Number Against Angular Position, Conjugate Case $\omega=10$, $\beta=2.0$, $\sigma=.72$, $G=10^3$

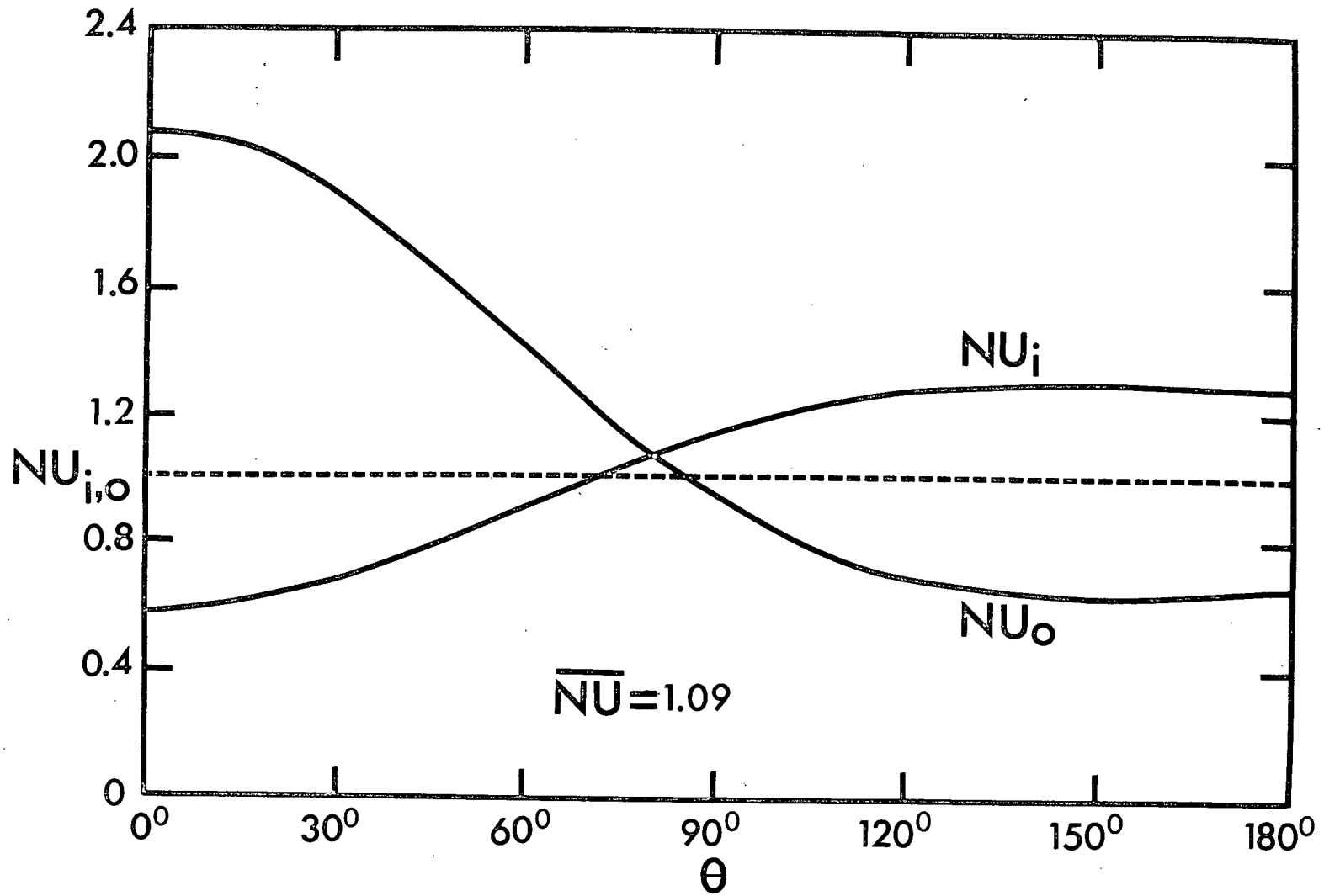

Figure 3.6.2 Nusselt Number Against Angular Position, Conjugate Case, ω=10, β=2.0, σ=10, G=72

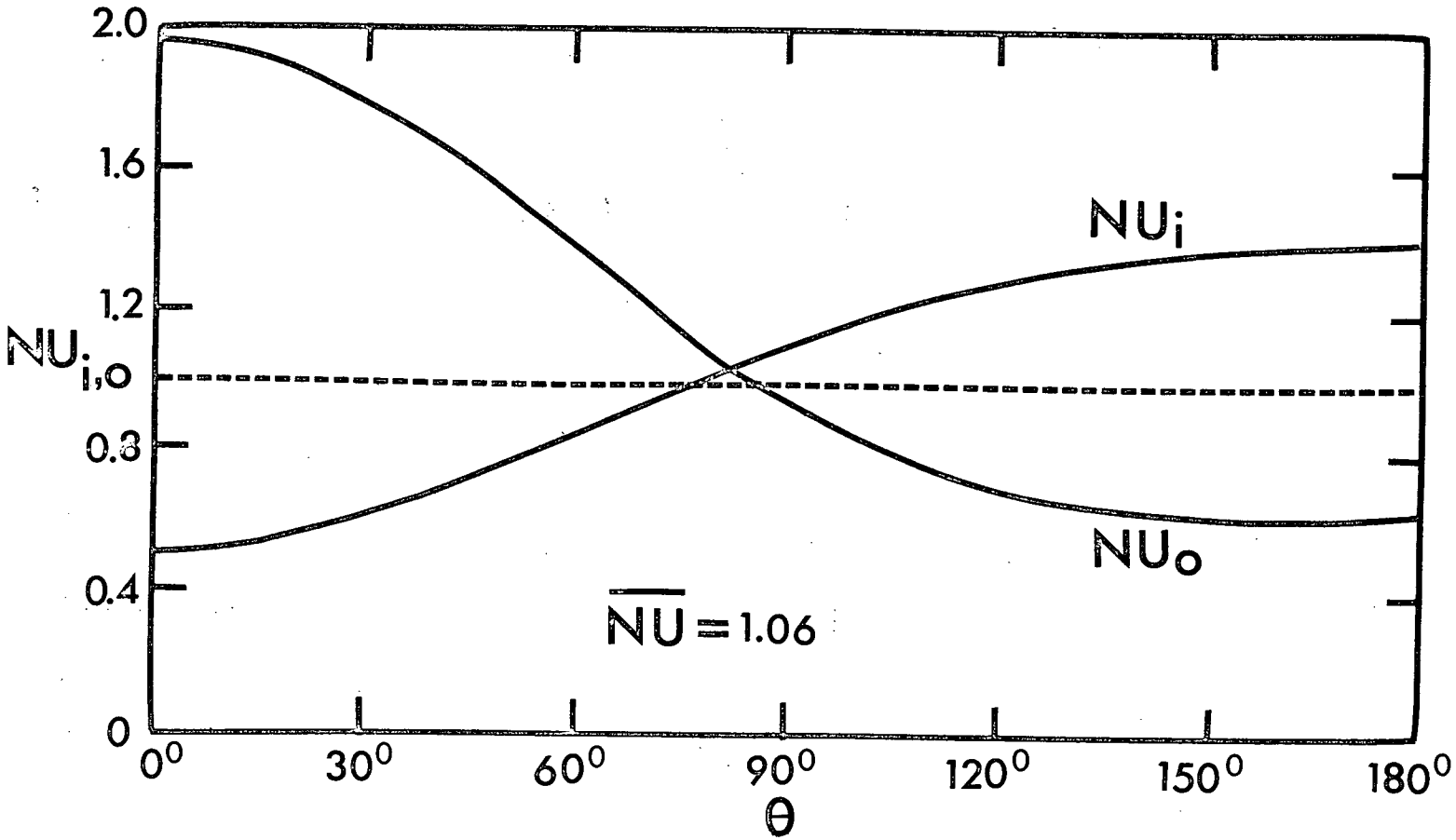

Figure 3.6.3 Nusselt Number Against Angular Position, Conjugate Case, $\omega=10^{15}$, $\beta=2.0$, $\sigma=.72$, $G=10^3$

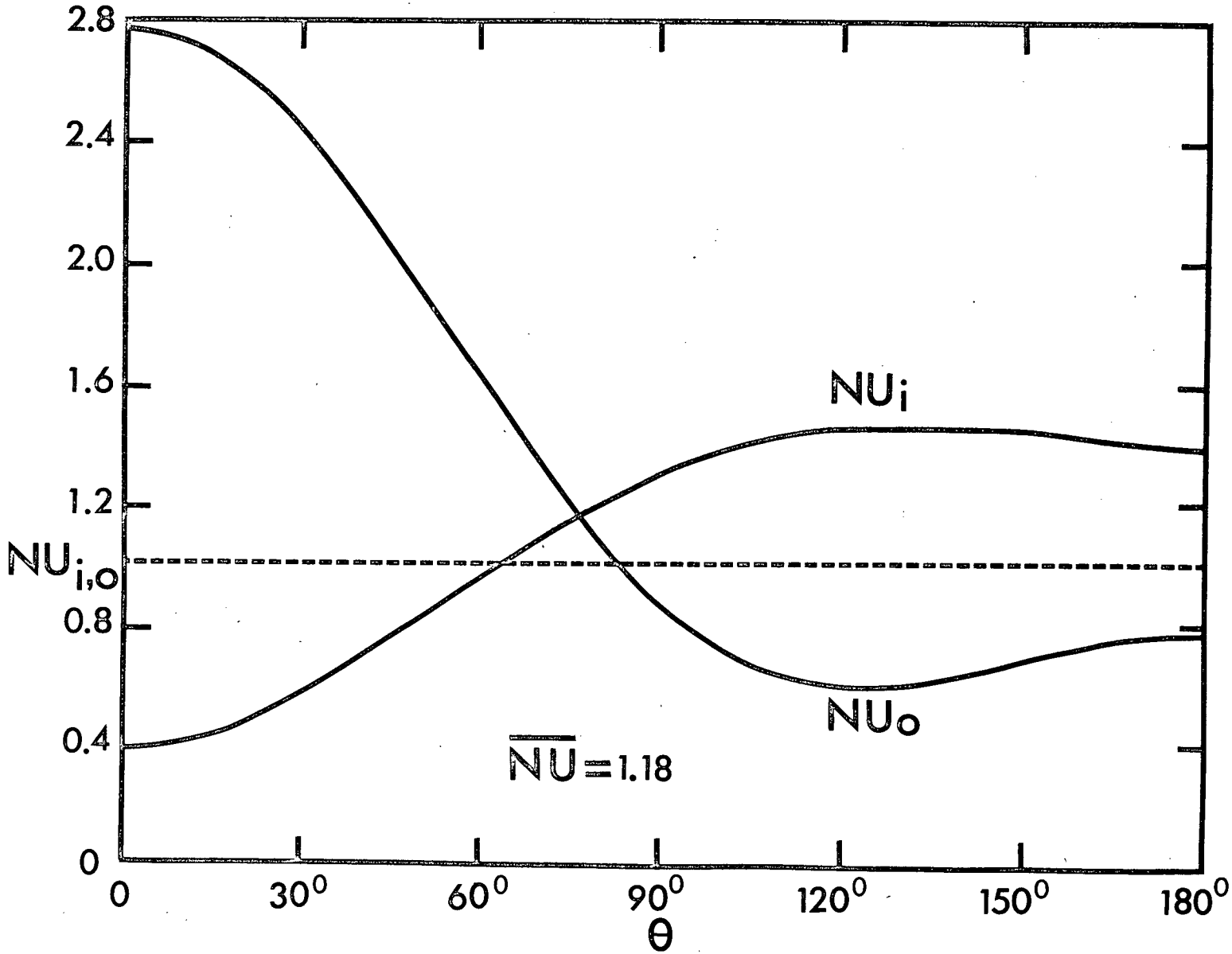

Figure 3.6.4 Nusselt Number Against Angular Position, Conjugate Case, ω=10, β=2.0, σ=.72, G=1400

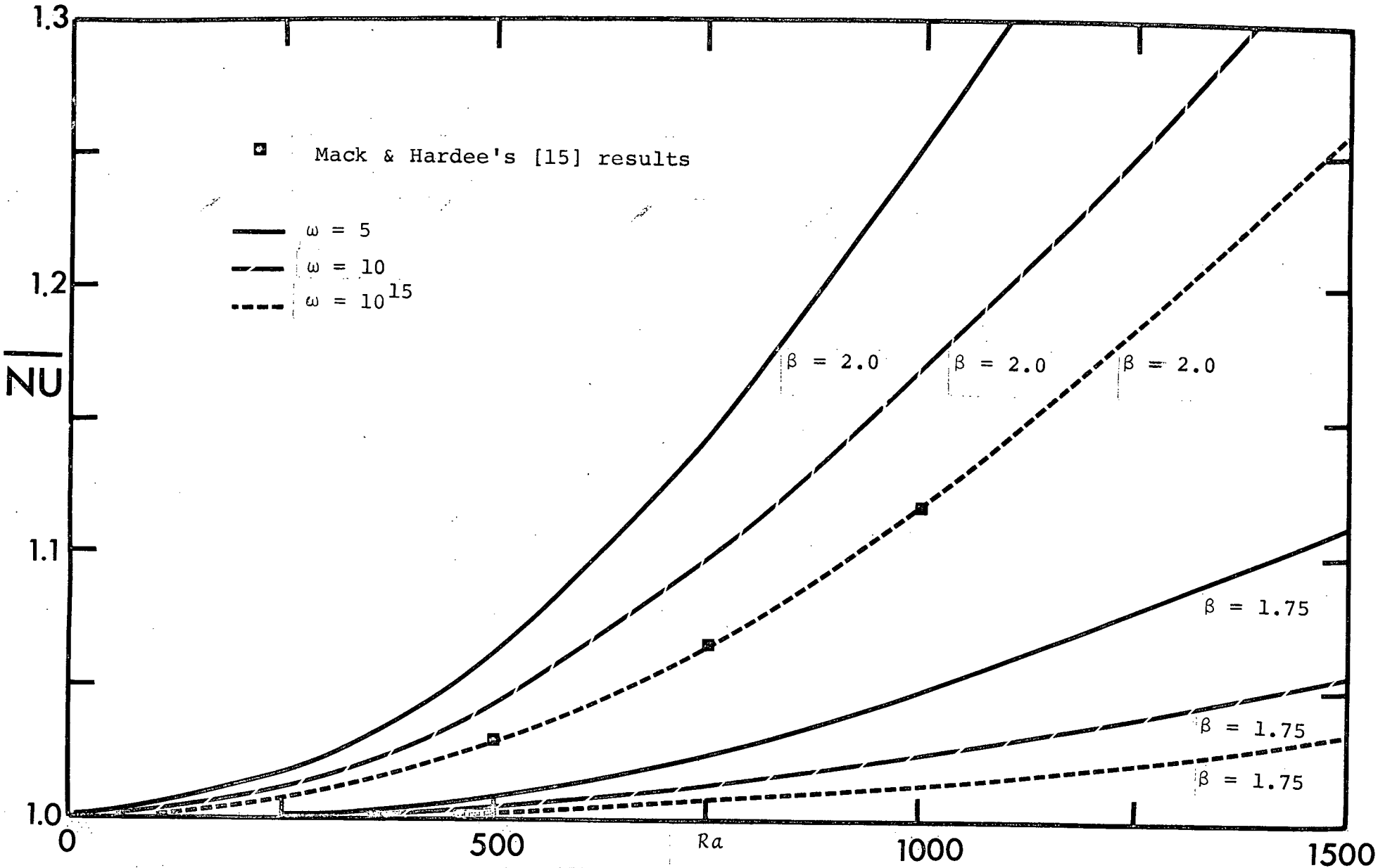

Figure 3.6.5 Overall Nusselt Number as Function of Rayleigh Number, Conjugate Case

TABLE I

OVERALL NUSSELT NUMBERS FOR CONJUGATE CASE, β = 1.15, 2.0, and 3.0

$Ra^* = Ra \times (\frac{\beta}{\beta-1})$			OVERALL NUSSELT NUMBER						
			β=1.15		β=2.0			β=3.0	
Ra^*	G	σ	ω=10	ω=5	$\omega=10^{15}$	ω=10	ω=5	ω=10	ω=5
10	10	0.01	1.000	1.000	1.00	1.00	1.00	1.00	1.00
100	10	0.10	1.000	1.000	1.00	1.00	1.00	1.06	1.08
500	10	0.50	1.000	1.000	1.01	1.01	1.01		
720	10	0.72	1.000	1.000	1.02	1.02	1.03		
1000	10	0.10	1.000	1.000	1.02	1.04	1.06		
1000	10	10	1.000	1.000	1.03	1.04	1.06		
2000	200	10	1.001	1.002	1.12	1.17	1.26		
2000	2800	0.72	1.001	1.002	1.12	1.17	1.26		
3000	300	10	1.001	1.004	1.26	1.36	1.57		
3000	4000	0.72	1.001	1.004	1.26	1.36	1.57		
5000	1000	5	1.004	1.008	1.74				

4. EXPERIMENT

The purpose of the experimental investigation was a flow visualization study of the conjugate natural convection pattern between two concentric spheres. The experimental equipment was designed so that it resembled as closely as possible the analytical model outlined in the previous chapters. The experimental results were expected to give a better understanding of the flow patterns and temperature distributions on the surface of the inner sphere. They were to confirm as well that the flow in the gap between the concentric spheres was steady, laminar and axisymmetrical.

Experiments of this type had been performed by Bishop et al. [6,7] on the convection patterns between concentric isothermal spheres.

4.1 Experimental Apparatus

The experimental apparatus, shown in Figure 4.1.1, consisted of two concentric spheres. The inner sphere was made out of two 6" diameter plexiglas hemispheres. Each of the hemispheres had a 3" diameter hemispherical cavity. Figure 4.1.2 shows the arrangement of the cylindrical heating element with the four thermocouples inside the spherical cavity and the eight thermocouples on the surface of the inner sphere. The positions of the thermocouples are shown

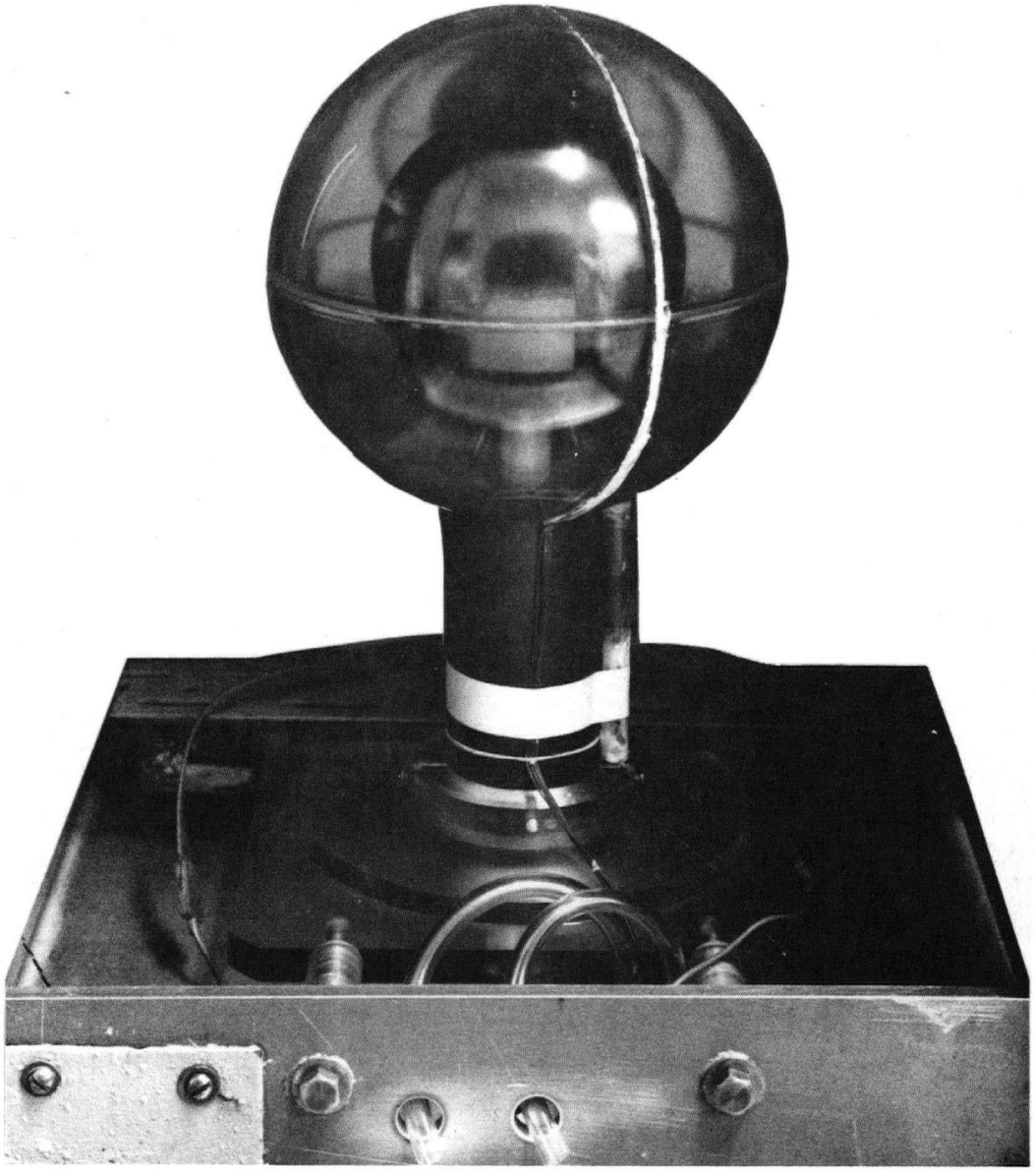

Figure 4.1.1 Experimental Apparatus

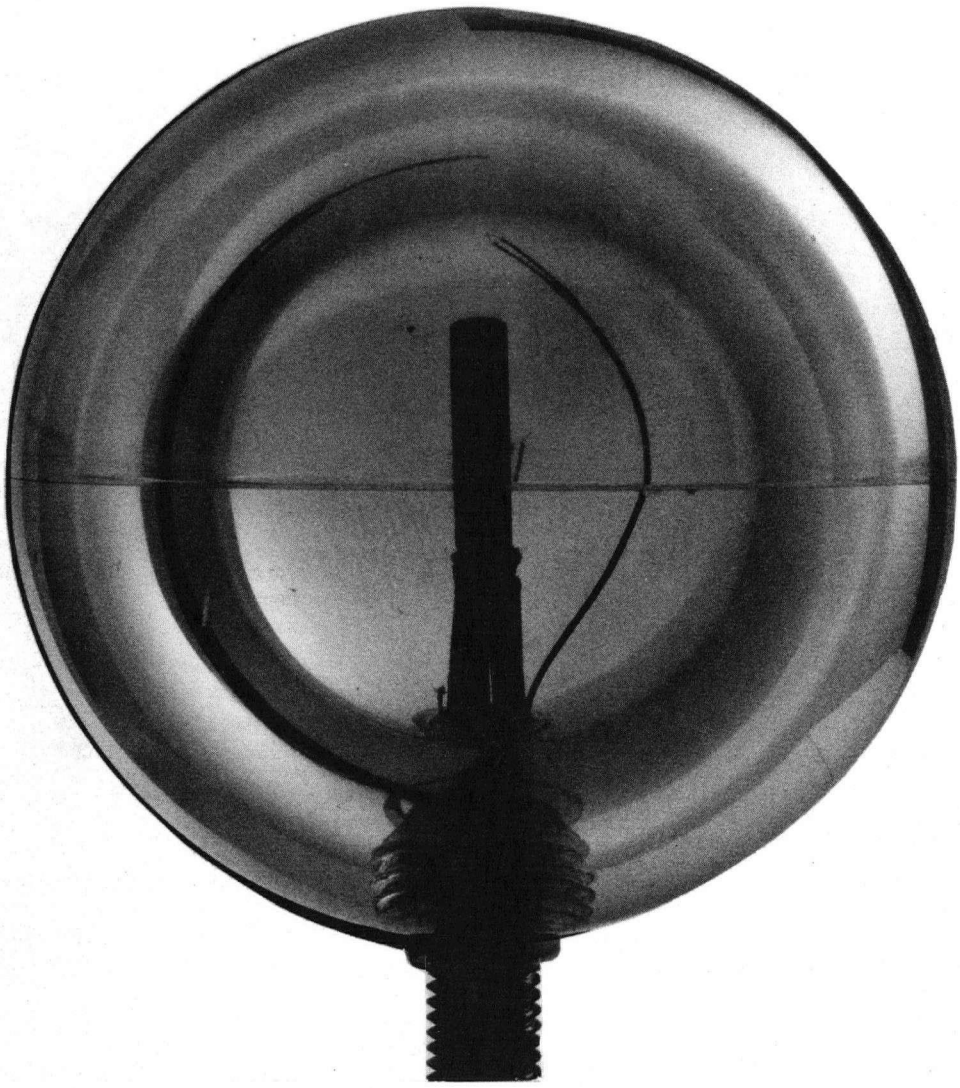

Figure 4.1.2 Plexiglas Inner Sphere

in Figure 4.1.3. The inner sphere was supported by a plexiglas stem, a central hole was drilled through the support stem for the passing of two .066" diameter polyethylene tubes (used for the introduction of silicone oil into the spherical cavity). The silicone oil was required to transfer heat from the heating element evenly to the envelope of the cavity. The heating element had an output of up to 50 watts.

The plexiglas sphere was sprayed with a flat black paint to reduce the reflection of light from it and thus facilitate the photographic work.

The outer sphere consisted of two 10" diameter Corning pyrex glass hemispheres with a .281" wall thickness. The lower half of the outer sphere had a 2" diameter hole. Through this hole a 2" diameter collar of 1/8" high, machined on the 3" outer support stem, was fitted, glued and sealed with silicone compound. As shown in Figure 4.1.4, part of the polystyrene support stem extended into the gap between the concentric spheres. This part was 1 3/4" long, 1" in diameter and threaded internally with a 1/2" diameter hole drilled along the whole length of the support stem. The thermocouple wires and the connecting leads to the heating element were passed through the central hole of both support stems. The inner stem with a 1" diameter, 1/4" high collar was then screwed onto the outer stem. This arrangement ensured the concentricity of the two spheres.

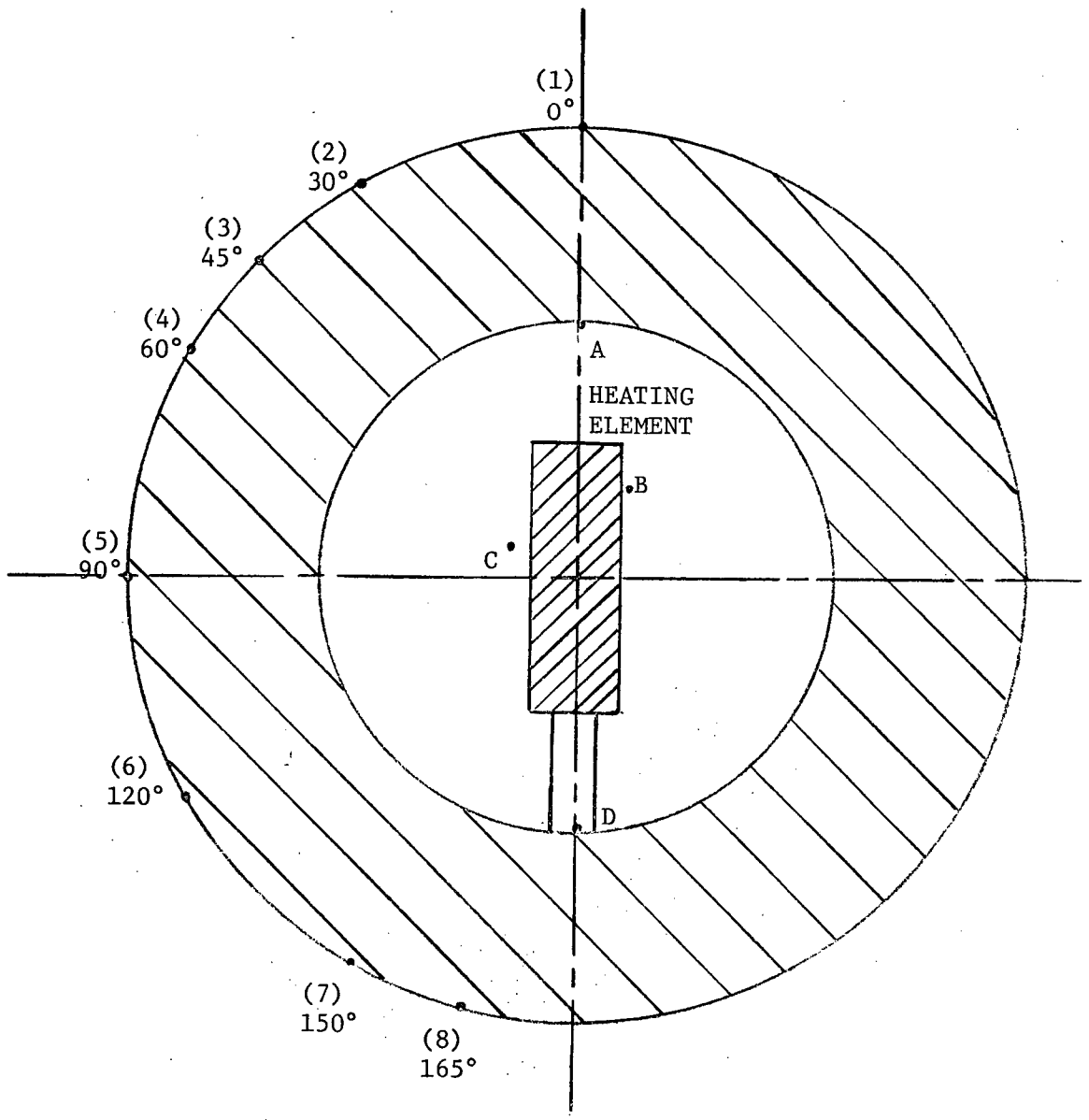

Figure 4.1.3 Locations of Thermocouples on Surface of Inner Sphere

Figure 4.1.4 Support Stem with Glass Hemisphere

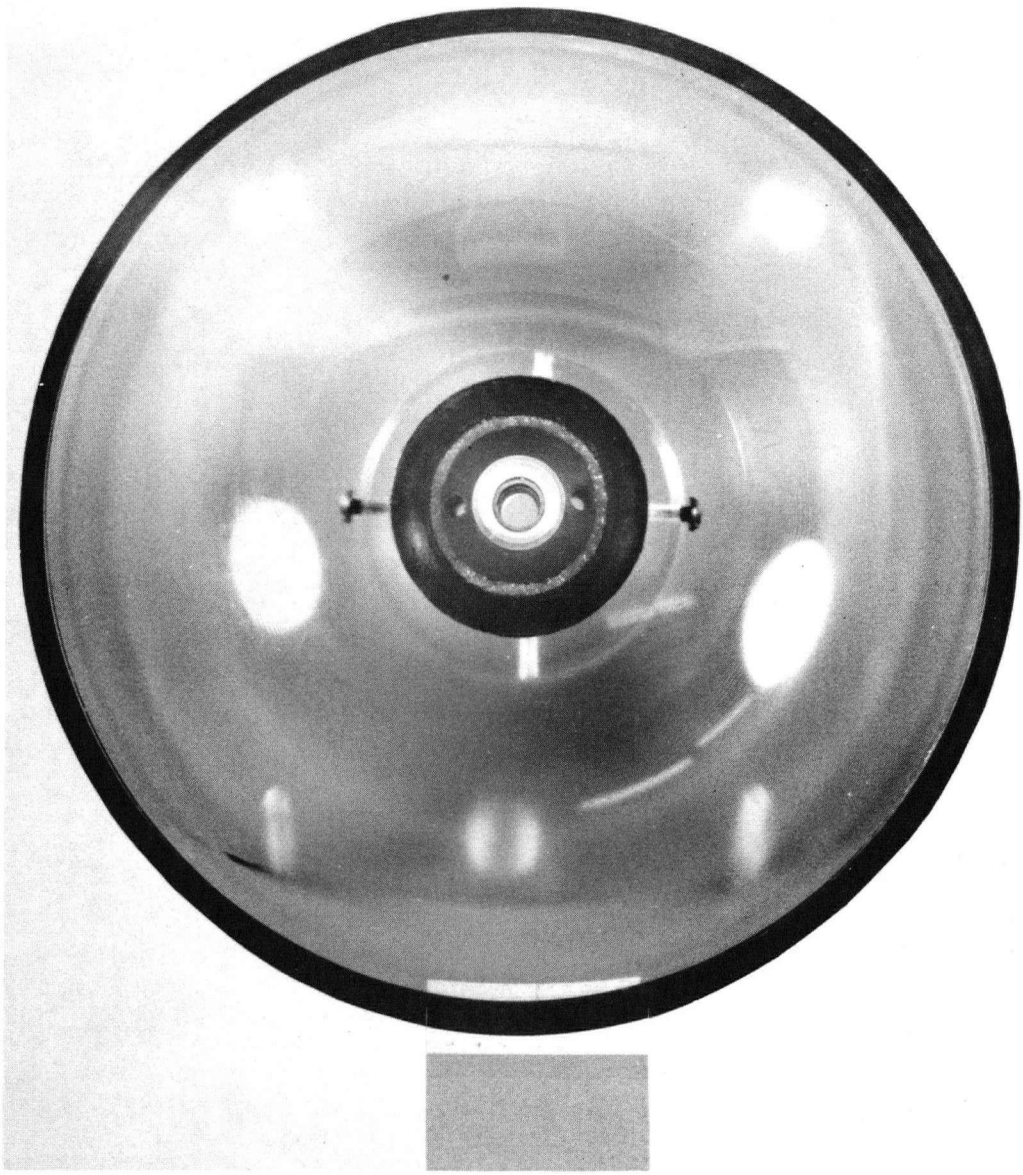

Figure 4.1.5 Top View of Support Stem and Glass Hemisphere

Smoke could be introduced to the gap between the concentric spheres through one of the two 5/8" diameter holes running through the whole length of the outer sphere support stem, Figure 4.1.5. The Pyrex hemispheres were sealed together with silicone glue. The surface temperature of the outer sphere was measured by four thermocouples at positions of 0°, 30°, 90° and 120°.

The outer sphere support stem was mounted onto a plexiglass base. The base was held in position by two brass bolts to the frame of a water tank (30" x 28" x 30") as shown in Figure 4.1.1. The water tank was used to provide a constant temperature bath. A temperature controller designed by the Geophysics Department,* University of British Columbia, was used to control the water temperature in the tank. The platinum wire temperature sensing probe of the temperature controller was taped to the side of the outer sphere support stem. A 'Brisket' heating tape (output capacity 60 watts) connected to the temperature controller was placed around the plexiglas base, Figure 4.1.1. The water in the tank was circulated from the top to the bottom of it by a 'Randolph' pump which was connected to the outlet and inlet pipes at the aluminium back-plate of the tank.

The thermocouple wires used were of 36 gauge Chromel-Alumel type. Figure 4.1.6 shows a typical calibration curve for the thermocouples. As the calibration data followed the

*The help of Dr. Russel and Mr. B. Goldberg in designing this item is gratefully acknowledged.

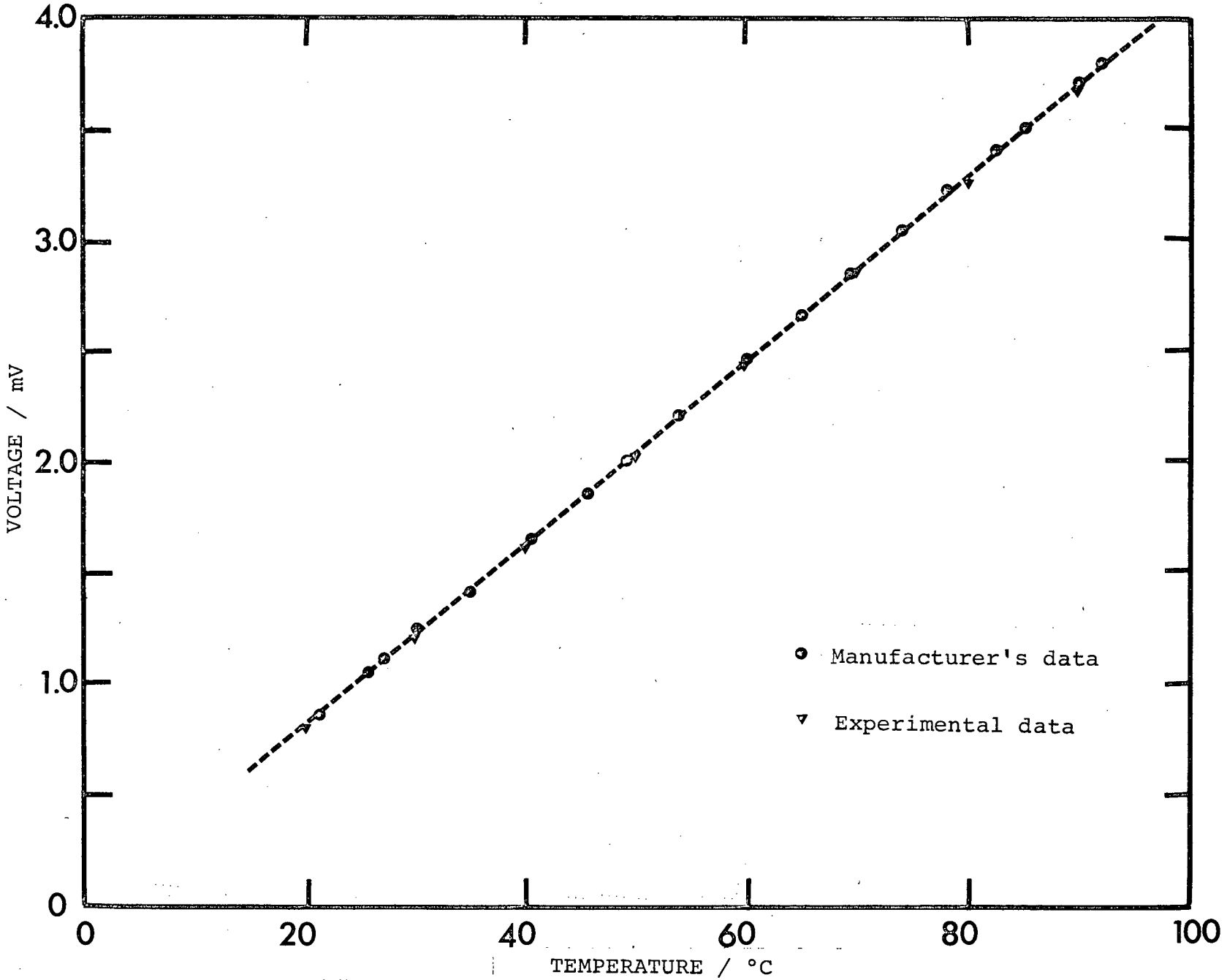

Figure 4.1.6 Typical Thermocouple Calibration Curve

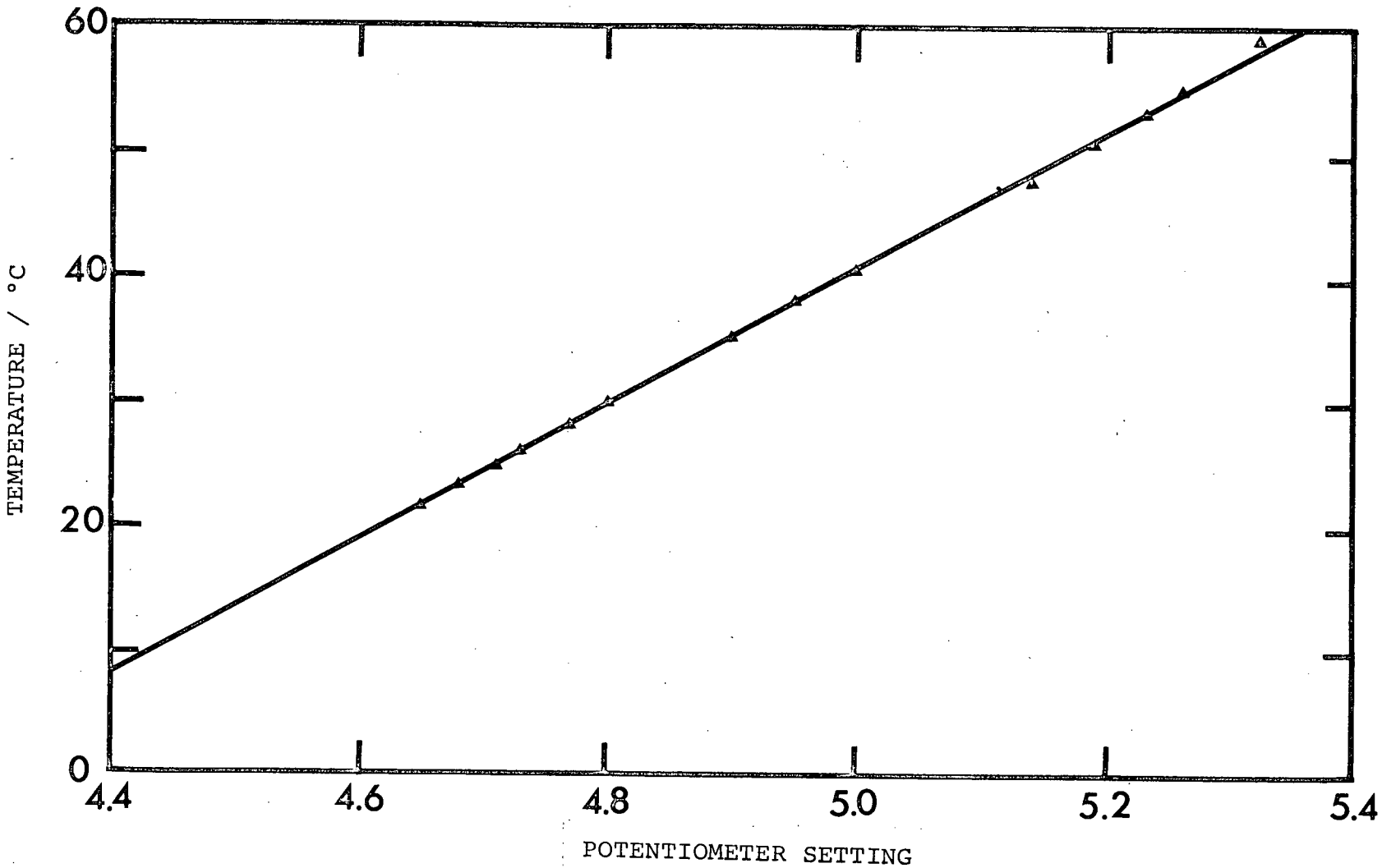

Figure 4.1.7 Platinum-Wire Temperature-Sensing Probe, Calibration Curve

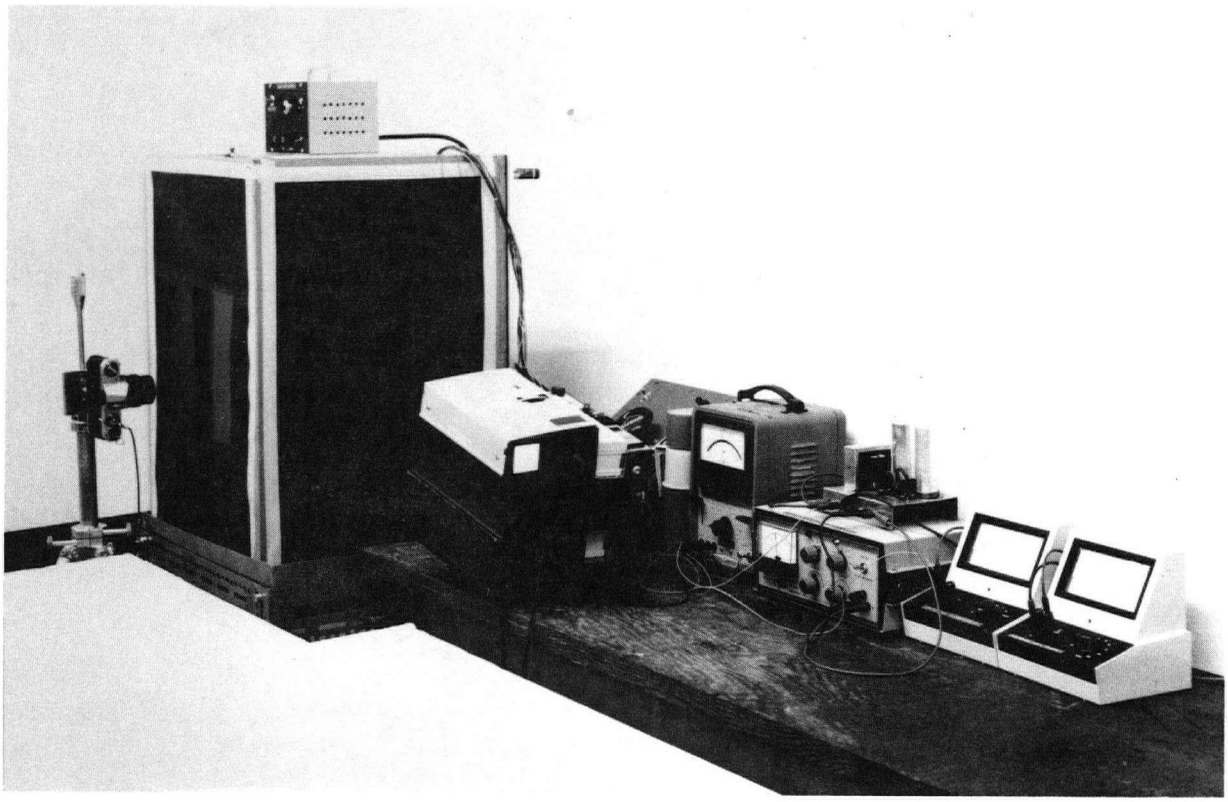

Figure 4.1.8 Layout of Experimental Apparatus

manufacturers' data very closely, only three of the thermo-couples were calibrated. The platinum wire sensing probe was also calibrated, Figure 4.1.8.

The sides of the tank were either painted black or lined with black construction paper so that the whole enclosure was dark to facilitate photographic work. A central narrow slit of 1/8" width was cut into the black paper lining at one side of the tank for collimating the illuminating light. Two 500-watts 35 mm slide projectors were positioned in front of the slit so that a vertical plane of light traversed the centre plane of the concentric spheres. On the adjacent side of the tank a rectangular opening was cut into the black paper lining to allow visual and photographic observation of the flow pattern in the illuminated vertical plane between the concentric spheres. Figure 4.1.8 shows the whole experimental apparatus assembled.

4.2 Experimental Procedure

Owing to the low thermal conductivity of plexiglas the inner sphere was heated up slowly in small increments of heating-rates until the desired value was achieved. Sufficient time was allowed to elapse before the heating rate was increased. A L-C filter unit was used to smooth out the heating current (supplied by a Heathkit regulated low voltage D.C. power source). At the same time, the water temperature

in the tank was kept constant. Before each experimental run, a period of approximately two days was allowed to achieve steady-state, such that the thermocouples' readings were constant over this period.

Cigar smoke was gently introduced into the gap between the concentric spheres through either one of the two tubings (Figure 4.1.1) which connected the two 1/8" holes in the outer sphere support stem to the two openings at the back plate of the tank. Sufficient time was allowed for the stabilization of the flow pattern before photographs were taken. A 35 mm camera and Kodak TRI-X film with a speed of 400 ASA were used for photography. The light source from the two projectors was switched on only when photographs were taken. This avoided supplementary heating of the inner sphere surface through absorption of radiation from the light source.

Focusing the camera directly on the illuminating plane was difficult and unsuccessful. So an indirect method was used whereby the camera was focused onto a finely printed surface placed adjacent to the outer sphere, in the plane of the path of the illuminating light. A polarizing filter was attached to the camera lens to eliminate most of the reflections from the inner sphere. Exposure times were either 1/2 second or 1 second with lens apertures setting at F5.6 and F8 respectively. The exposed film was developed using Kodak D-19 developer for 10 minutes so as to raise the film speed to 800 ASA. The photographs were printed on high contrast paper for better contrast of the smoke patterns.

4.4 Experimental Results

Figures 4.4.1 to 4.4.3 are photographs of the flow pattern in the gap between the concentric spheres obtained under three operating conditions. Due to the thickness of the outer glass sphere, its inner surface acted as a reflector. This caused the bright and dark regions over the surface of the outer sphere. There are two dark lines across the gap in the photographs. These are the shadows of the horizontal seal between the two halves of the outer sphere. There are some dust particles on the surface of the outer sphere which appear as bright scatter spots in the photographs. Similarly, the white line starting from the top of gap is the reflection of the outer sphere surface thermocouples. The reflection of light by the outer sphere support stem appears as a white region in the bottom of the gap.

From both visual and photographic observations it is seen that the flow pattern in the gap between the concentric spheres is steady and axisymmetrical about the vertical axis. At the diameter ratio used (β=1.67) and for all three temperature differences, the flow pattern is of the 'crescent-eddy' type as predicted in the analysis. The flow patterns can essentially be divided into two regions as follow:
(a) the region in the immediate vicinity of each sphere where there is a thin-layer of high velocity flow;
(b) the central eddy region where the fluid is moving relatively slowly. The fluid velocity near the inner sphere

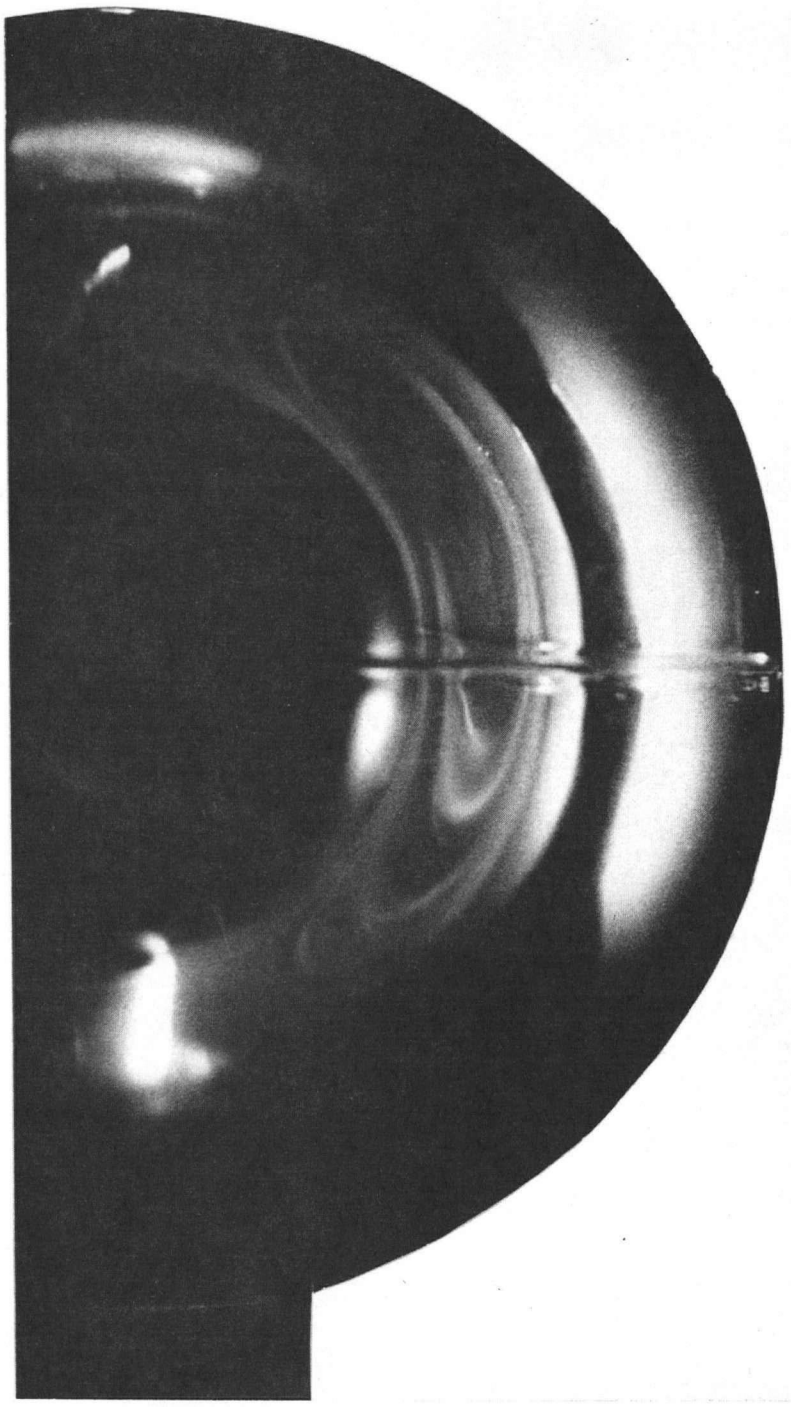

Figure 4.4.1 Smoke Pattern at $G=1.32 \times 10^4$, $\Delta T = .024°C$

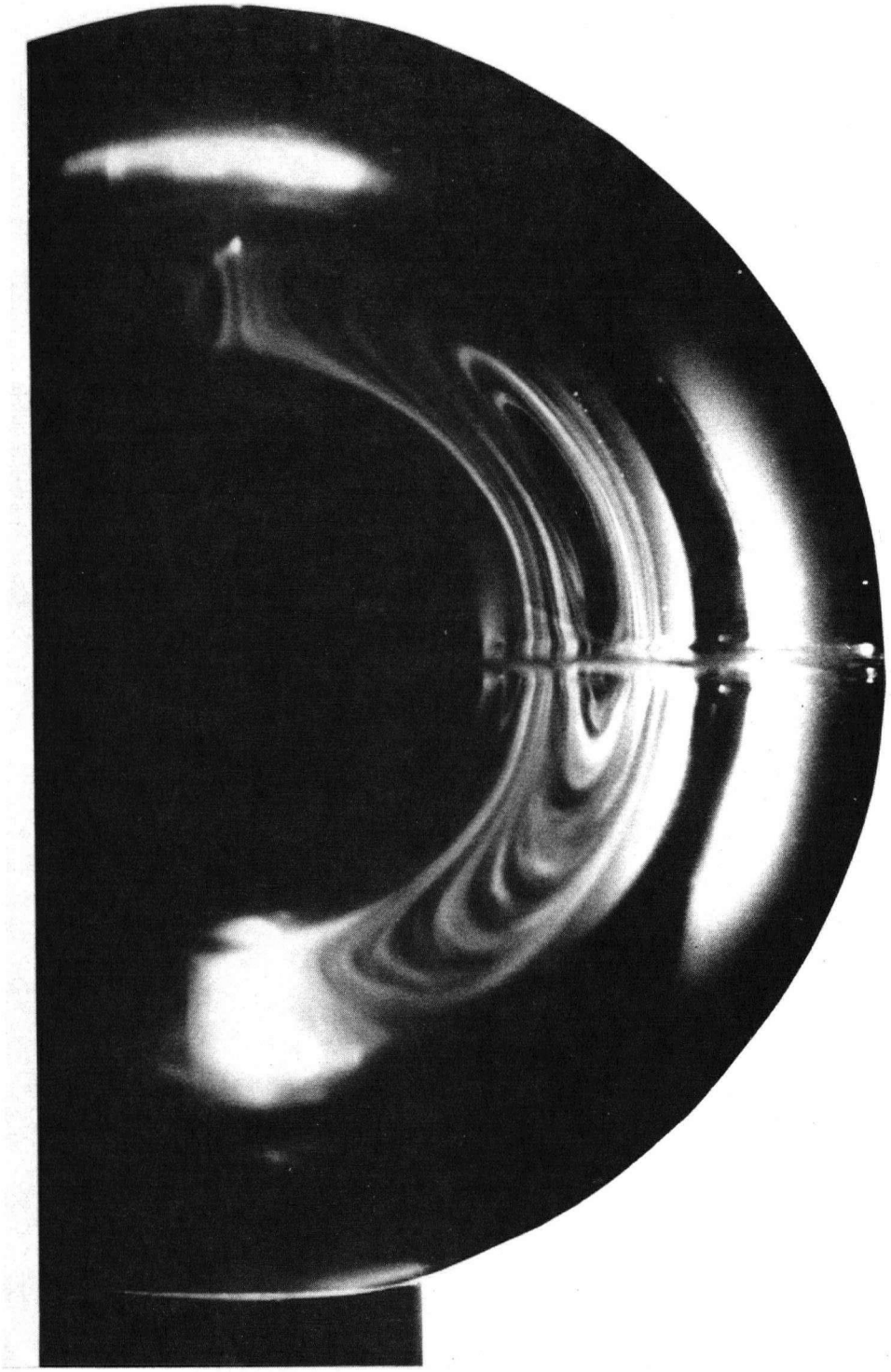

Figure 4.4.2 Smoke Pattern at $G=3.72 \times 10^5$, $\Delta T = 7.21°C$

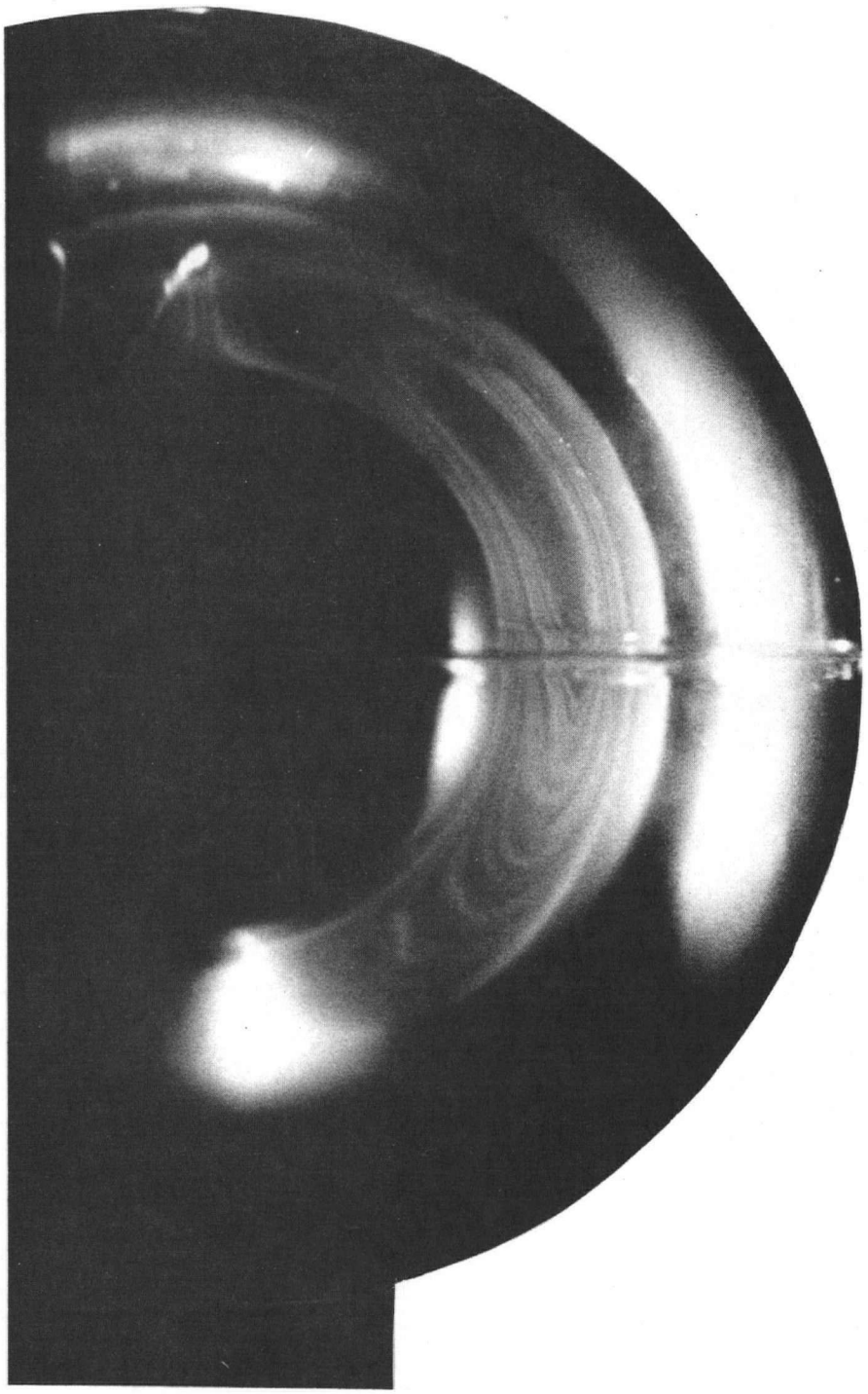

Figure 4.4.3 Smoke Pattern at $G = 5.78 \times 10^5$, $\Delta T = 10.3°C$

is higher than that near the outer sphere. At the top of the inner sphere there is a jet-like flow polarization. The fluid separates from the inner sphere near the top and flows downward along the outer sphere into the bottom of the gap. This region is relatively stagnant and acts as if it were a reservoir. The centre of the eddy is in the upper half of the gap between the concentric spheres. Its position remains relatively stationary for all three temperature differences tested.

Bishop et al. [7] had reported that in their experiment on natural convention between concentric isothermal spheres, as the high speed flow separated from the top of the inner sphere, a corner eddy was observed in the 'corner' formed by the intersection of the surface of the inner sphere with the vertical axis of symmetry. However, this phenomenon is not observed here for natural conjugate convection.

Tables II, III and IV show the temperature distributions on the surface of the inner sphere, the temperature of the oil in various positions (Figure 4.1.2) in the cavity inside the inner sphere and the surface temperature of the outer sphere. In each case, the temperature on the surface of the inner sphere decreases as θ increases, as predicted theoretically.

The following Tables (II to IV) show the temperature distribution on the surfaces of the concentric spheres at the positions indicated in Figure 4.1.2.

TABLE II

$\dot{Q}$ = 1.4 watts		ΔT = .024°C ,		$G = 1.32 \times 10^4$	
	Position	Temperature		Position	Temperature
(1)	0°	28.3	(9)	A	33°C
(2)	30°	28°C	(10)	B	34.2°C
(3)	45°	28°C	(11)	C	-
(4)	60°	27.5°C	(12)	D	36.6°C
(5)	90°	26.5°C	(13)	0°*	24.5°C
(6)	120°	-	(14)	30°*	24.5°C
( )	150°	25.5°C	(15)	90°*	24.5°C
(8)	165°	25.3°C	(16)	120°*	24.5°C

*Outer Sphere.

TABLE III

$\dot{Q}$ = 4.29 watts		ΔT = 7.21°C ,		$G = 3.72 \times 10^5$	
	Position	Temperature		Position	Temperature
(1)	0°	35.5°C	(9)	A	48.5°C
(2)	30°	35.4°C	(10)	B	49.5°C
(3)	45°	35.1°C	(11)	C	36.2°C
(4)	60°	32.5°C	(12)	D	54°C
(5)	90°	31°C	(13)	0°*	25.3°C
(6)	120°	-	(14)	30°*	25.3°C
(7)	150°	28.8°C	(15)	90°*	25.3°C
(8)	165°	28.3°C	(16)	120°*	25.3°C

*Outer Sphere.

TABLE IV

$\dot{Q}$ = 6.14 watts		ΔT = 10.3°C ,		$G = 5.78 \times 10^5$	
	Position	Temperature		Position	Temperature
(1)	0°	37.5°C	(9)	A	61°C
(2)	30°	37.0°C	(10)	B	68.5°C
(3)	45°	37.0°C	(11)	C	-
(4)	60°	36.8°C	(12)	D	72.5°C
(5)	90°	36.5°C	(13)	0°*	24.5°C
(6)	120°	-	(14)	30°*	24.5°C
(7)	150°	31.4°C	(15)	90°*	24.5°C
(8)	165°	31.2°C	(16)	120°*	24.5°C

*Outer sphere.

Although the experimental results obtained here are for the values of $\omega \simeq 15$, $\beta = 1.67$, $\sigma = 0.72$ and appreciably higher G numbers than those for which the perturbation expansions will be valid, the flow pattern and the temperature distributions on the surface of the inner sphere are qualitatively similar to those predicted by the analysis. Moreover, the experimental results confirm that the flow in the gap between the concentric spheres is steady, laminar and axisymmetrical, assumptions used in the analysis.

5. CONCLUSIONS

The present investigation has led to the following results:

1. Theoretical solutions for the governing equations for steady laminar axisymmetrical conjugate natural convection between two concentric spheres were obtained. The case of a constant flux inner sphere with an isothermal outer sphere was solved separately.
2. The limits of the applicability of the solutions were defined.
3. The streamline configuration was found to be of the crescent-eddy type. The existence of secondary cells was found not to be a genuine feature of either the conjugate or the non-conjugate cases considered here.
4. Contours of isovorticity lines, isotherms and distributions of velocity and temperature of the fluid in the gap between the concentric spheres were obtained and discussed.
5. Local heat transfer rates from both inner and outer spheres were determined.
6. The influence of Prandtl number on the overall heat transfer rate was found to be a higher-order effect.

7. The flow pattern obtained experimentally is steady, laminar, axisymmetrical and of the crescent-eddy type.
8. The experimental results support the analysis at the very least qualitatively.

REFERENCES

1. G.K. Batchelor, Heat transfer by free convection across a closed cavity between vertical boundaries at different temperatures, Quart. J. Applied Math. 3, 1954, 209-233.

2. G. Poots, Heat transfer by laminar free convection in enclosed plane gas layers, Quart. J. Mech. Applied Math. 11, 1958, 257-273.

3. J.O. Wilkes and S.W. Churchill, The finite-difference computation of natural convection in a rectangular enclosure, A.I. Ch. E. 12, 161-166.

4. J.W. Elder, Numerical experiments with free convection in a vertical slot, J. Fluid Mech. 24, 1966, 823-843.

5. G. de Vahl Davis, Laminar Natural convection in an enclosed rectangular cavity, Intern. J. Heat/Mass Transfer 11, 1968, 1675-1693.

6. E.H. Bishop, R.S. Kolfat, L.R. Mack and J.A. Scanlan, Photographic studies of convection patterns between concentric spheres, S.P.I.E. J. 3, 1964, 47-49.

7. E.H. Bishop, R.S. Kolfat, L.R. Mack and J.A. Scanlan, Convective heat transfer between concentric spheres, Proc. 1964 Heat Transfer / Fluid Mech. Inst., (Stanford U.P. 1964), 69-80.

8. E.H. Bishop, L.R. Mack and J.A. Scalan, Heat transfer by natural convection between concentric spheres, Intern. J. Heat/Mass Transfer 9, 1966, 6949-662.

9. L.R. Mack and E.H. Bishop, Natural convection between horizontal concentric cylinders for low Rayleigh numbers, Quart. J. Mech. Applied Math. 21, 1968, 223-241.

10. L.R. Mack and H.C. Hardee, Natural convection between concentric spheres at low Rayleigh numbers, Intern. J. Heat/Mass Transfer 11, 1968, 387-396.

11. T.L. Perelman, On Conjugated problems of heat transfer, Intern. J. of Heat/Mass Transfer 3, 1961, 293-303.

12. Z. Rotem, The effect of thermal conduction of the wall upon convection from a surface in a laminar boundary layer, Intern. J. Heat/Mass Transfer 10, 1967, 461-466.

13. M.D. Kelleher and K-T. Yang, A steady conjugate heat transfer problem with conduction and free convection, Applied Sci. Res. 17, 1967, 249-269.

14. G.S.H. Lock and J.C. Gunn, Laminar free convection from a downward-projecting fin, J. Heat Transfer ASME Series C, 1968, 63-70.

15. E.J. Davis and W.N. Gill, The effects of axial conduction in the wall on heat transfer with laminar flow, Intern. J. Heat/Mass Transfer 13, 1970, 459-470.

16. Z. Rotem. Conjugate free convection from horizontal conducting circular cylinders, Int. J. of Heat/Mass Transfer 19, 1971, in press.

17. L. Knopoff, The convection current hypothesis, Reviews of Geophysics 2, 1964, 89-122.

18. M. Van Dyke, Perturbation methods in fluid mechanics, Academic Press 1964.

19. F.E. Fendell, Laminar natural convection about an isothermal heated sphere at small Grashof number, J. Fluid Mech. 34, 1968, 163-176.

20. C.A. Hieber and B. Gebhart, Mixed convection from a small sphere at small Reynolds and Grashof numbers, J. Fluid Mech. 38, 1969, 137-159.

21. J.A. Scanlan, E.H. Bishop and R.E. Powe, Natural convection heat transfer between concentric spheres, Intern. J. Heat/Mass Transfer 13, 1970, 1857-1872.

22. J. Proudman and J.R.A. Pearson, Expansions at small Reynolds numbers for the flow past a sphere and a circular cylinder. J. Fluid Mech. 2, 1957, 237-262.

23. J.J. Mahoney, Heat transfer at small Grashof number. Proc. Roy. Soc. A238, 1957, 412-423.

24. Md. A. Hossain and B. Gebhart, Natural convection about a sphere at low Grashof number, Fourth Intern. Heat Transfer Conference, Paris, 1970, Vol. 4, 1-12.

APPENDIX I

CALCULATION OF VISCOUS DISSIPATION EFFECT

The energy equation of the fluid including the viscous dissipation terms (with rotational symmetry) expressed in spherical coordinates is

$$K_f \nabla^2 T - \rho C_p \left(V'_R \frac{\partial T}{\partial R'} + \frac{V'_\theta}{R'} \frac{\partial T}{\partial \theta} \right) + \mu \Phi_v = 0 \qquad \text{(A-1)}$$

where $\mu\Phi_v$ is the dissipation term of mechanical energy by viscous effects per unit volume. The dissipation function,

$$\Phi_v = 2 \left\{ \left(\frac{\partial V'_R}{\partial R} \right)^2 + \left(\frac{V'_R}{R'} + \frac{1}{R'} \frac{\partial V'_\theta}{\partial \theta} \right)^2 + \left(\frac{V'_R}{R} + \frac{V'_\theta}{R'} \cot \theta \right)^2 \right\}$$

$$+ \left[R' \frac{\partial}{\partial R'} \left(\frac{V'_\theta}{R'} \right) + \frac{1}{R'} \frac{\partial V'_R}{\partial \theta} \right]^2 \quad .$$

The dimensionless radial and tangential components of velocity are introduced as follows,

$$V_R = \frac{R'_i}{\nu'} V'_R \quad ; \quad V_\theta = \frac{R'_i}{\nu'} V'_\theta \quad .$$

Rendering the energy equation (A-1) dimensionless,

$$\nabla^2\Theta - \sigma \left(V_R \frac{\partial\Theta}{\partial R} + \frac{V_\theta}{R} \frac{\partial\Theta}{\partial\theta}\right) + \mathcal{D}\Phi_v = 0 \qquad \text{(A-2)}$$

where the viscous dissipation number is

$$\mathcal{D} = \frac{\mu \nu^2}{R_i^2 K_f \Delta T_{ref}} .$$

Let

$$\varepsilon = \frac{\mathcal{D}\Phi_v}{\nabla^2\Theta}$$

denote the dimensionless ratio of the viscous dissipation term to the conduction term.

Let

$$\lambda = \frac{\mathcal{D}\Phi_v}{\sigma\left(V_R \frac{\partial\Theta}{\partial R} + \frac{V_\theta}{R} \frac{\partial\Theta}{\partial\theta}\right)}$$

denote the dimensionless ratio of the viscous dissipation term to the convection term.

For air with G=1000, σ=0.72, R_i'=1 ft, β=2.0, ω=10 and $\mathcal{D}$=1.146 x 10^{-10}, the values of $|\varepsilon|$ and $|\lambda|$ at both angular and radial positions in the gap between the two concentric spheres are given in Table V.

TABLE V

RATIO OF VISCOUS DISSIPATION TERM TO CONDUCTION TERM: RATIO OF VISCOUS DISSIPATION TERM TO CONVECTION TERM (AIR)

R	1.1	1.3	1.5	1.8	θ
$\|\varepsilon\|$	6.58×10^{-11}	3.56×10^{-11}	3.16×10^{-11}	3.27×10^{-11}	15°
$\|\lambda\|$	2.72×10^{-9}	9.25×10^{-10}	1.84×10^{-8}	5.00×10^{-10}	15°
$\|\varepsilon\|$	1.89×10^{-9}	9.10×10^{-10}	7.95×10^{-10}	8.15×10^{-10}	60°
$\|\lambda\|$	5.42×10^{-10}	2.28×10^{-10}	3.54×10^{-9}	1.80×10^{-10}	60°
$\|\varepsilon\|$	3.23×10^{-10}	1.64×10^{-10}	1.45×10^{-10}	1.49×10^{-10}	135°
$\|\lambda\|$	8.00×10^{-10}	4.94×10^{-10}	1.43×10^{-9}	4.10×10^{-10}	135°

For water with $G=62$, $\sigma=11.6$, $R_i'=1$ ft, $\beta=2.0$, $\omega=10$ and $\mathcal{D}=4.42\times10^{-12}$, the values of $|\varepsilon|$ and $|\lambda|$ at both angular and radial positions in the gap between the two concentric spheres are given in Table VI.

TABLE VI

RATIO OF VISCOUS DISSIPATION TERM TO CONDUCTION TERM: RATIO OF VISCOUS DISSIPATION TERM TO CONVECTION TERM (WATER)

R	1.1	1.3	1.5	1.8	θ
$\|\varepsilon\|$	6.33×10^{-13}	6.78×10^{-14}	4.21×10^{-14}	3.07×10^{-14}	15°
$\|\lambda\|$	8.98×10^{-12}	4.14×10^{-12}	8.99×10^{-12}	9.05×10^{-12}	15°
$\|\varepsilon\|$	4.65×10^{-13}	1.22×10^{-12}	9.45×10^{-13}	1.17×10^{-12}	60°
$\|\lambda\|$	2.19×10^{-11}	6.63×10^{-12}	1.33×10^{-9}	2.80×10^{-12}	60°
$\|\varepsilon\|$	5.12×10^{-13}	2.57×10^{-13}	1.81×10^{-13}	1.37×10^{-13}	135°
$\|\lambda\|$	2.58×10^{-11}	1.05×10^{-11}	7.60×10^{-11}	5.62×10^{-12}	135°

Tables V and VI show that the relative order of magnitude of the viscous dissipation term to either the conduction term ($|\varepsilon|$) or the convection term ($|\lambda|$) is at least of the order of 10^{-8}. Thus the assumption that the viscous dissipation of energy in the fluid assumed in section 2.1 to be negligible is found to be valid.

APPENDIX II

CONJUGATE PROBLEM WITH INNER SPHERE CONTAINING DISTRIBUTED SOURCES

Consider now the inner sphere of the conjugate problem in section 2 with uniform distributed heat sources instead of a single heat source at its centre. The energy equation of the inner sphere then becomes

$$K_s \times \nabla^2 \tilde{T}_i = \mathcal{B}(R) \qquad \text{(B-1)}$$

where $\mathcal{B}(R)$ is the heat source function per unit volume assumed constant. The reference temperature, ΔT_{ref}, defined in section 2.2, with $\dot{Q}$ replaced here by $\mathcal{B} \times \frac{4}{3} \pi R_i'^3$

$$\Delta T_{ref} = \frac{\mathcal{B} \times \frac{4}{3} \pi R_i'^3 \times (\beta-1)}{4\pi \beta R_i' K_f}$$

$$= \frac{\mathcal{B} R_i'^2 (\beta-1)}{3\beta K_f}$$

Rendering the energy equation (B-1) dimensionless, it becomes

$$\nabla^2 \tilde{\Theta} = \frac{3\beta}{\omega (\beta-1)} \qquad \text{(B-2)}$$

$$= \text{constant for given values of } \omega \text{ and } \beta .$$

Then the energy equation (2.2.3) given in section 2.2 for the inner sphere is replaced here by equation (B-2). The boundary conditions and the method of solution for this case are exactly the same as previously described in section 2. Also the set of uncoupled linear differential equations given in section 2.3 remains essentially the same with the sole exception that the equation (2.3.7) is replaced here by

$$\nabla^2 \tilde{\Theta}_o^o = \frac{3\beta}{\omega\ (\beta-1)} \qquad \text{(B-3)}$$

Equation (B-3) is solved simultaneously with equation (2.3.8) subject to the boundary conditions (2.3.18) and (2.3.19). The solutions are

$$\tilde{\Theta}_o^o = \frac{\beta}{\omega\ (\beta-1)} \left(\frac{2}{R} - \frac{5}{2} + \frac{r^2}{2} \right)$$

$$\Theta_o^o = \frac{\beta}{(\beta-1)} \left(\frac{1}{R} - 1 \right)$$

As the equations for ψ and the higher order terms of the Θ, and $\tilde{\Theta}$ expansions and the boundary conditions remain unchanged; their solutions are those given in section 2.4 .

Hence for the conjugate problem the stream function, Ψ and the temperature distribution Θ of the fluid in the gap of the two concentric spheres do not depend on what form of heat source distribution inside the inner sphere. However, the inner sphere temperature distribution does depend on the heat source distribution inside the inner sphere.

APPENDIX III

A BRIEF REVIEW ON SMALL GRASHOF NUMBERS NATURAL CONVECTION ABOUT A HEATED SPHERE

In the analysis of conjugate natural convection between concentric spheres, it is seen that as the radius ratio, $\beta \to \infty$ the problem reduces to a single heated sphere in an unbounded expanse of fluid. The resulting flow field is essentially confined to a vertical plume above the heat source. The temperature vanishes outside the plume and as $R \to \infty$ the velocity should vanish everywhere except in the narrow wake region above the sphere, wherein it should be bounded. The regular perturbation expansion scheme employed in this thesis is inadequate except in the region near the sphere. For it is in the solution for Ψ_1° (eq. 2.4.4), as $R \to \infty$ the $O(R^3)$ term of Ψ_1° corresponds to an $O(R)$ behaviour in V_R (eq. 3.3.1a).

Thus the velocity boundary condition at infinity is not satisfied. This is analogous to the Whitehead paradox [22] for small Reynolds number flow past a finite size three-dimensional body (i.e. the convective effect must be considered at the distant region away from the sphere, although diffusive effect is predominant near the sphere). Therefore, there exists an outer region in which the con-

vective, diffusive and bouyancy effects are of the same order of magnitude. An inner-and-outer matched asymptotic expansions will be required for the solution of the flow field. Note that at a large distance away from the sphere, although there is conjugate effect at the surface of the sphere, it will appear as a heat point source.

In order to obtain the governing equations in the outer region where the convective and diffusive effects are of the same order, Mahoney [23] introduced an appropriate length scale (i.e. $R=R_i G^{-\frac{1}{2}}$) together with an asymptotic expansion in terms of $G^{-\frac{1}{2}}$. He noted the complexity of obtaining exact solutions for the outer region. Instead he obtained similarity solutions to the equations by assuming the existence of a vertical plume in this region. However, it is impossible to match the outer solution to the regular perturbation expansion in the inner region.

Recently, Fendell [19] obtained an approximate solution, first by seeking a similarity solution, and then by linearizing the equations in the outer region in the manner of Oseen's equation. The magnitude of the assumed uniform stream is based upon the coordinate perturbation solution in the plume. Hence the velocity above the sphere is reduced from unbounded growth with distance from the sphere to a constant magnitude. This procedure can be expected to yield qualitative results only. In their conjectures, Hieber and Gebhard [20] showed that it seems plausible to assume that

velocity in the wake behave as a uniform stream only in the matching region. This is based on their results on free and forced convection from a sphere at low Reynolds and Grashof numbers.

Hossain and Gebhart [24] employed a single parameter perturbation scheme in their analysis to this problem. The Grashof number is used as the expansion parameter in combination with exponentially decaying functions. These decaying functions will ensure the velocity and temperature vanish as $R \to \infty$. However, the disadvantages of this scheme are (a) it is only valid for very small G, (b) the temperature boundary condition at the surface of the inner sphere is not satisfied completely.

The difficulties in the analysis of small Grashof numbers from a heated sphere seem to be that the flow field is divided into regions where the predominance of particular physical effects varies for each region i.e. (a) in the vicinity of the sphere the diffusive effect is predominant, (b) in the matching region of the inner and outer flow field the convective, diffusive and bouyancy effects are of equal importance, (c) at infinity the velocity should be zero. The limits of these regions in the flow field are apparently very complicated. Hence not all scaling lengths or velocities are known. The techniques [20] which are employed successfully for the forced convection flows are not successful here except qualitatively. This is due to the entirely different flow field being encountered. Therefore a study of conjugate natural convection from a single heated sphere would be interesting and challenging.